THE UNIVERSITY OF WISCONSIN—MILWAUKEE

CENTER FOR GREAT LAKES STUDIES

SPECIAL REPORT NO. 12

LARGE-SCALE OSCILLATORY MOTIONS AND SEASONAL TEMPERATURE CHANGES IN LAKE MICHIGAN AND LAKE ONTARIO

Part II, Illustrations

by

C. H. MORTIMER

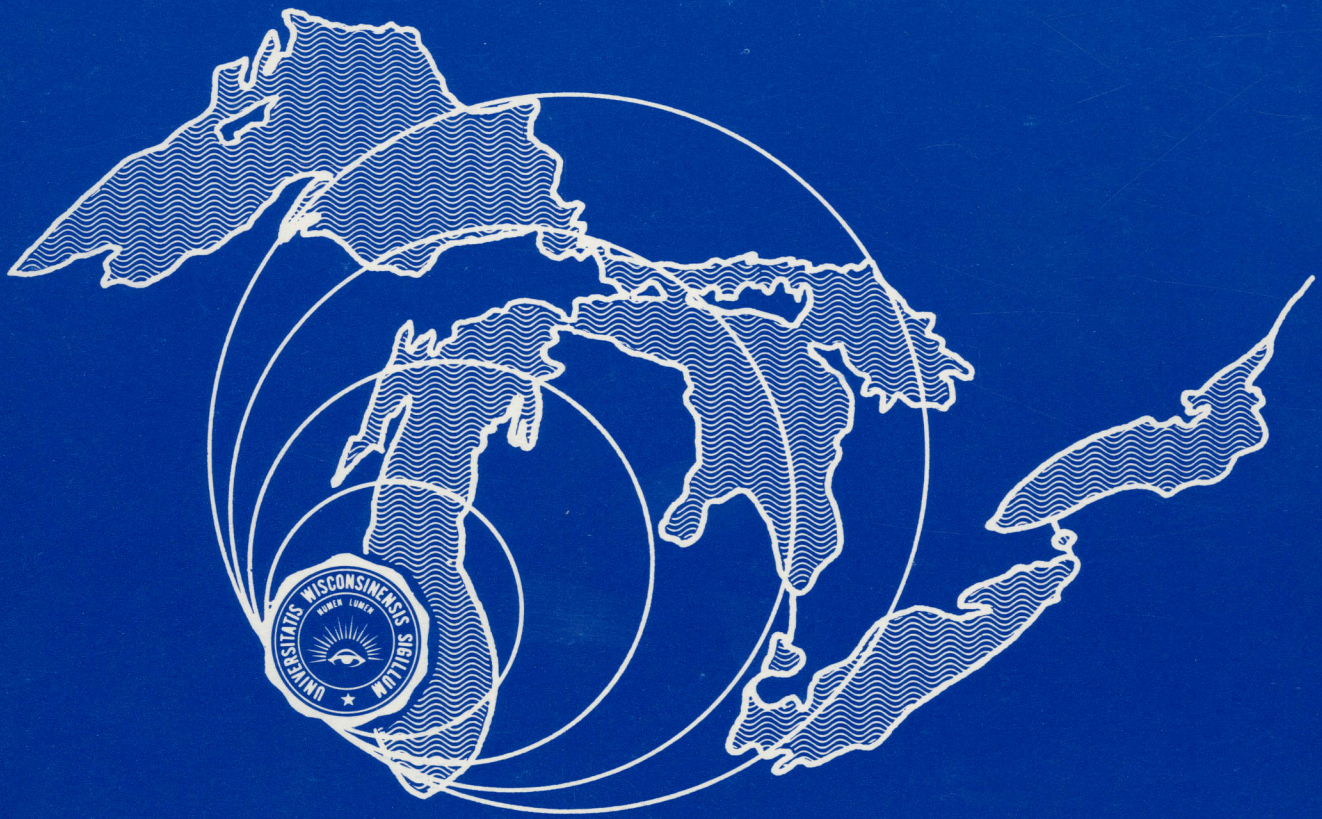

MILWAUKEE, WISCONSIN 53201 U.S.A.

SPECIAL REPORT NO. 12

LARGE-SCALE OSCILLATORY MOTIONS AND SEASONAL TEMPERATURE CHANGES IN LAKE MICHIGAN AND LAKE ONTARIO

Part II, Illustrations*

by

C. H. MORTIMER

A Preparatory Analysis for the International Field Year on the Great Lakes (International Hydrological Decade)

Prepared under U. S. Army Engineers Contract No. DACW-35-68-C-0072

*Part I, Text, is bound separately

Center for Great Lakes Studies
University of Wisconsin-Milwaukee
Milwaukee, Wisconsin 53201

1971

ILLUSTRATIONS GROUPED BY CHAPTER

LIST OF ILLUSTRATIONS*

---

*(Short form; further details in some figure legends)

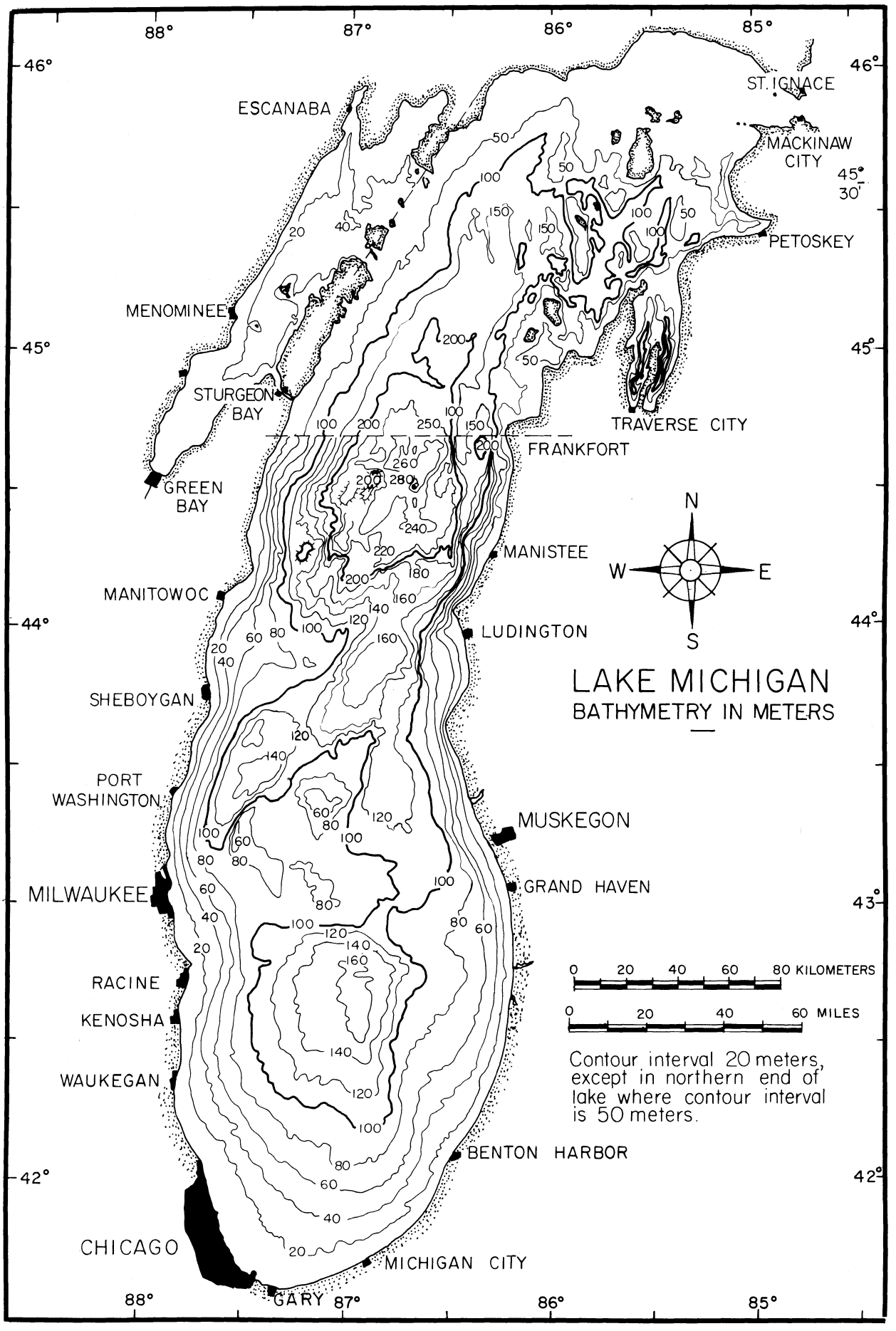

Fig. 1. Bathymetric chart of Lake Michigan (prepared by R. Ristić from U.S. Army Engineers, Lake Survey, soundings).

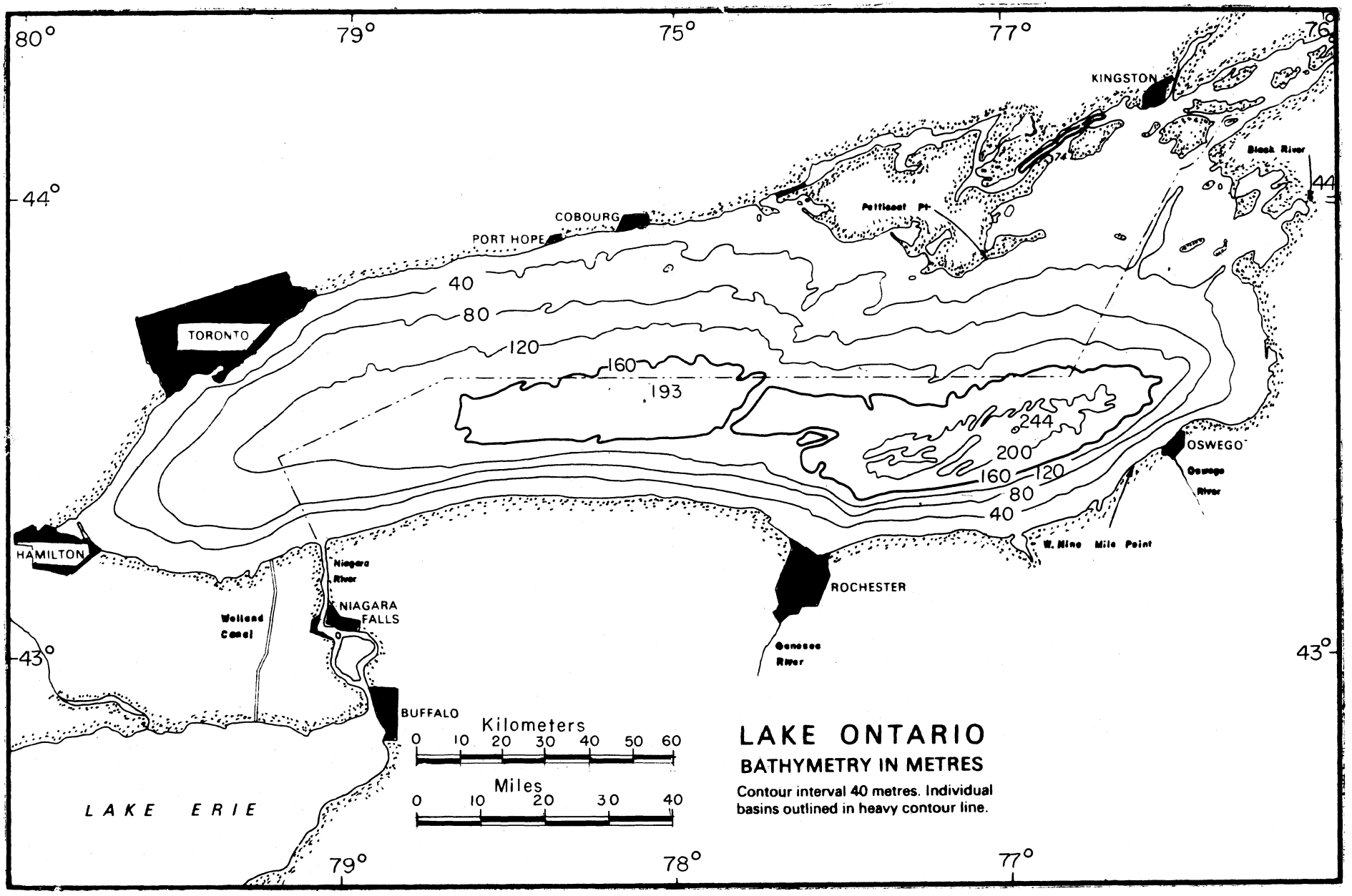

Fig. 2. Bathymetric chart of Lake Ontario (from Sweers 1969).

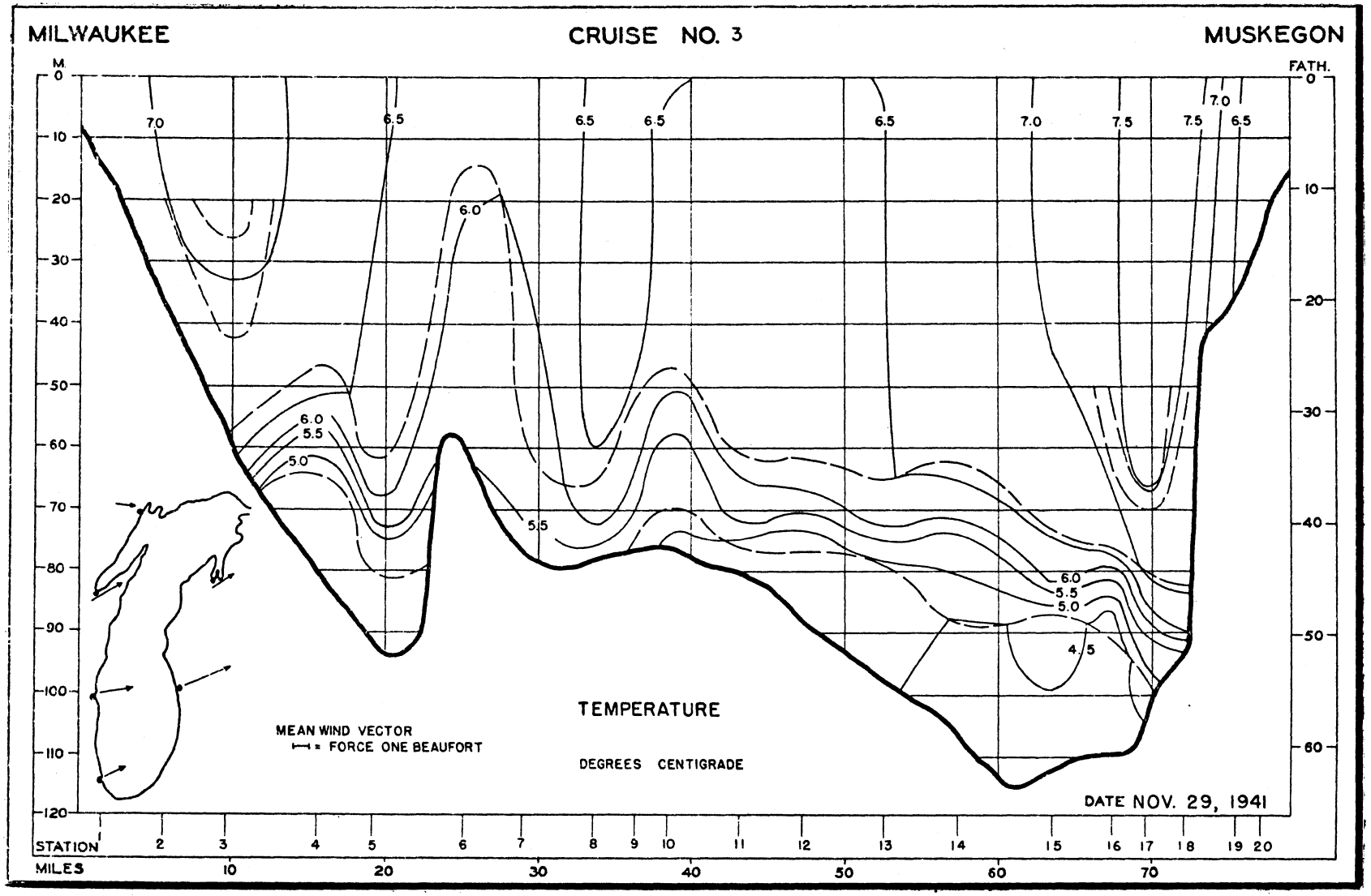

Fig. 3. Lake Michigan, 29 November 1941. Distribution of temperature, °C, observed from a ferry, Milwaukee-Muskegon transection, see fig. 1 (Church 1945).

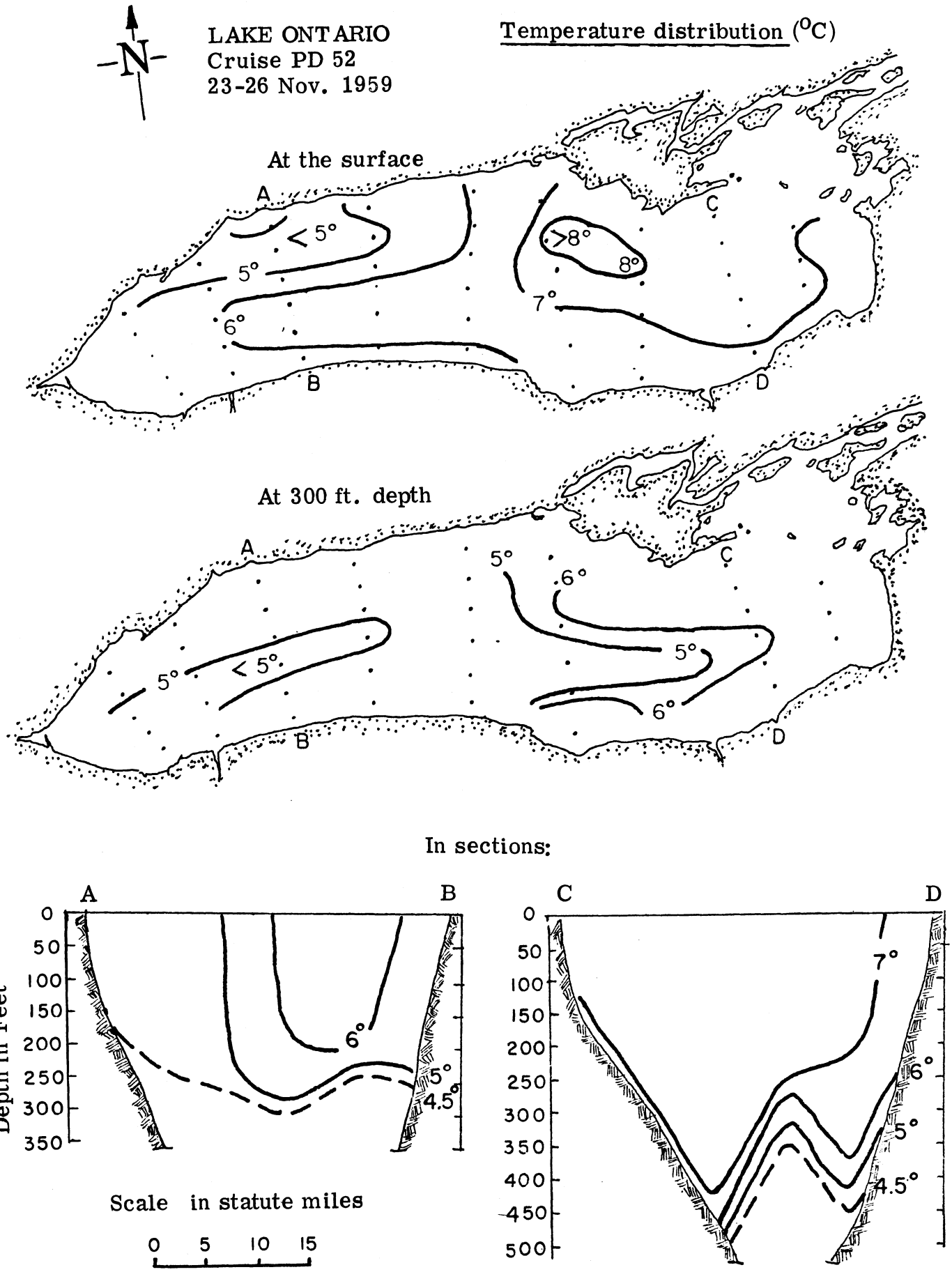

Fig. 4. Lake Ontario, 23-26 November 1959. Distribution of temperature, °C, basin-wide at the surface and at 300 ft depth, and in two cross-sections (re-drawn from Anderson 1967).

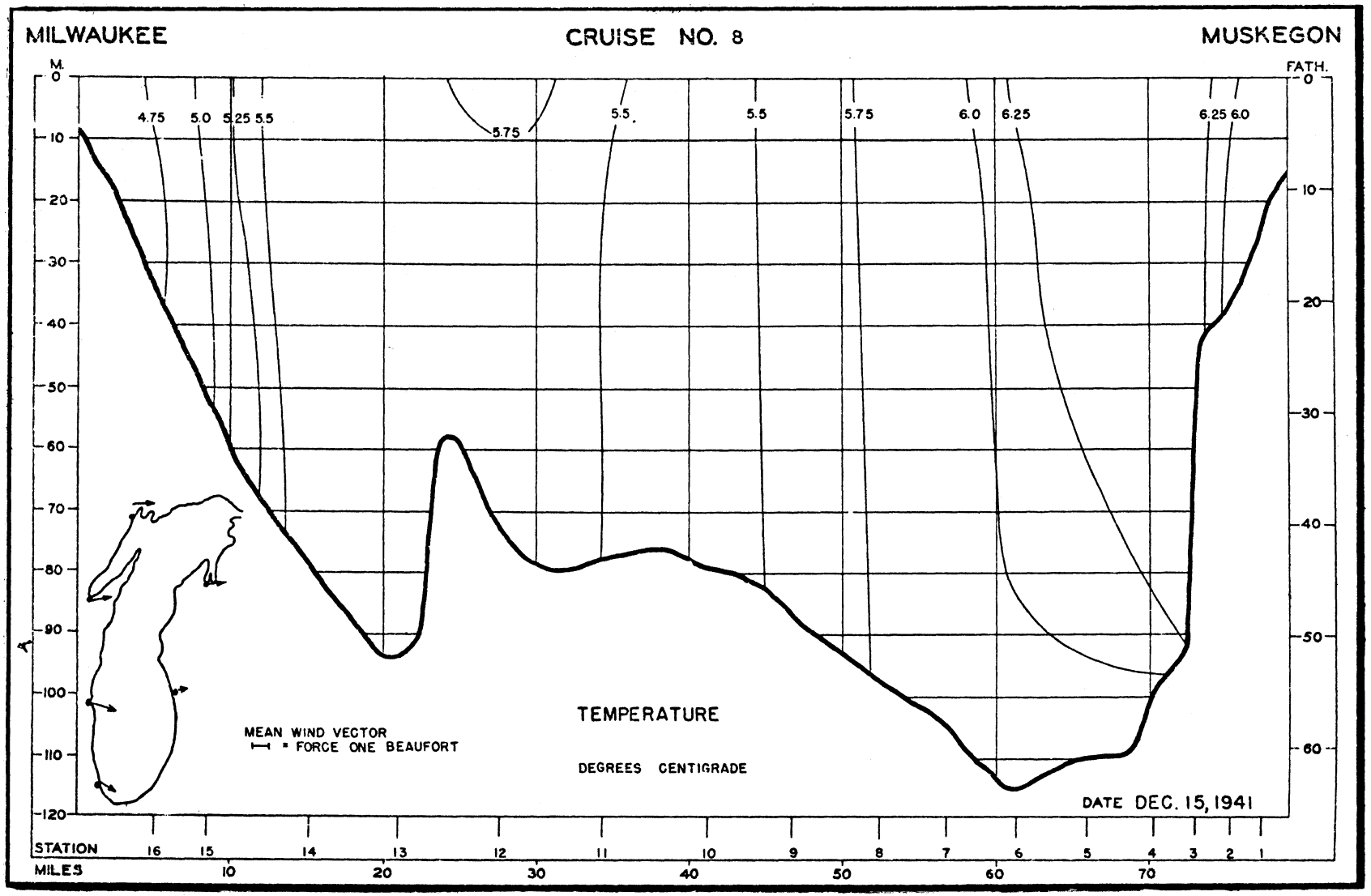

Fig. 5. Lake Michigan, 15 December 1941. Distribution of temperature, °C, observed from a ferry, Milwaukee-Muskegon transection (Church 1945).

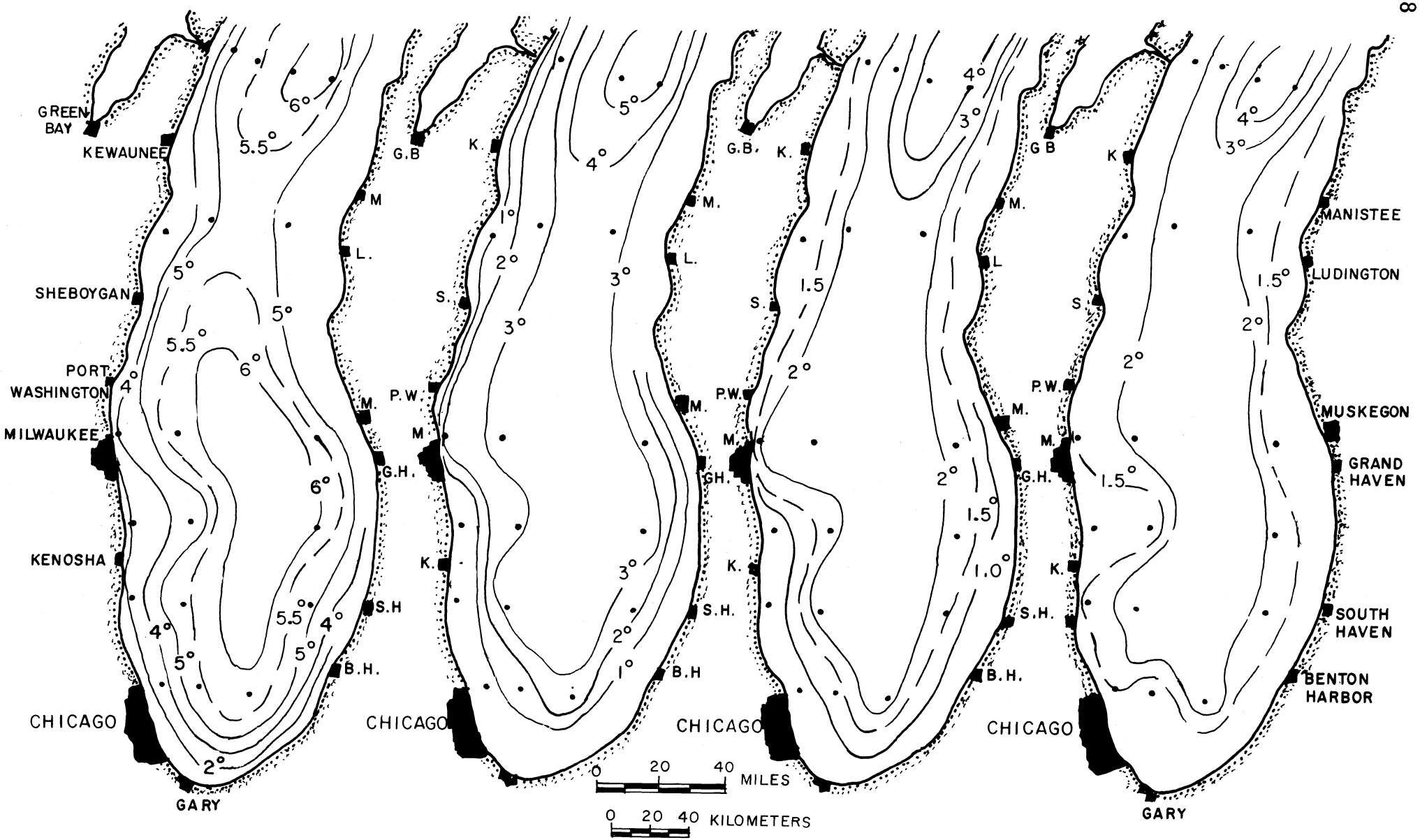

Fig. 6. Lake Michigan. Distribution of temperature, °C, at 10 m depth in the southern 2/3 of the basin, representative for 15th-20th of each month, Dec. 1963 and Jan., Feb., and March. 1964 (prepared from data in Noble and Michaelis 1968).

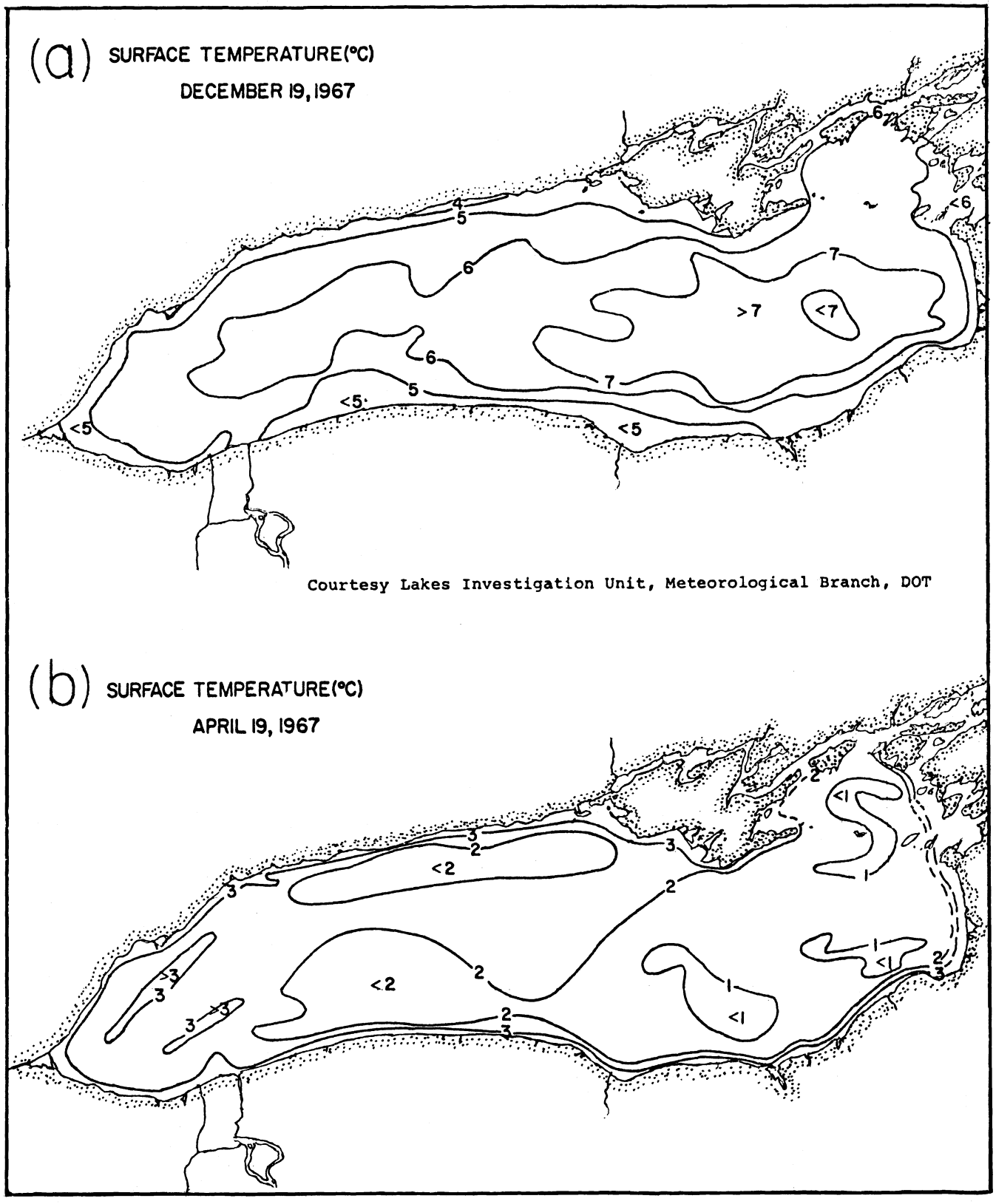

Fig. 7. Lake Ontario. Distribution of temperature, °C, at the surface; (a) 19 Dec. 1967; and (b) 19 Apr. 1967 (from Sweers 1969).

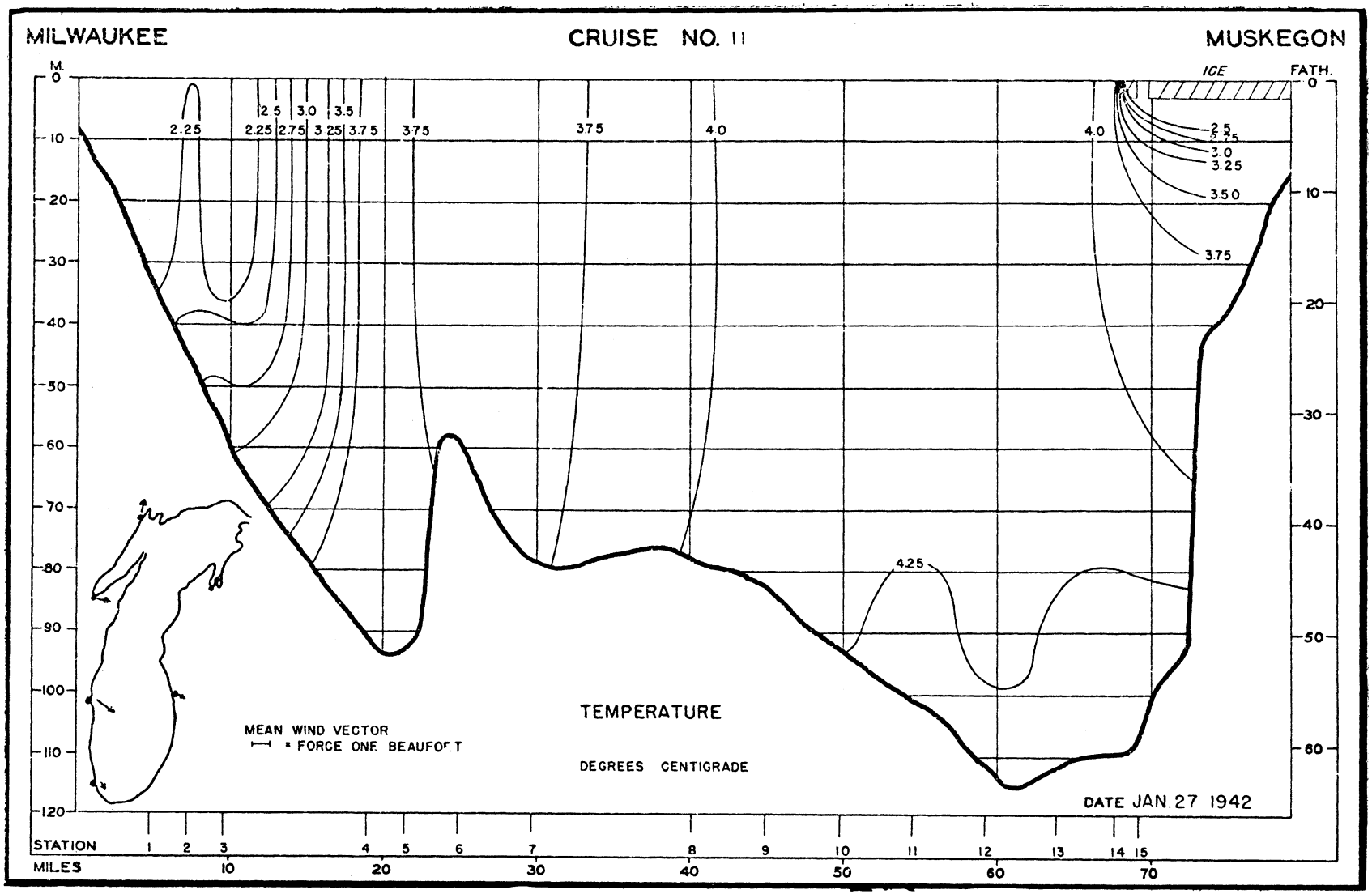

Fig. 8. Lake Michigan, 27 January 1942. Distribution of temperature, °C, observed from a ferry, Milwaukee-Muskegon transection (Church 1945).

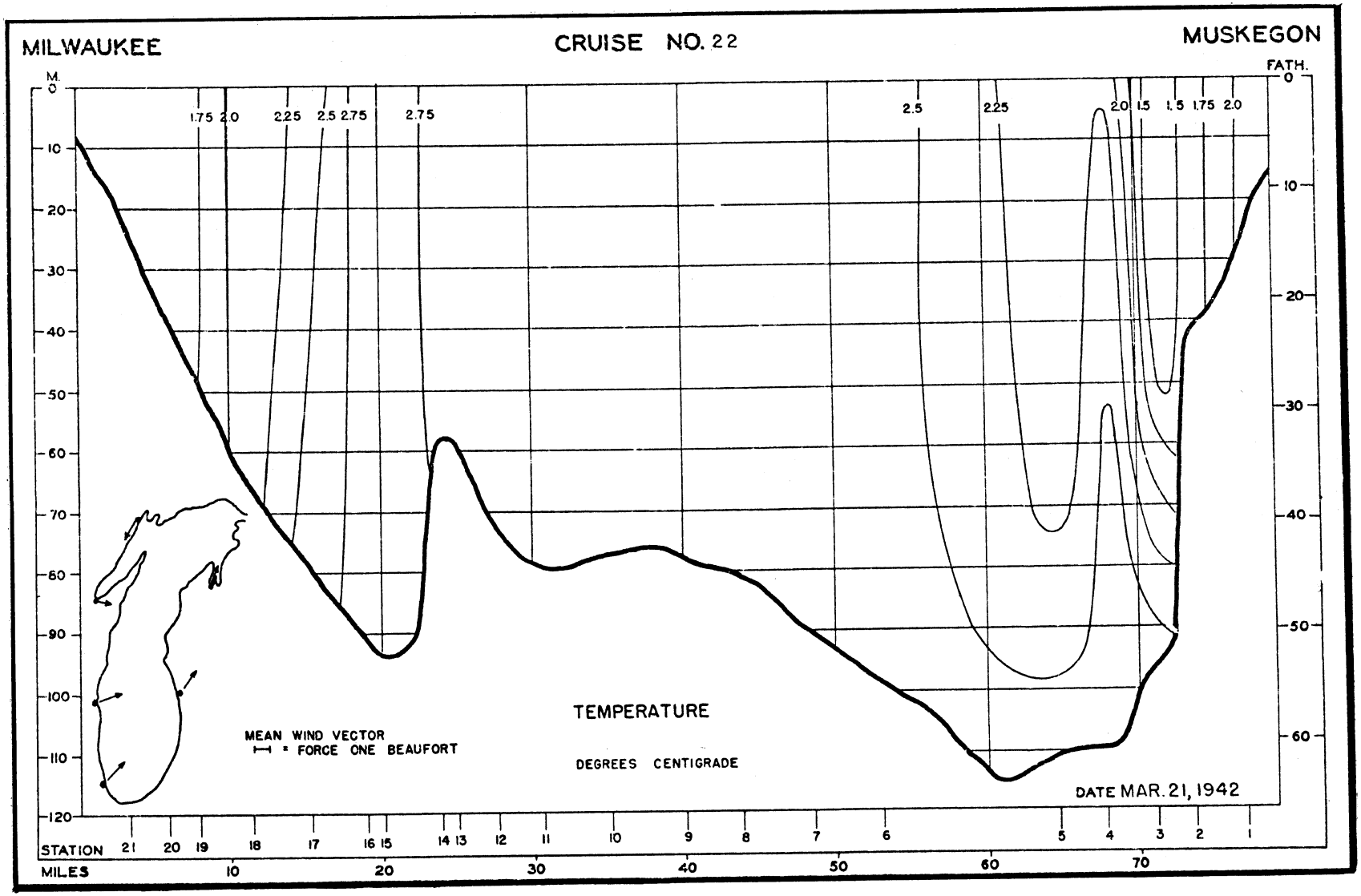

Fig. 9. Lake Michigan, 21 March 1942. Distribution of temperature, °C, observed from a ferry, Milwaukee-Muskegon transection (Church 1945).

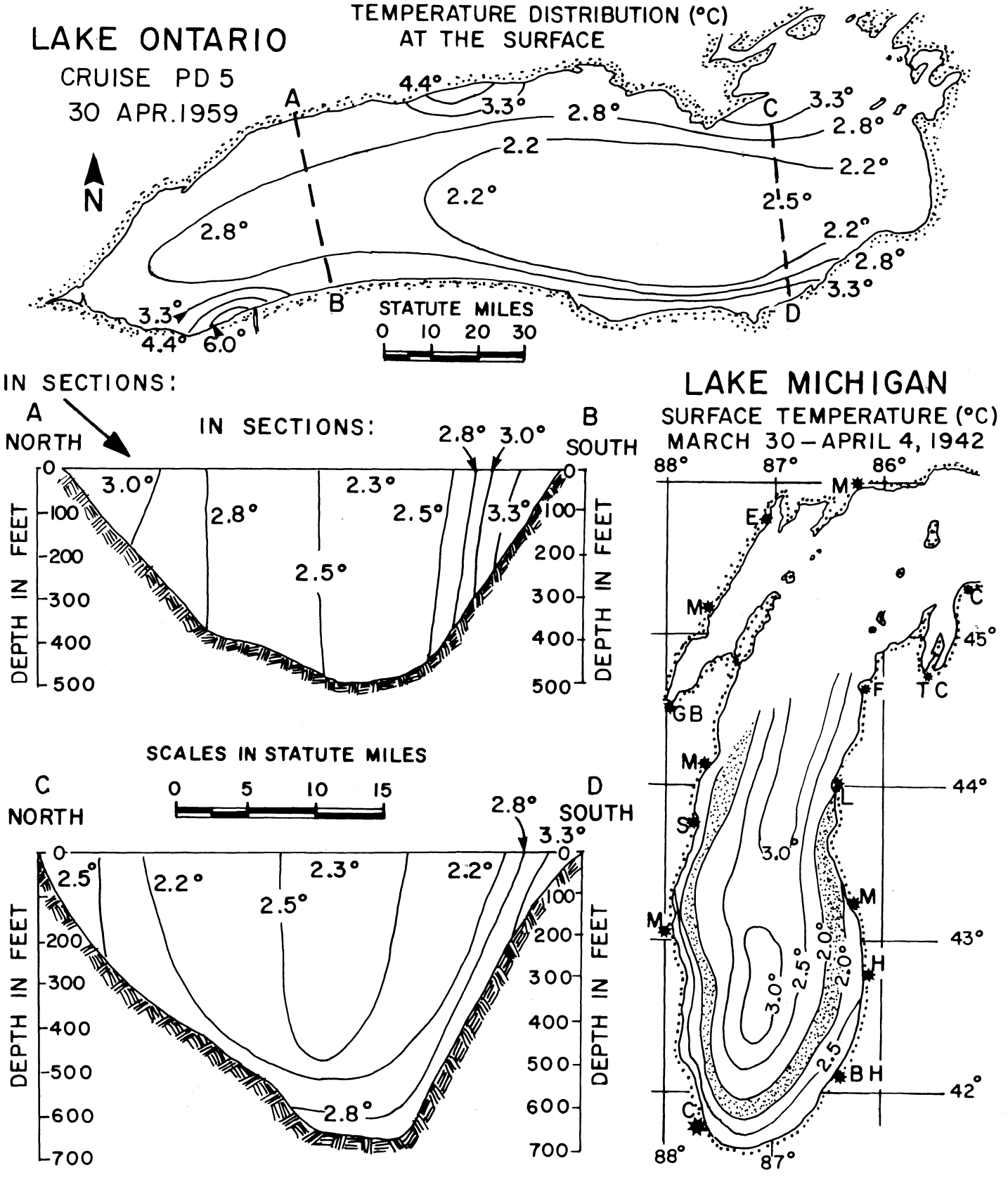

Fig. 10. Lake Ontario, 30 April 1959. Distribution of temperature, °C, at the surface and in two sections (re-drawn from Anderson 1967).

Lake Michigan, 30 March - 4 Apr. 1942. Distribution of surface temperature, °C, in the southern 2/3 of the basin (Church 1945).

Fig. 11. The thermal bar: (a) early winter in Lac Lèman (Forel 1895); (b) in spring and early winter in Lake Ladoga (Tikhomirov 1963, illustrations from Kalesnik 1968); (c) development in Lake Ontario (re-drawn from Rodgers 1966); (d) aftermath (?) of a thermal bar in northern Lake Michigan (Church 1945).

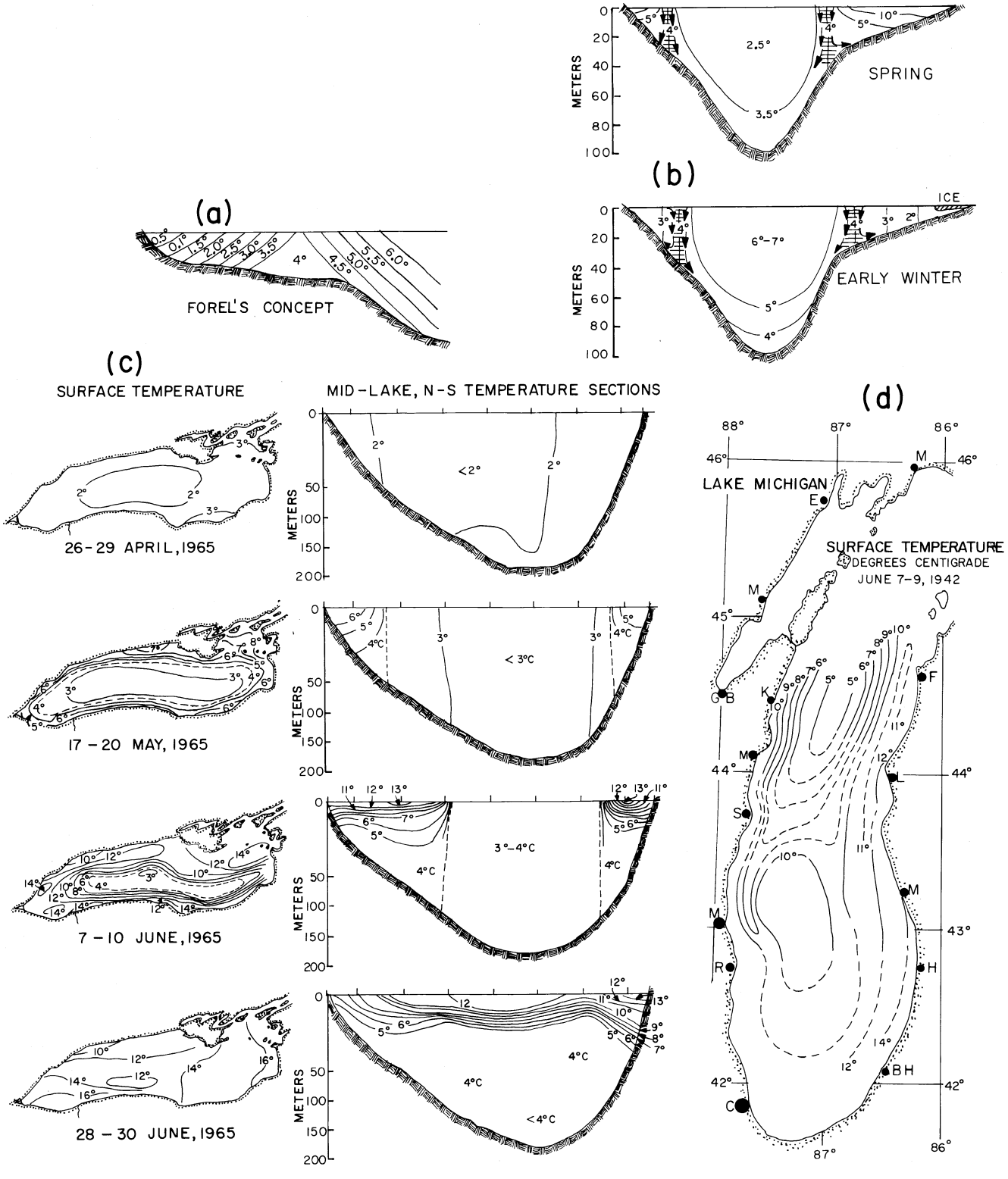

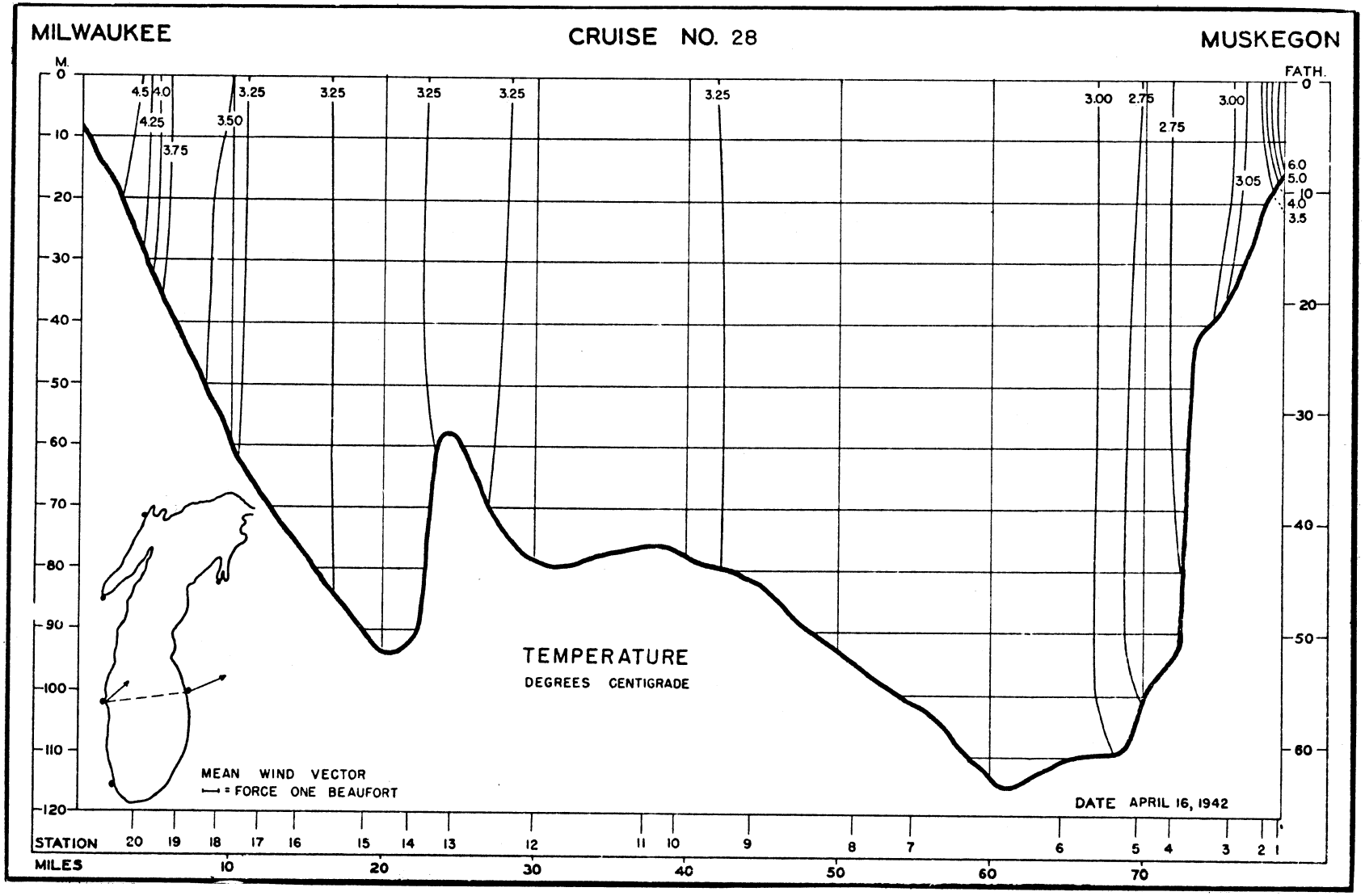

Fig. 12. Lake Michigan, 16 April 1942. Distribution of temperature, °C, observed from a ferry, Milwaukee-Muskegon transection (Church 1945).

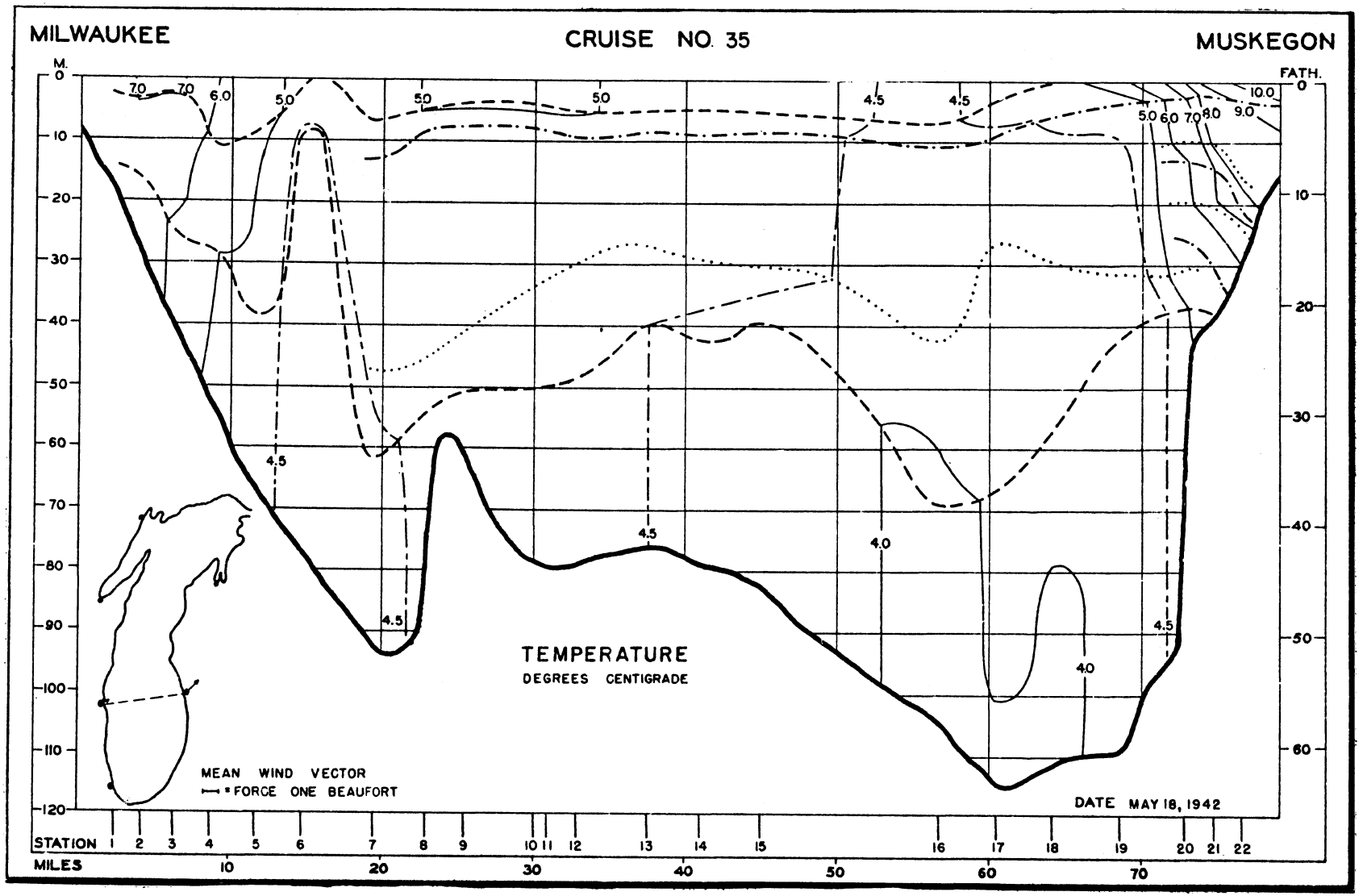

Fig. 13. Lake Michigan, 18 May 1942. Distribution of temperature, °C, observed from a ferry, Milwaukee-Muskegon transection (Church 1942).

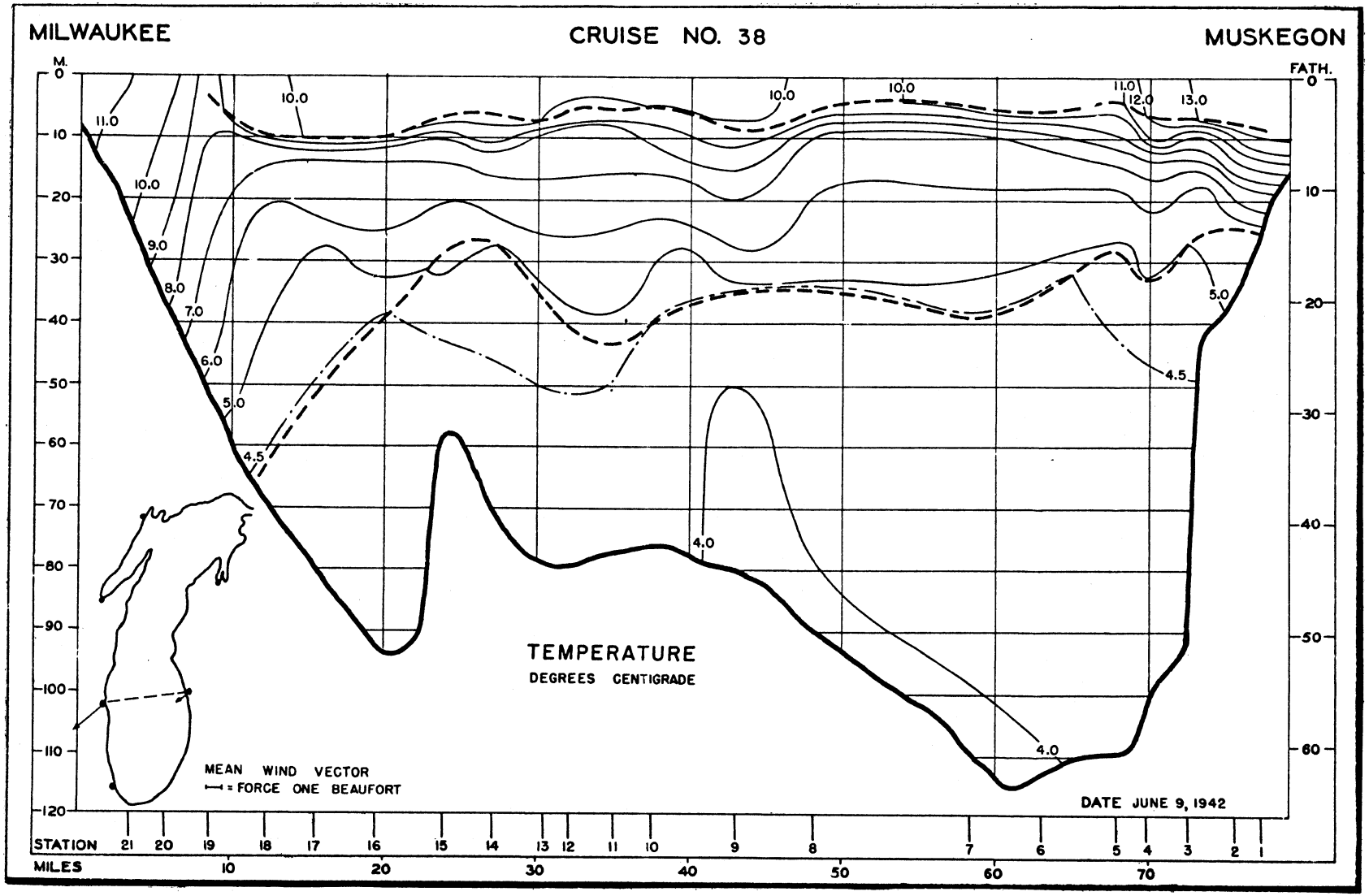

Fig. 14. Lake Michigan, 9 June 1942. Distribution of temperature, °C, observed from a ferry, Milwaukee-Muskegon transection (Church 1945).

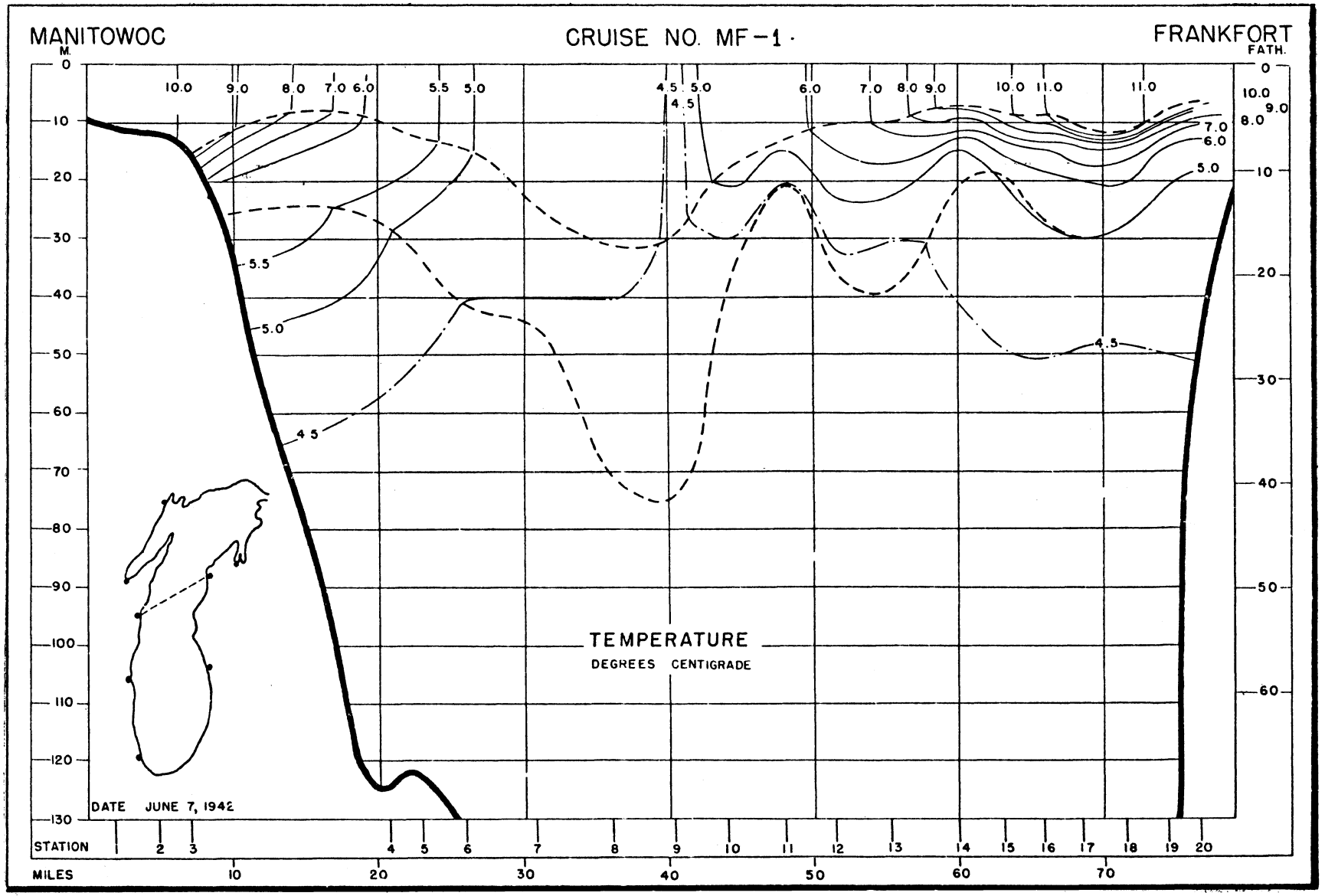

Fig. 15. Lake Michigan, 7 June 1942. Distribution of temperature, °C. observed from a ferry, Manitowoc-Frankfort transection (Church 1945).

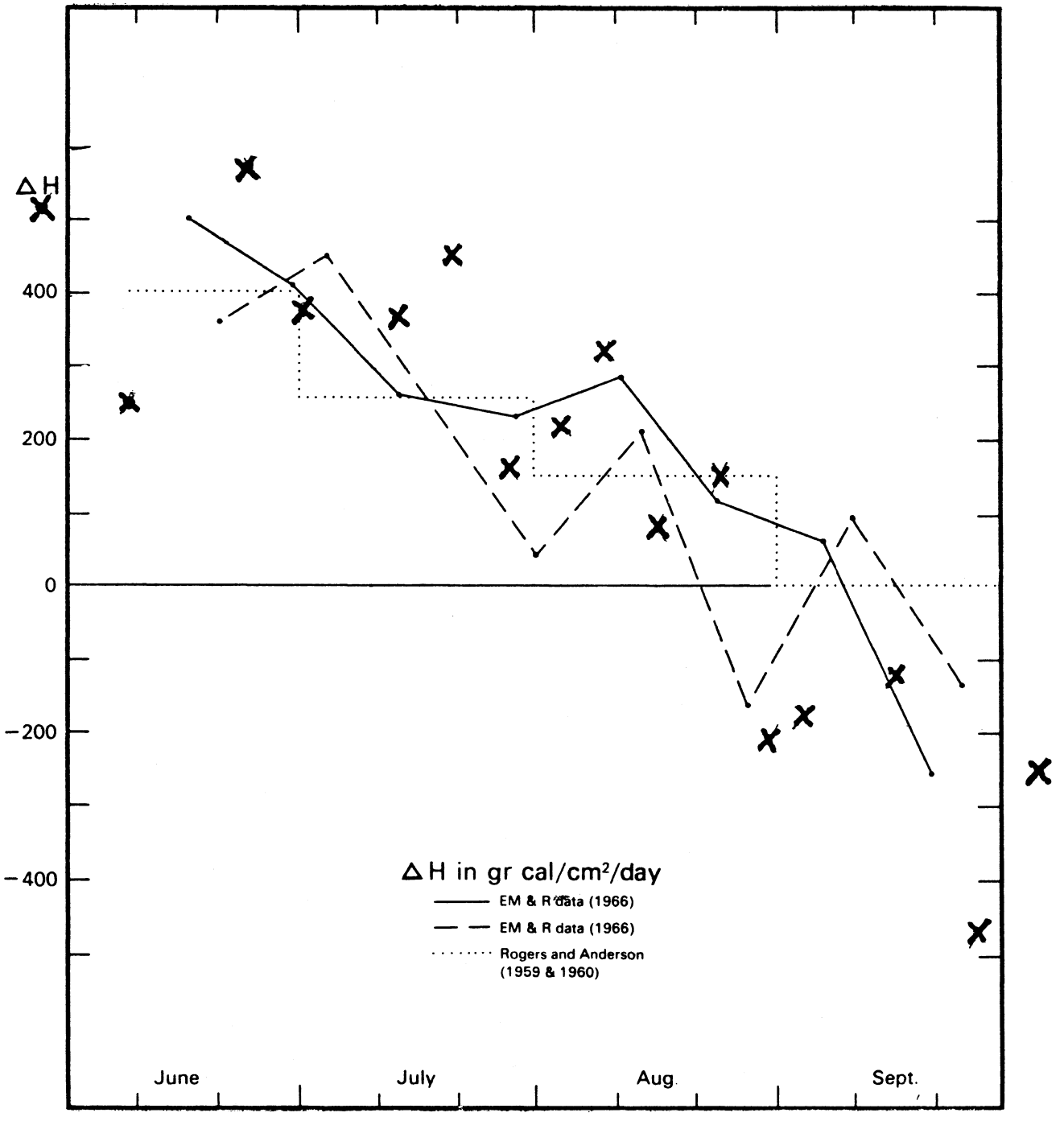

Fig. 16. Lakes Ontario and Michigan, mean net heat input, ΔH in g cal /cm^2/day, based on fig. 35 of Sweers (1969), which presents Δ H for Lake Ontario during 1966 (solid line), during 1967 (broken line), and as monthly means for 1959 and 1960 (dotted line). Superimposed on the figure (as crosses) are corresponding 1942 values of Δ H for the Milwaukee-Muskegon transection of Lake Michigan, from Church (1947).

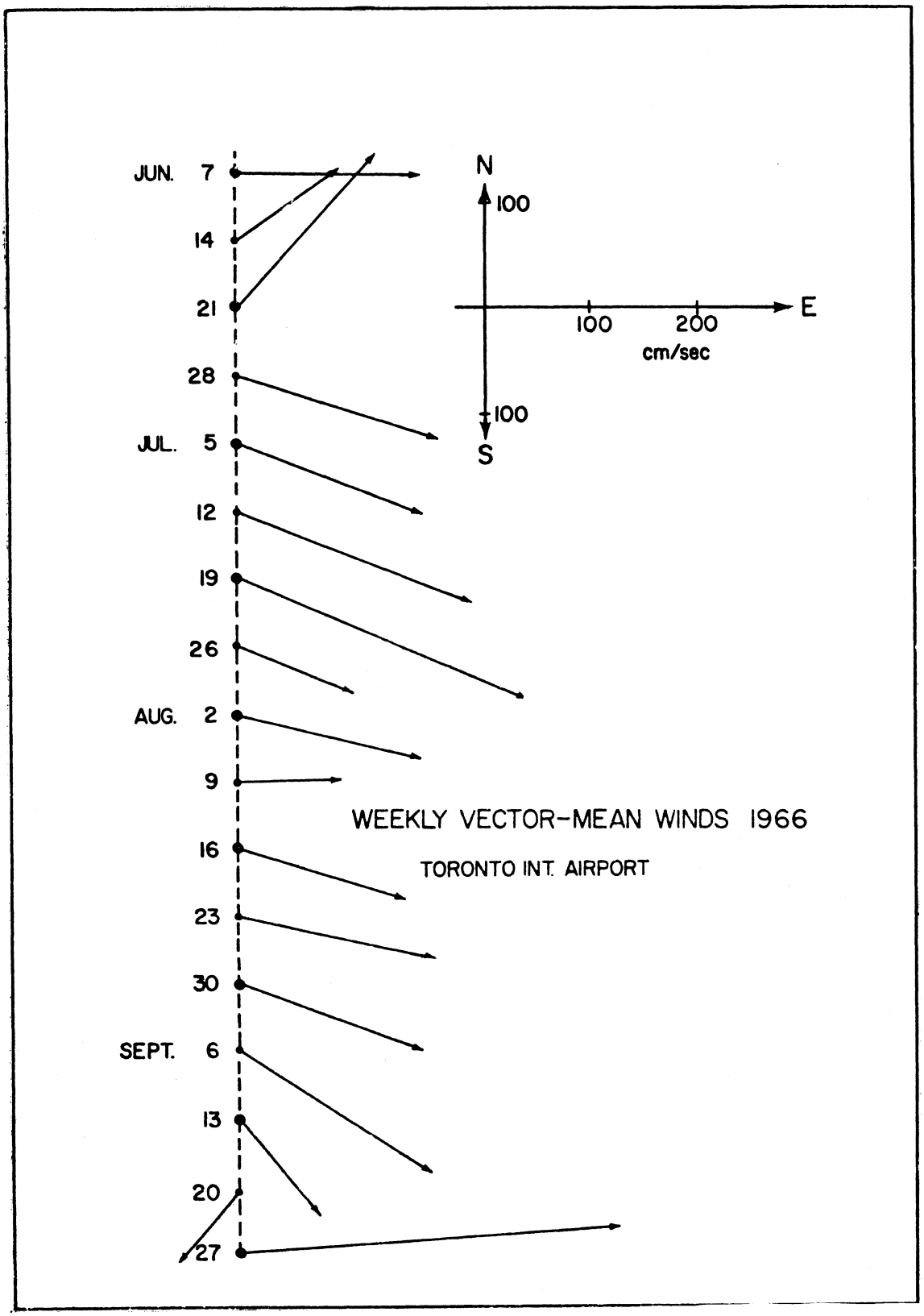

Fig. 17. Weekly vector-mean winds at Toronto International Airport, 7 June - 27 September 1966 (fig. 7 in Sweers 1969).

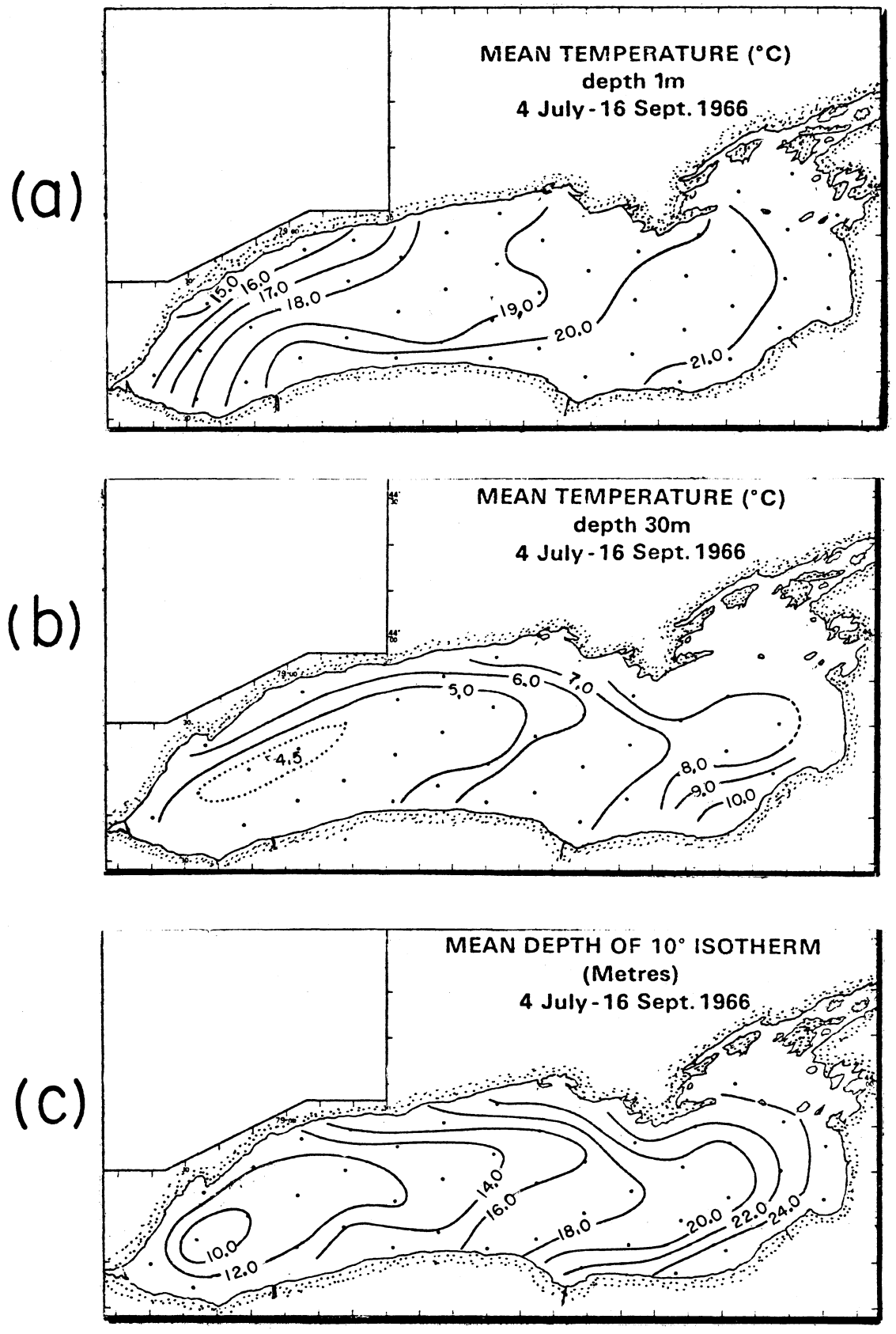

Fig. 18. Lake Ontario, 4 July - 16 September 1966: (a) mean temperature, °C, at 1 m; (b) mean temperature at 30 m; (c) mean depth of the 10° C isotherm (from Sweers 1969).

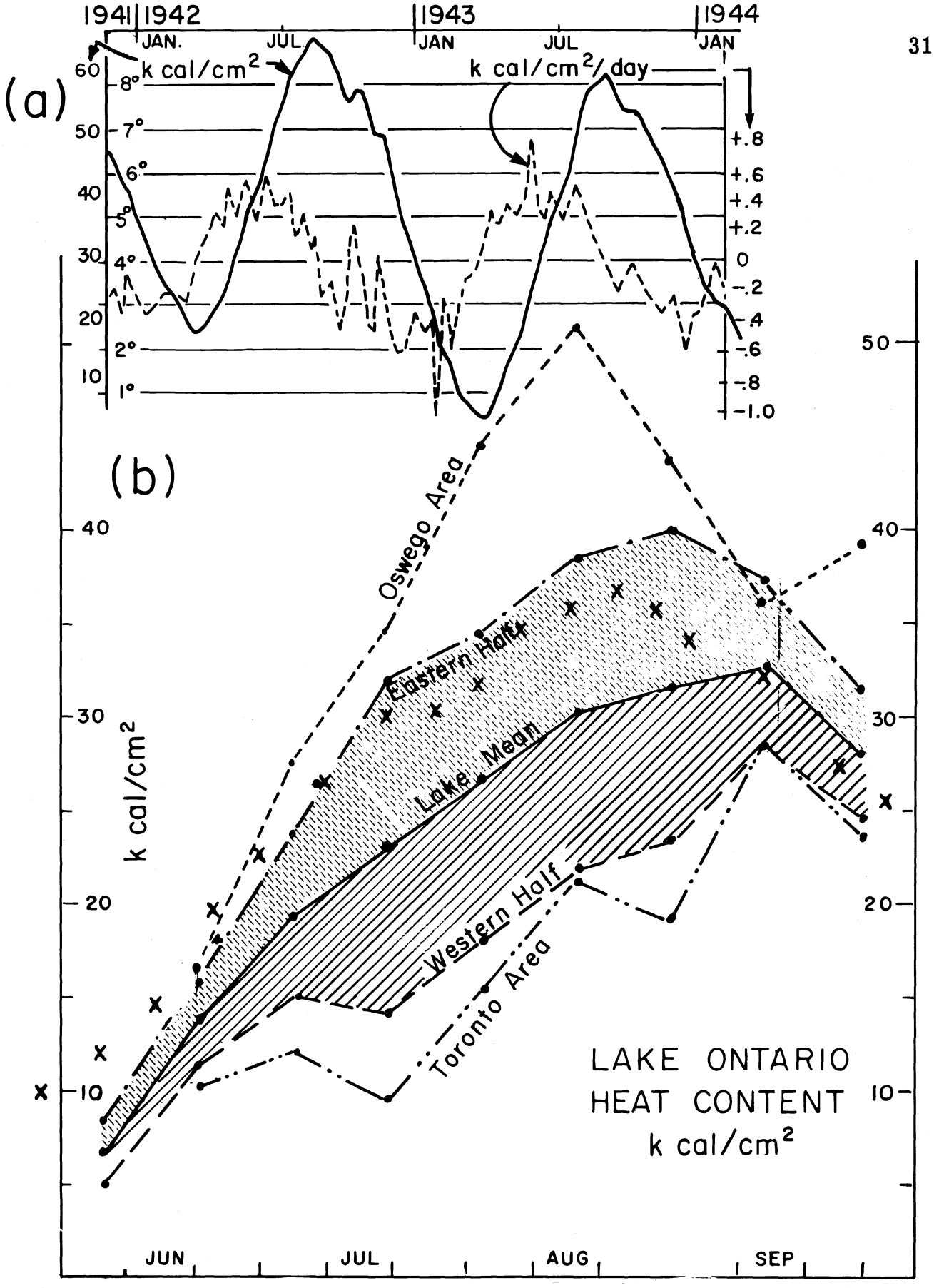

Fig. 19. Mean heat content, k cal/cm^2; (a) Lake Michigan, Milwaukee-Muskegon section, 1941-42 (Church 1947, daily rates of change also shown); (b) Lake Ontario, June - Sept. 1966, for the whole basin and regions of the basin (Sweers 1969), with corresponding 1942 L. Michigan values entered, from (a), as crosses.

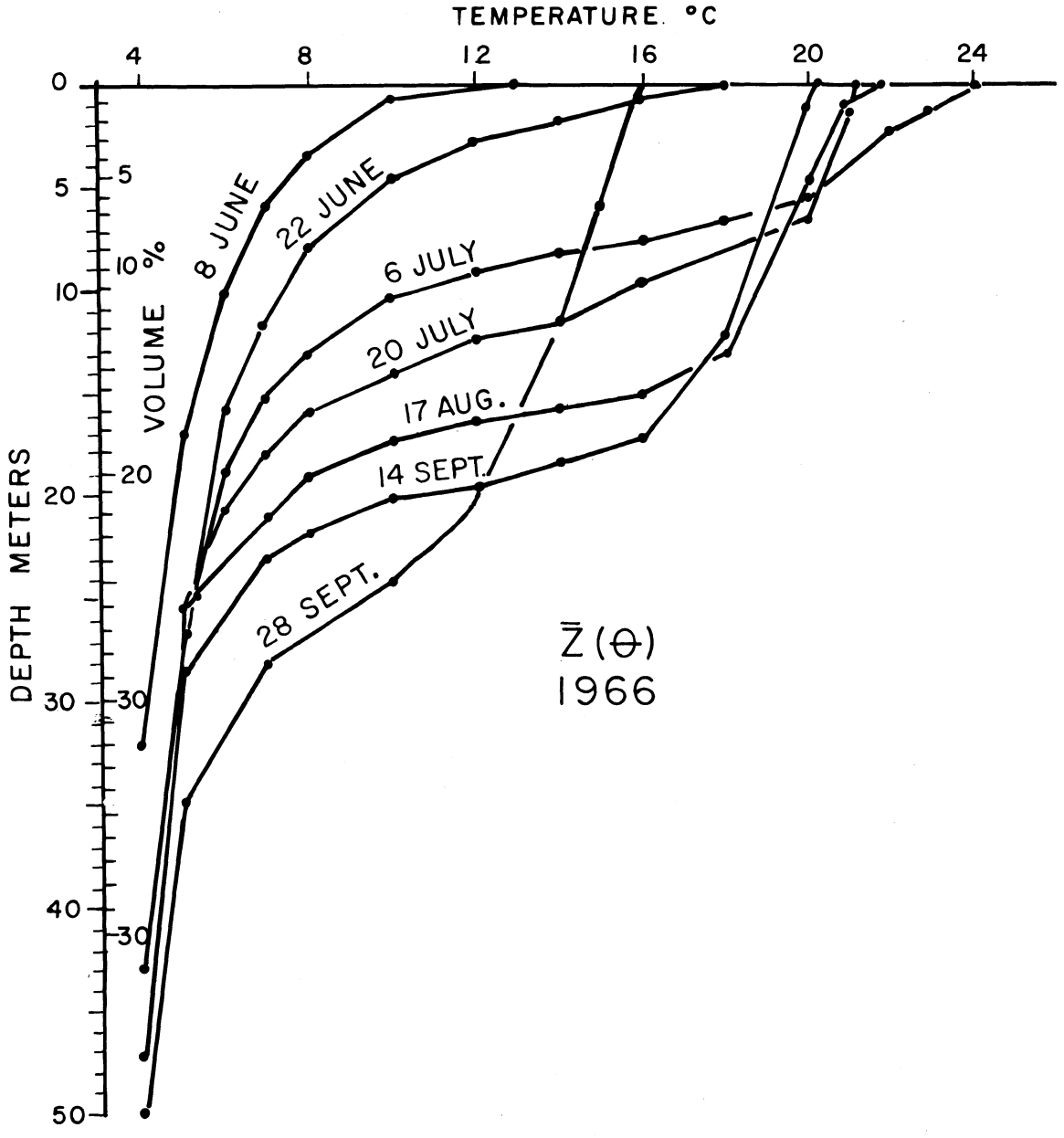

Fig. 20. Lake Ontario, 8 June - 28 September 1966. Whole-basin mean vertical depth distribution of temperature (fig. 26 in Sweers 1969).

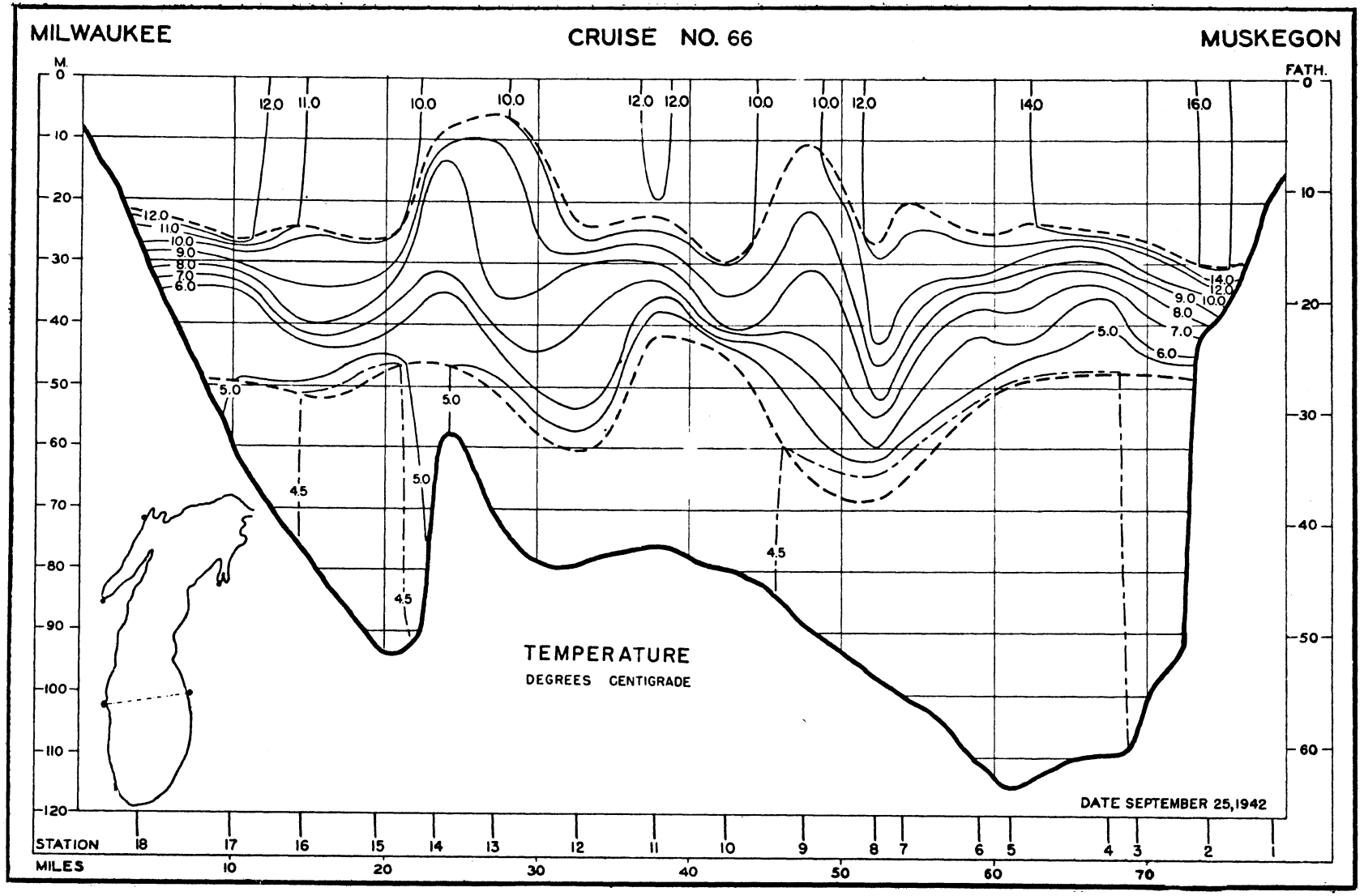

Fig. 21. Lake Michigan, 25 September 1942. Distribution of temperature, °C, observed from a ferry, Milwaukee-Muskegon transection (Church 1945).

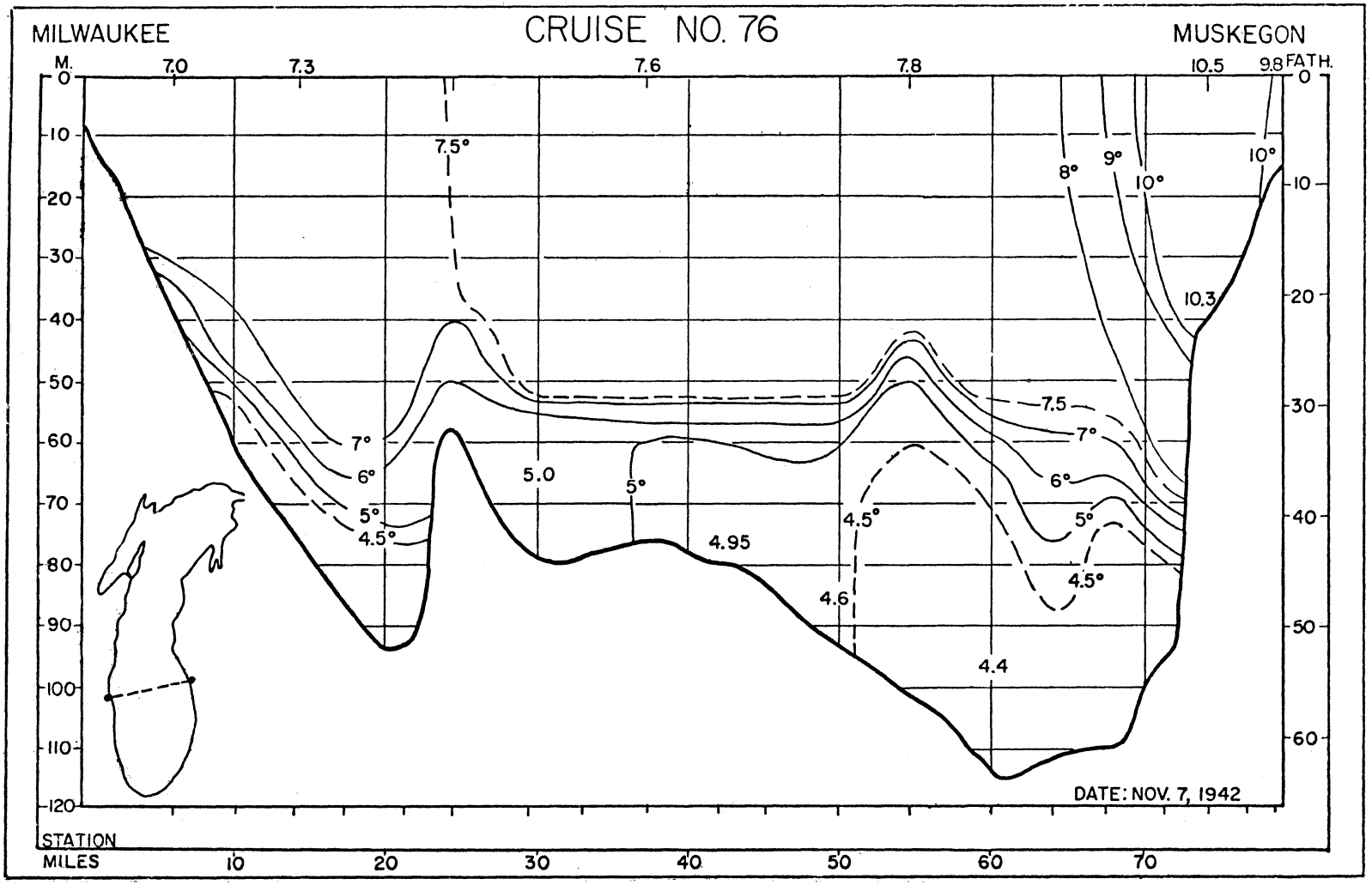

Fig. 22. Lake Michigan, 7 November 1942. Distribution of temperature, °C, observed from a ferry, Milwaukee-Muskegon transection (unpublished data, Church, personal communication).

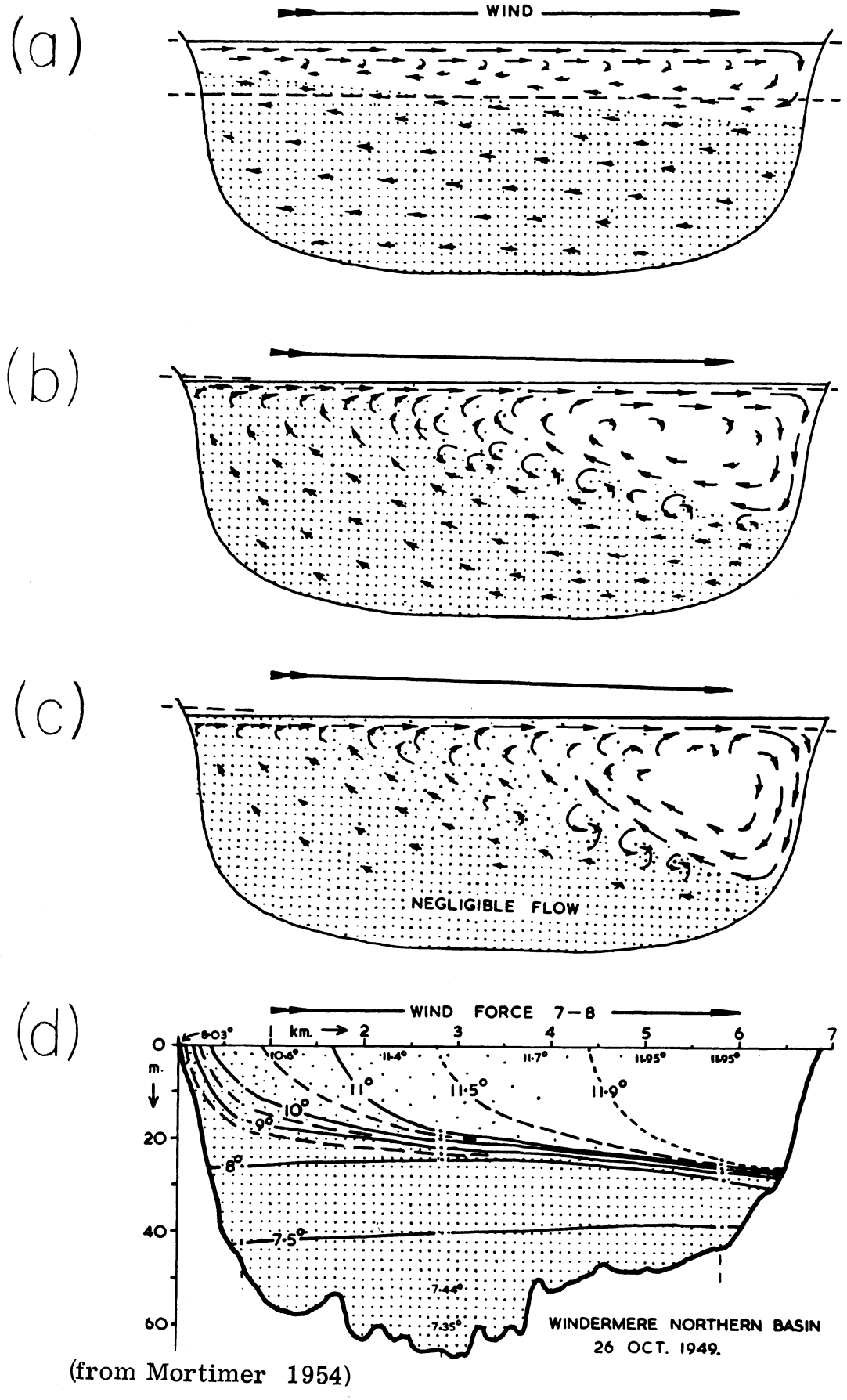

(from Mortimer 1954)

Fig. 23. Circulation and upwelling produced by the stress of a steady wind on a small lake: (a) - (c) three hypothetical stages in flow development; (d) isotherm distribution in an actual lake after 12 hrs of wind stress.

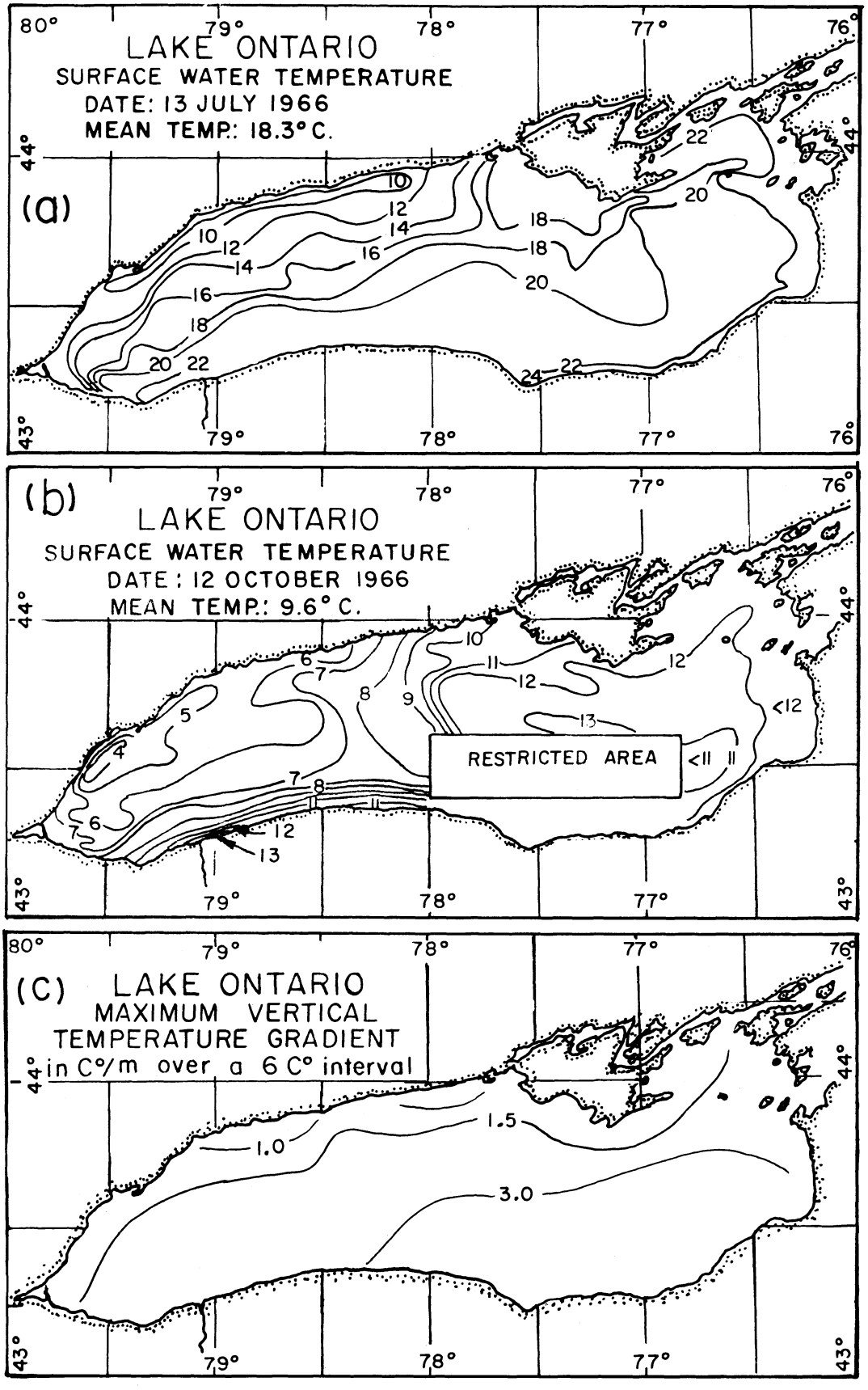

Fig. 24. Lake Ontario: (a) surface temperature, °C, 13 July 1966; (b) surface temperature, 12 Oct. 1966 (Richards, Irbe, and Massey 1969); (c) distribution of maximum vertical temperature gradient during the summer of 1966 (Sweers 1969).

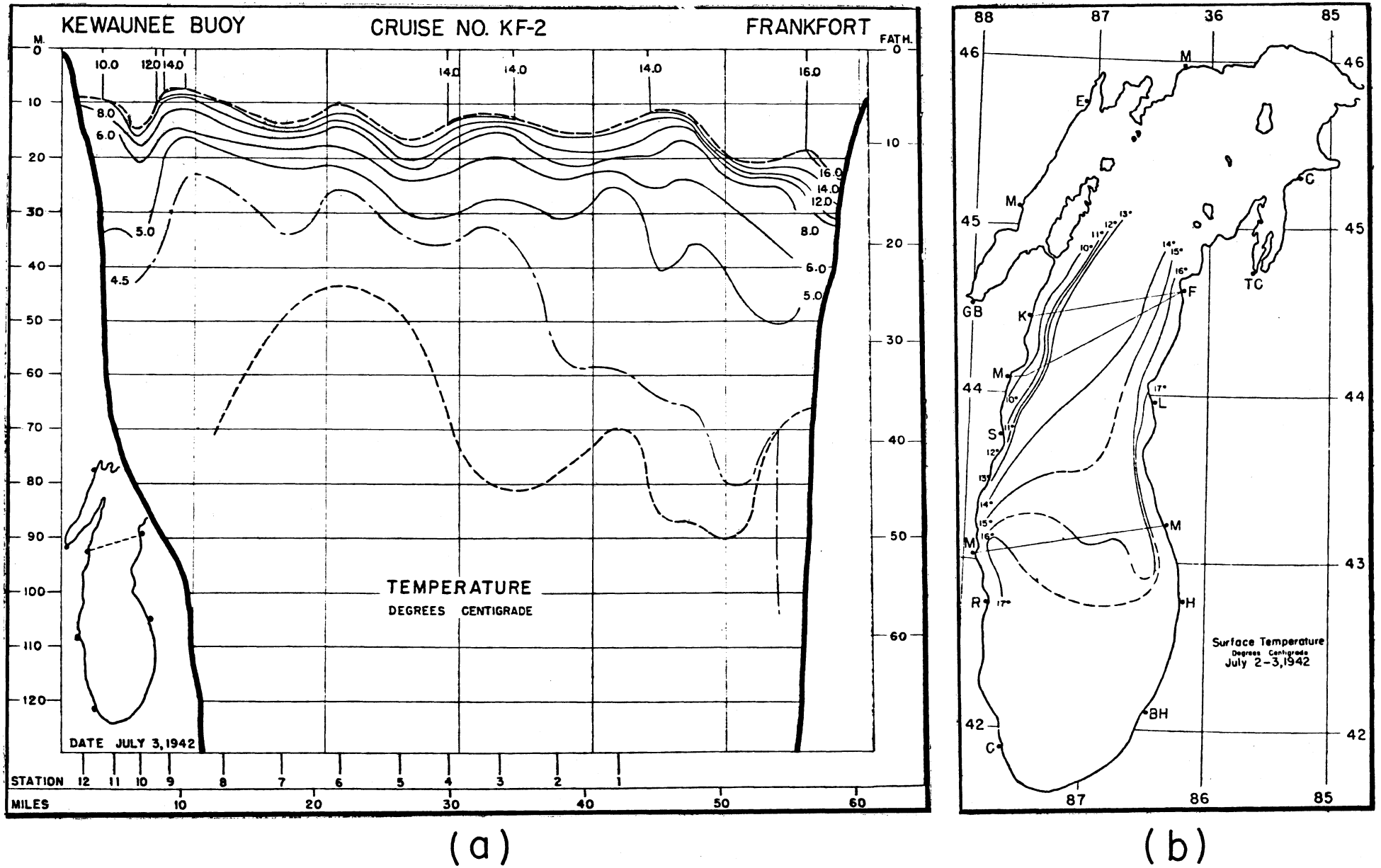

Fig. 25. Lake Michigan: (a) distribution of temperature, °C. observed from a ferry, Kewaunee-Frankfort transection, 3 July 1942; (b) distribution of surface temperature, 2-3 July 1942 (Church 1945).

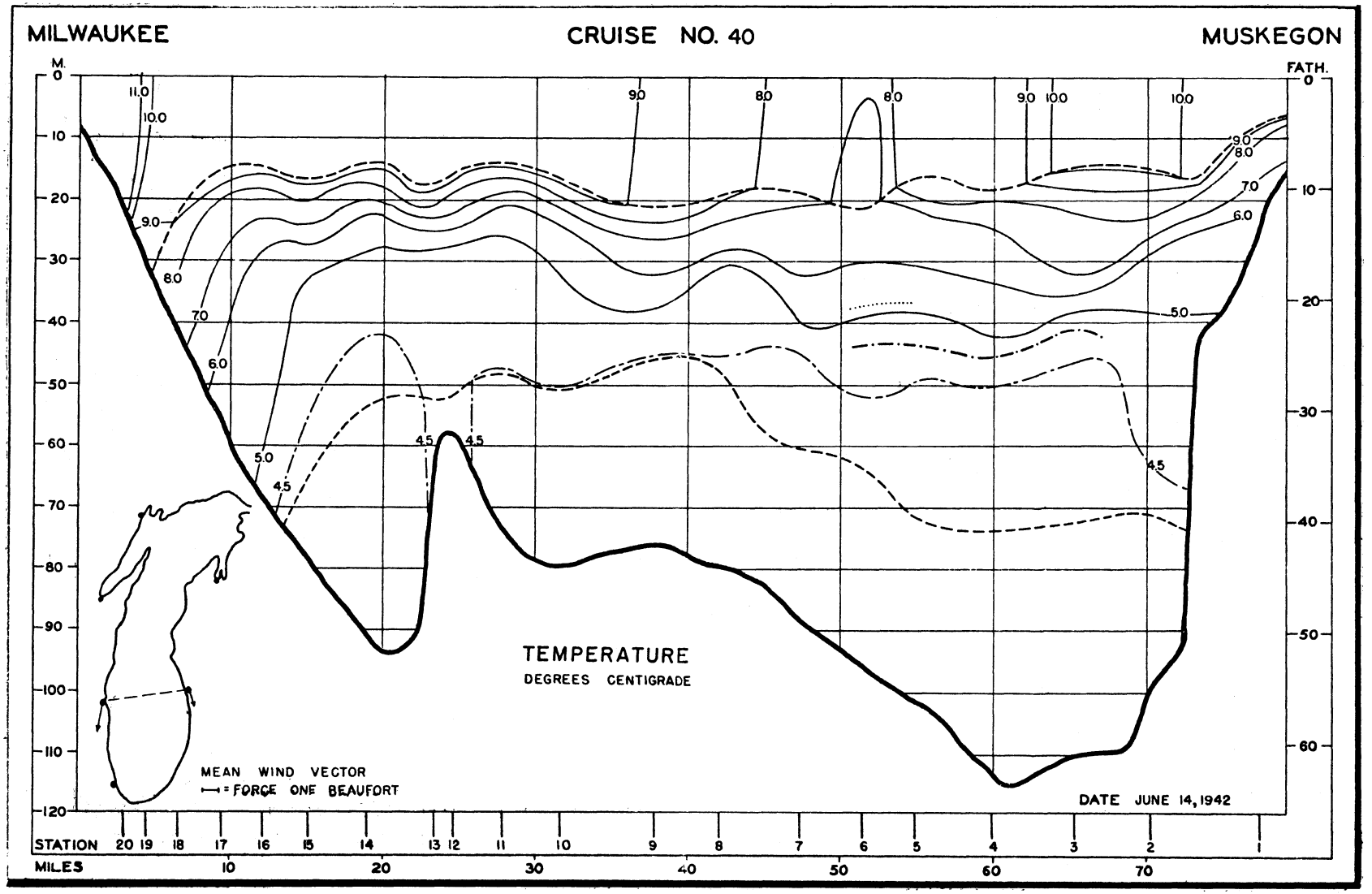

Fig. 26. Lake Michigan, 14 June 1942. Distribution of temperature, °C, observed from a ferry, Milwaukee-Muskegon transection (Church 1945).

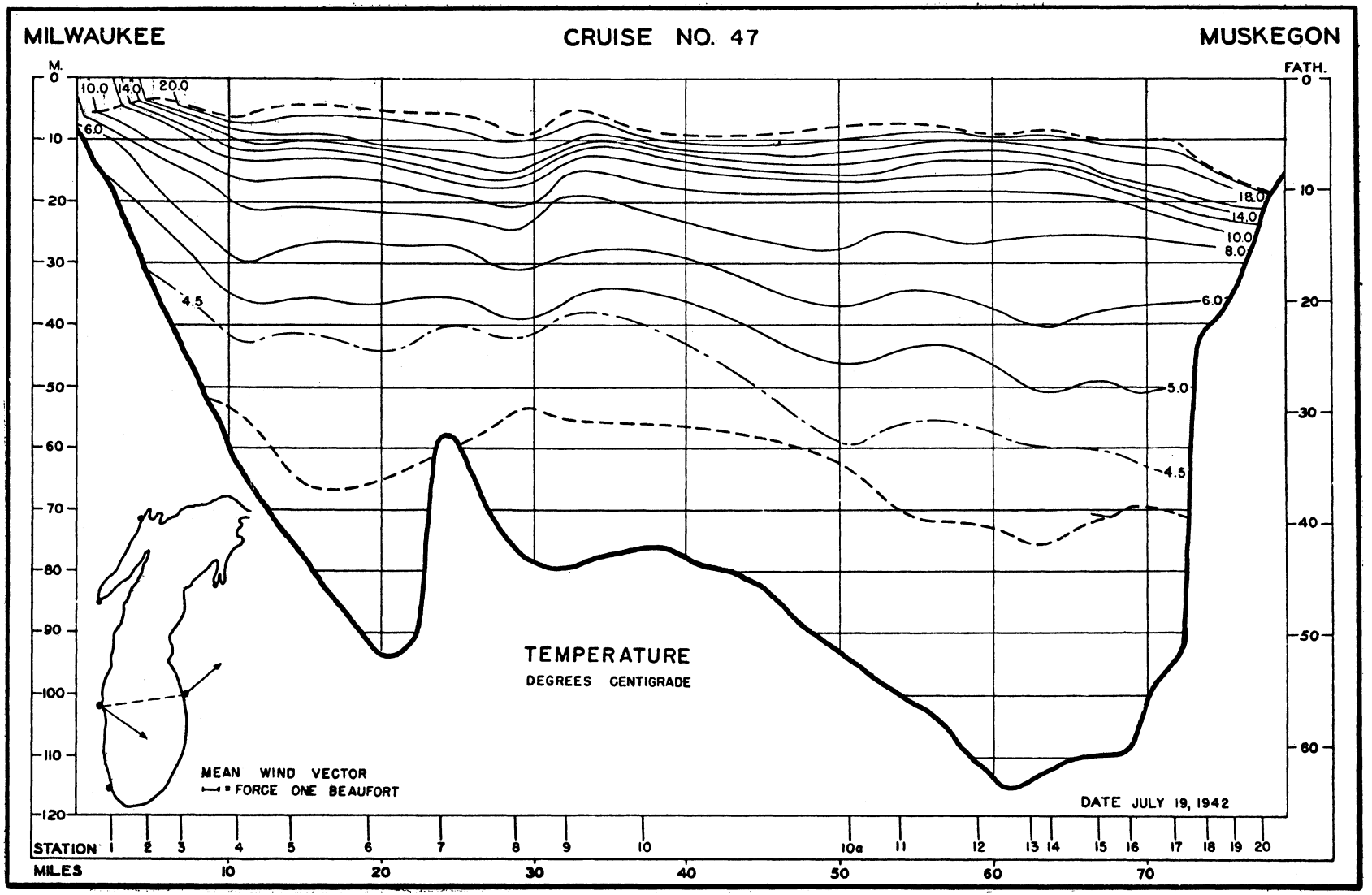

Fig. 27. Lake Michigan, 19 July 1942. Distribution of temperature, °C, observed from a ferry, Milwaukee-Muskegon transection (Church 1945).

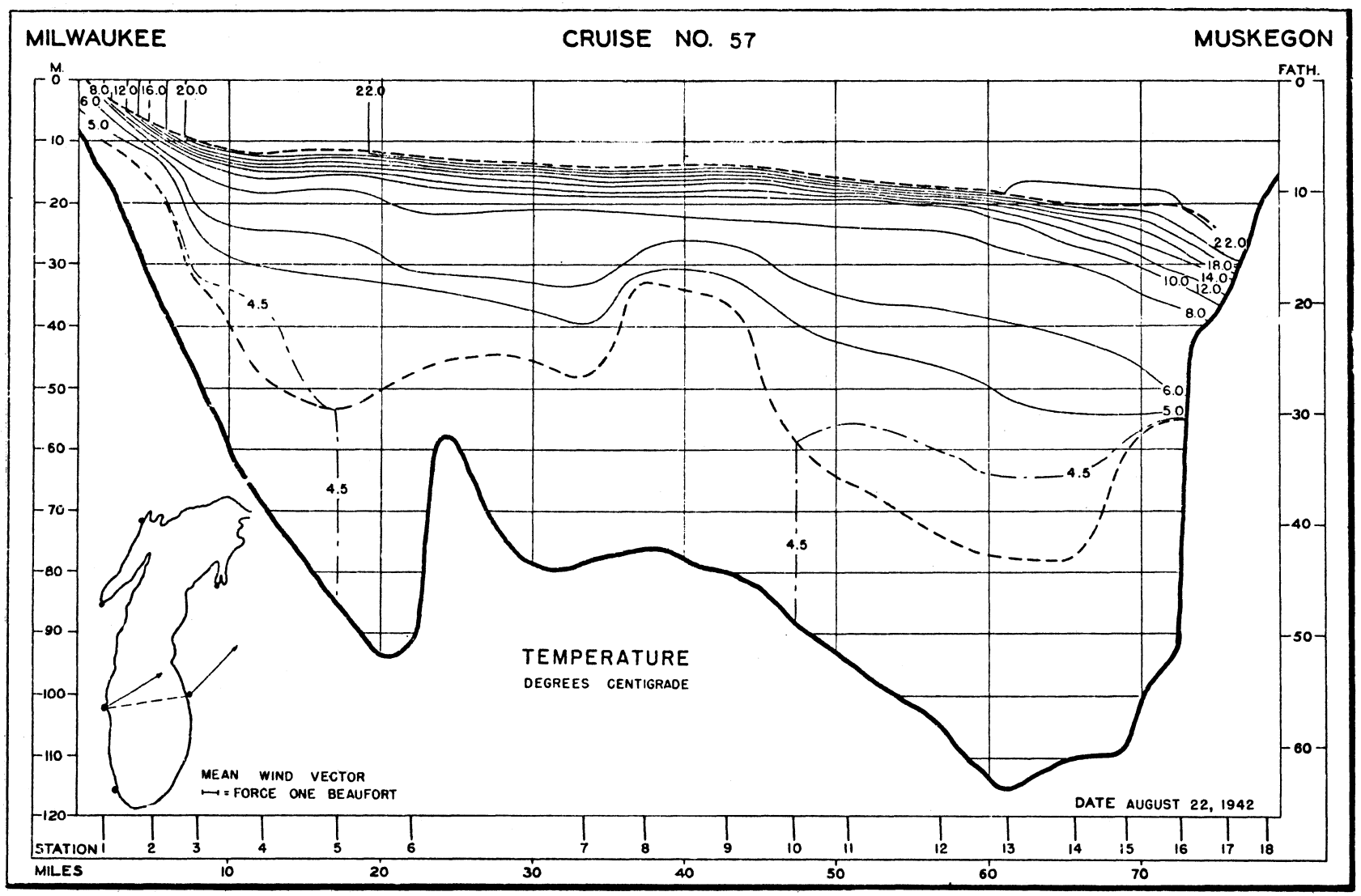

Fig. 28. Lake Michigan, 22 August 1942. Distribution of temperature, °C, observed from a ferry, Milwaukee-Muskegon transection (Church 1945).

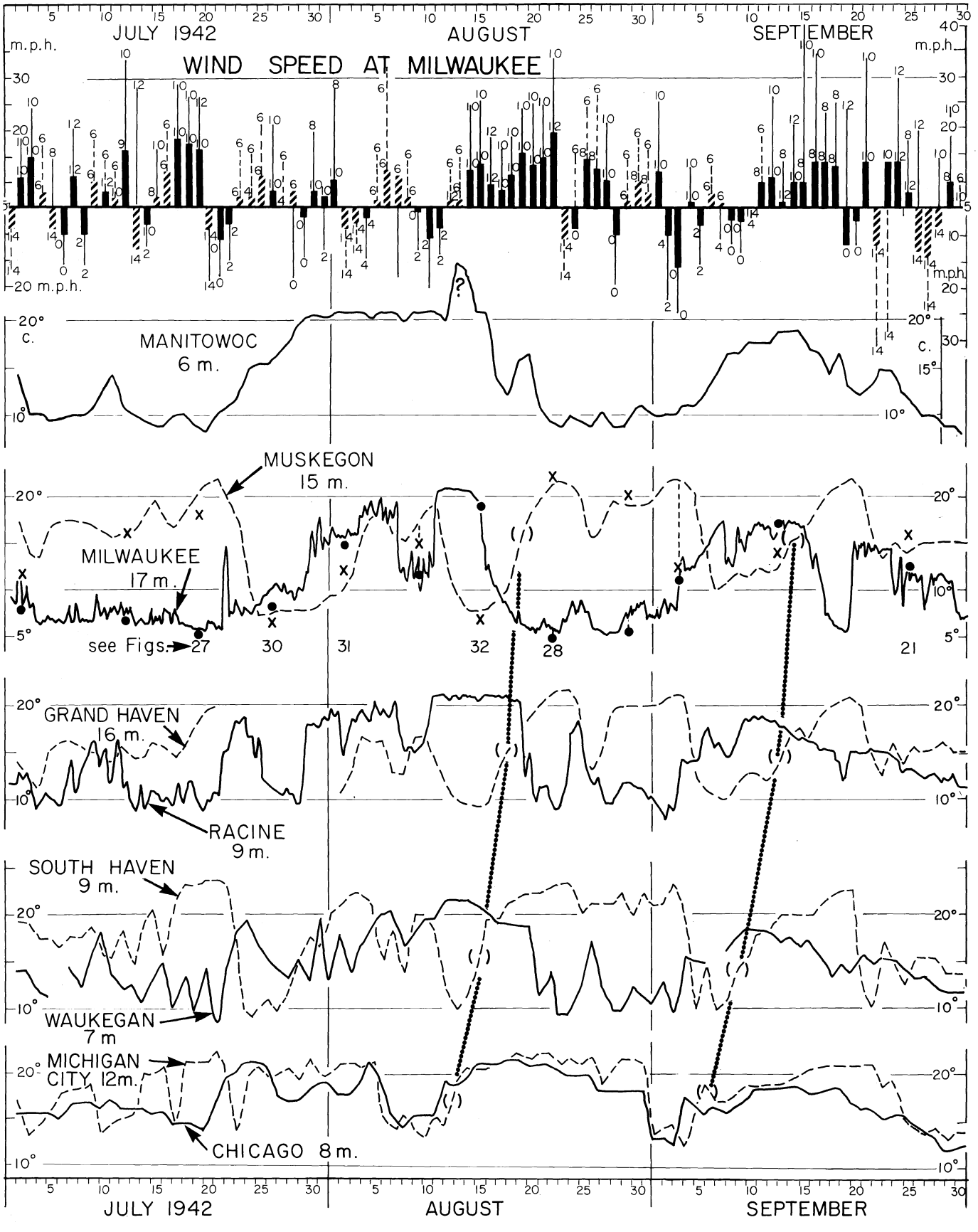

Fig. 29. Lake Michigan 1942. Temperatures at municipal water intakes, compared with wind speed and direction. Details overleaf.

Fig. 29 (overleaf). Lake Michigan, July - September 1942: temperatures, at municipal water intakes (positions shown in fig. 34, intake depths as indicated), °C, 6-hourly means at Milwaukee, 6-hourly readings at Racine, otherwise daily readings. Also illustrated are daily means (and "fastest mile") of wind speed and direction at Milwaukee. Directions are indicated by number code, 0 to 15 quarter quadrants, starting with 0 at N. Winds from the prevalent quadrant, S-W, are shown as black bars above the line. Further explanation is given on p. 9 of the text.

Also inserted, as dots and crosses, are the temperatures at those points on the Church (1945) transections, nearest to the Milwaukee and Muskegon intakes, respectively. The figure numbers are given for those transections reproduced in this report. The two heavy, dotted lines are referred to on p. 50 of the text. (Re-drawn from Mortimer 1963.)

Legends for later figures

Fig. 33. Lake Michigan, July - September 1955: temperatures, °C, at municipal water intakes (positions shown in fig. 34, depths as indicated), 6-hourly means at Milwaukee, 6-hourly readings at Racine, otherwise daily readings. Also illustrated are daily means (and "fastest mile") of wind speed and direction at Milwaukee, as explained in the legend to fig. 29 and on p. 9 of the text. Vertical arrows indicate the date, 9 August, of the fig. 34-36 cruises. The heavy, dotted line is referred to on p. 50 of the text. (Re-drawn from Mortimer 1963).

Fig. 43. Lake Ontario, July - September 1950 and 1951: hourly temperature readings or hourly means, °C, at municipal water intakes, compared with wind speed (daily mean and fastest hourly reading) at Toronto, with direction indications, as explained on p. 13 of the text, by number code, 0 to 15 quarter quadrants starting with 0 at N. Winds from the prevalent quadrant SW to NW are shown as black bars above the line.

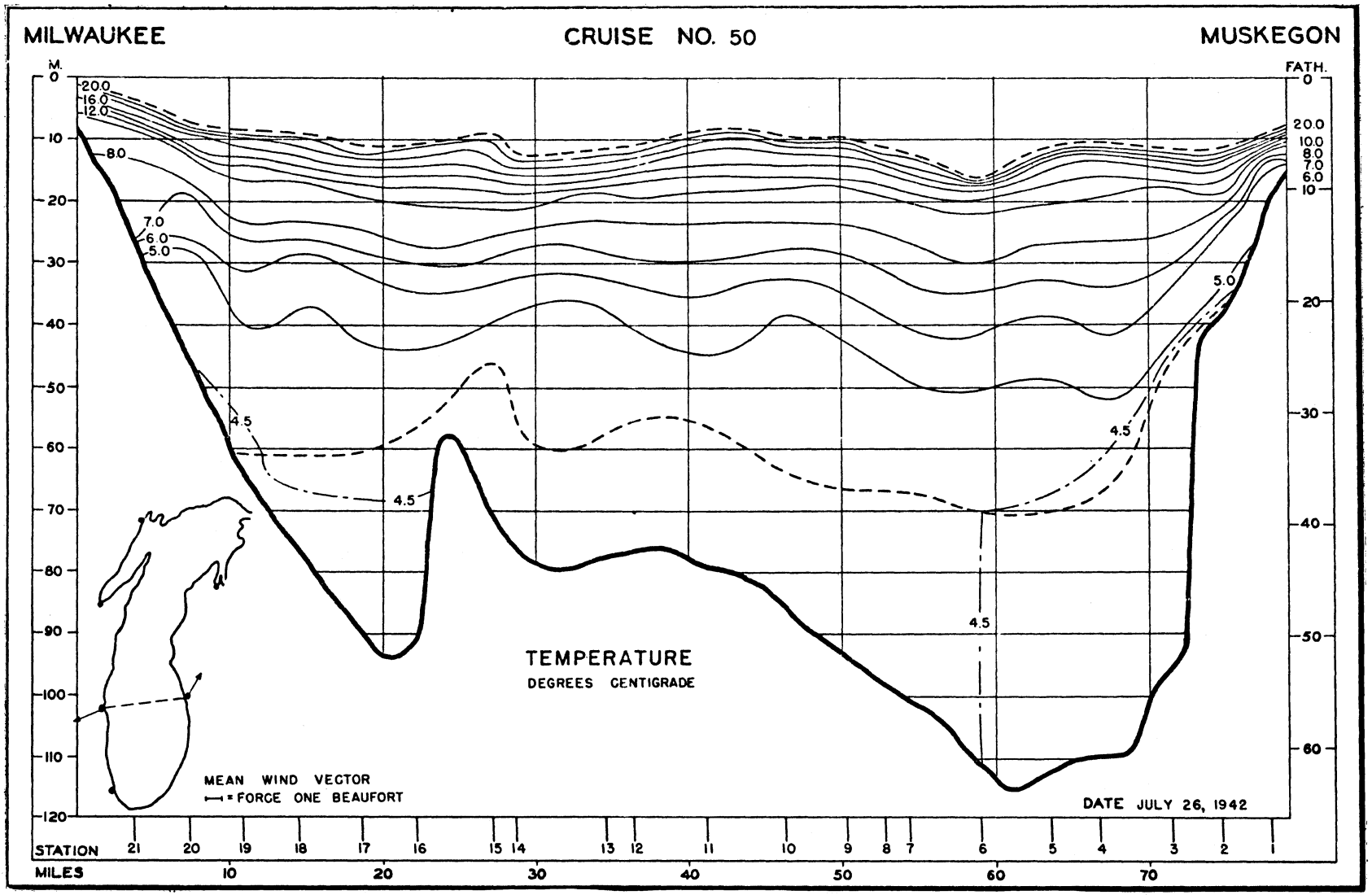

Fig. 30. Lake Michigan, 26 July 1942. Distribution of temperature, °C, observed from a ferry, Milwaukee-Muskegon transection (Church 1945).

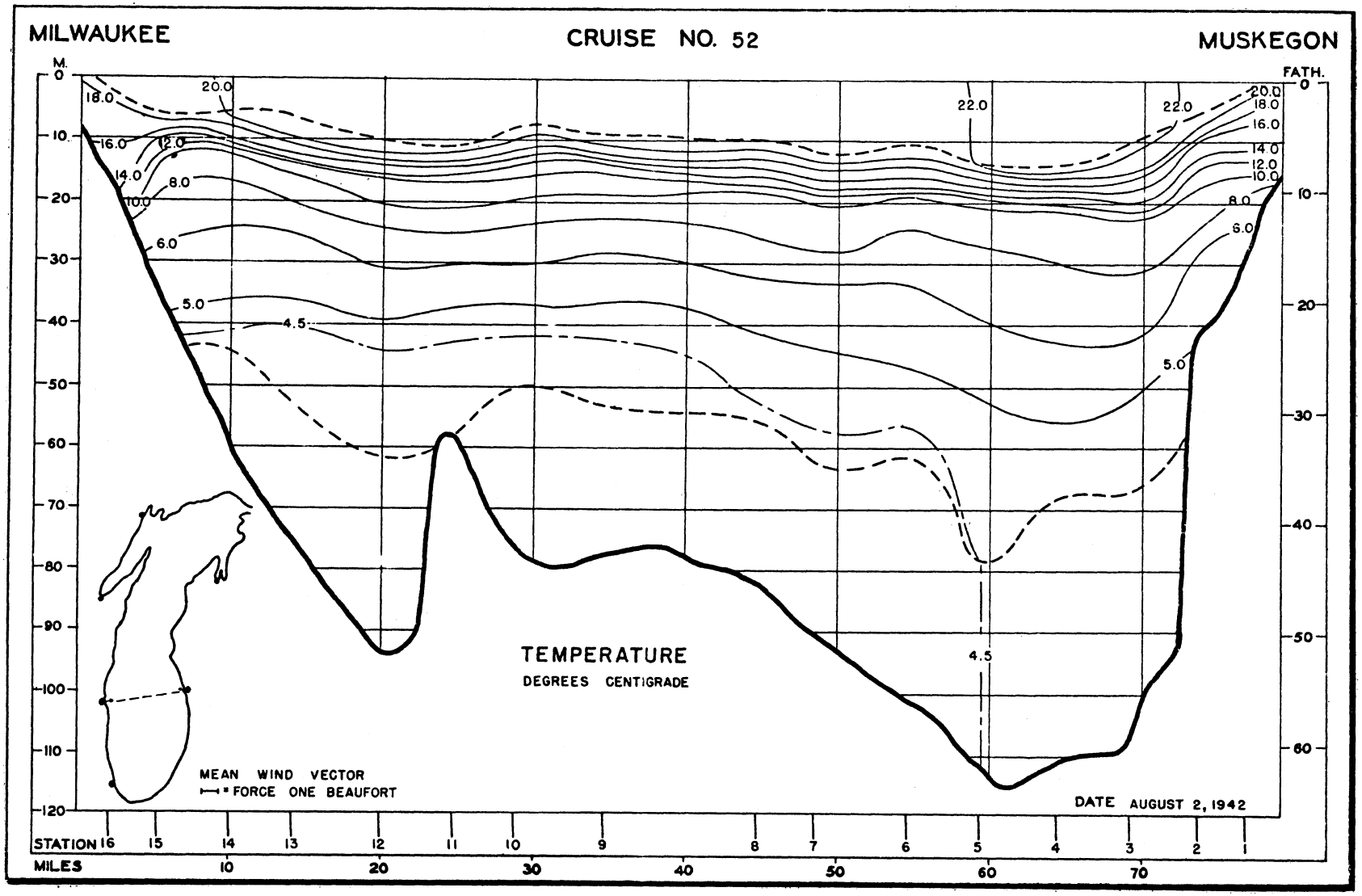

Fig. 31. Lake Michigan, 2 August 1942. Distribution of temperature, °C, observed from a ferry, Milwaukee-Muskegon transection (Church 1945).

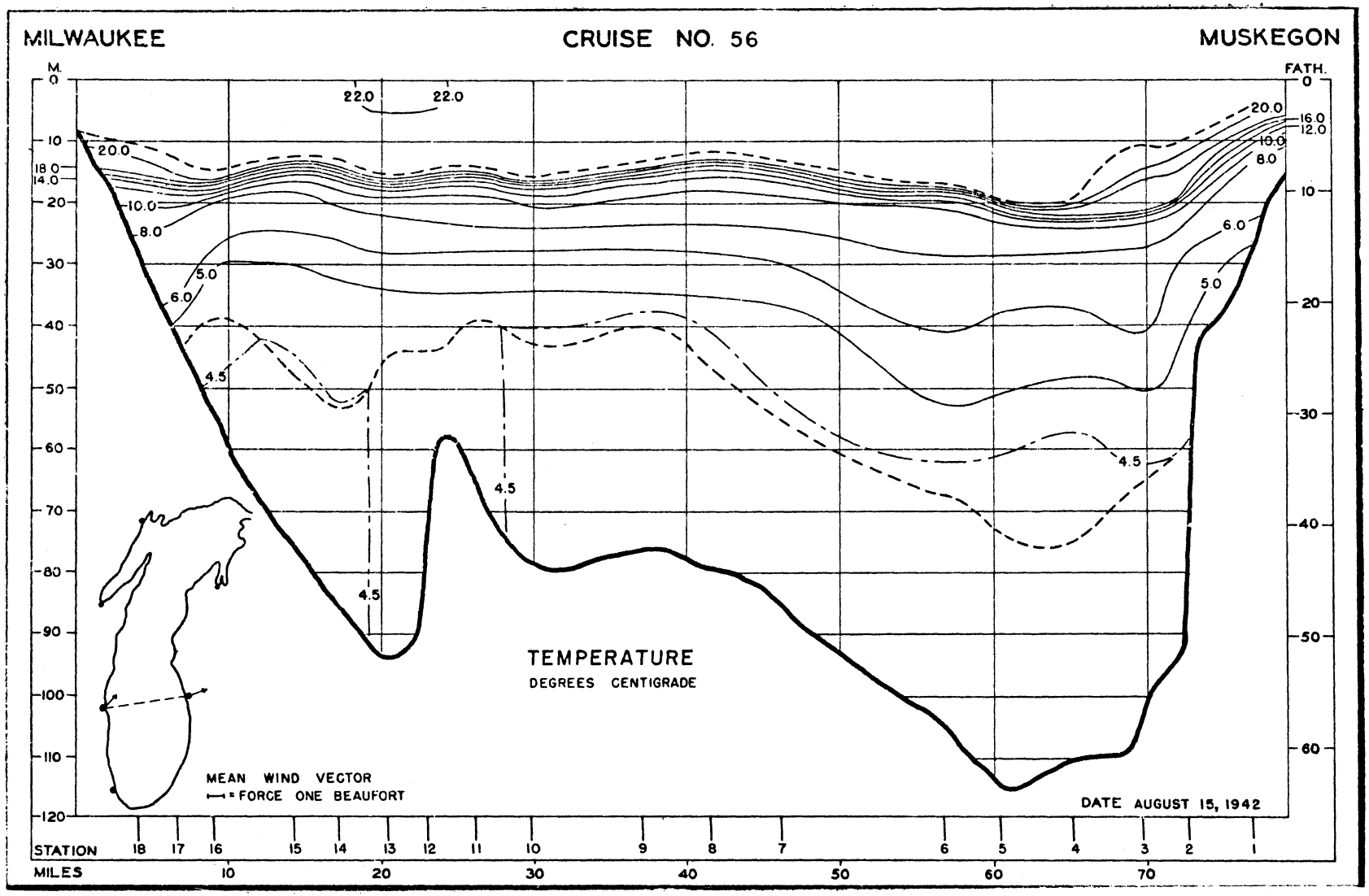

Fig. 32. Lake Michigan, 15 August 1942. Distribution of temperature, °C, observed from a ferry, Milwaukee-Muskegon transection (Church 1945).

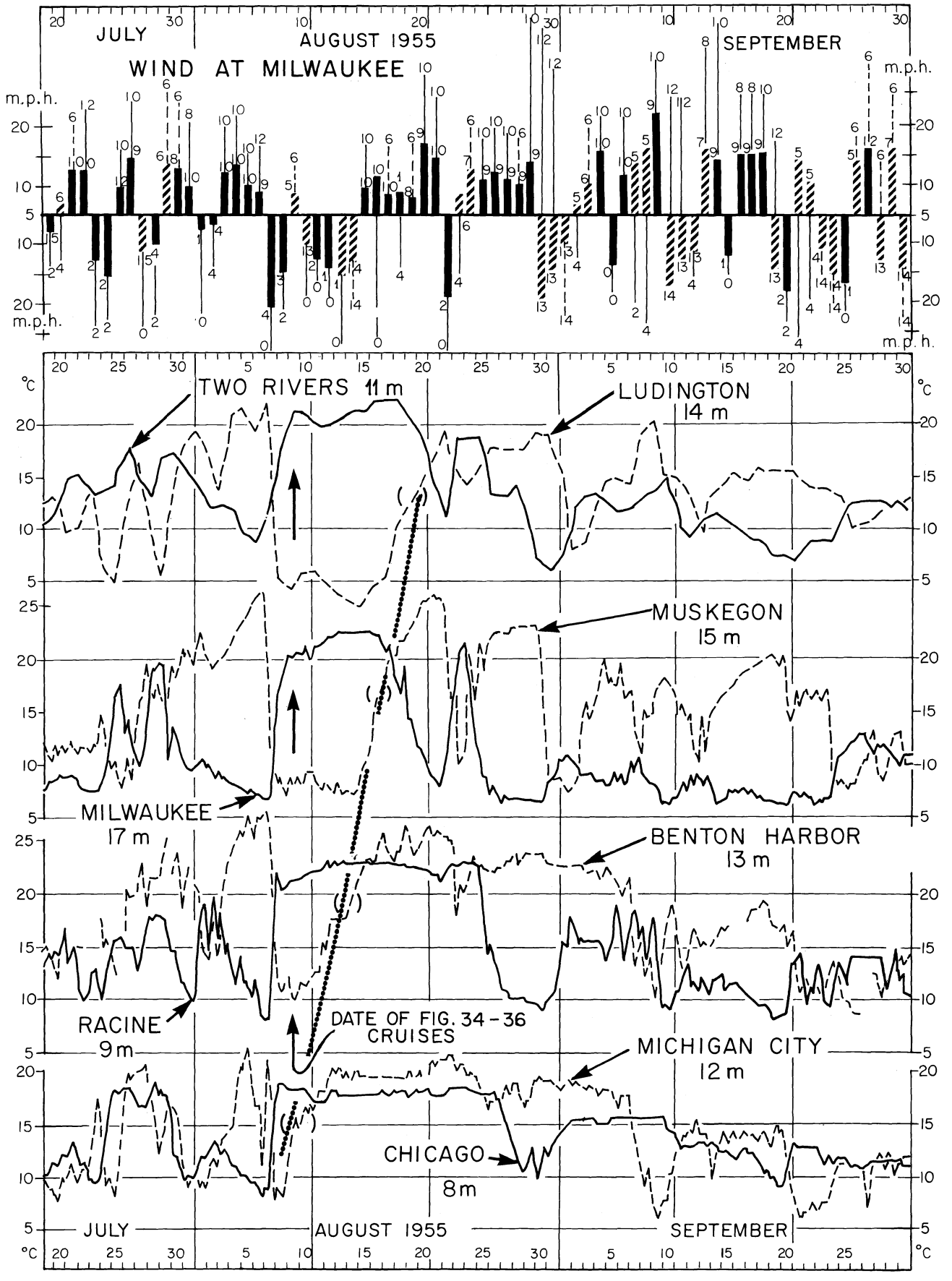

Fig. 33. Lake Michigan 1955. Temperatures at municipal water intakes, compared with wind speed and direction. Full legend and further details on page opposite fig. 30.

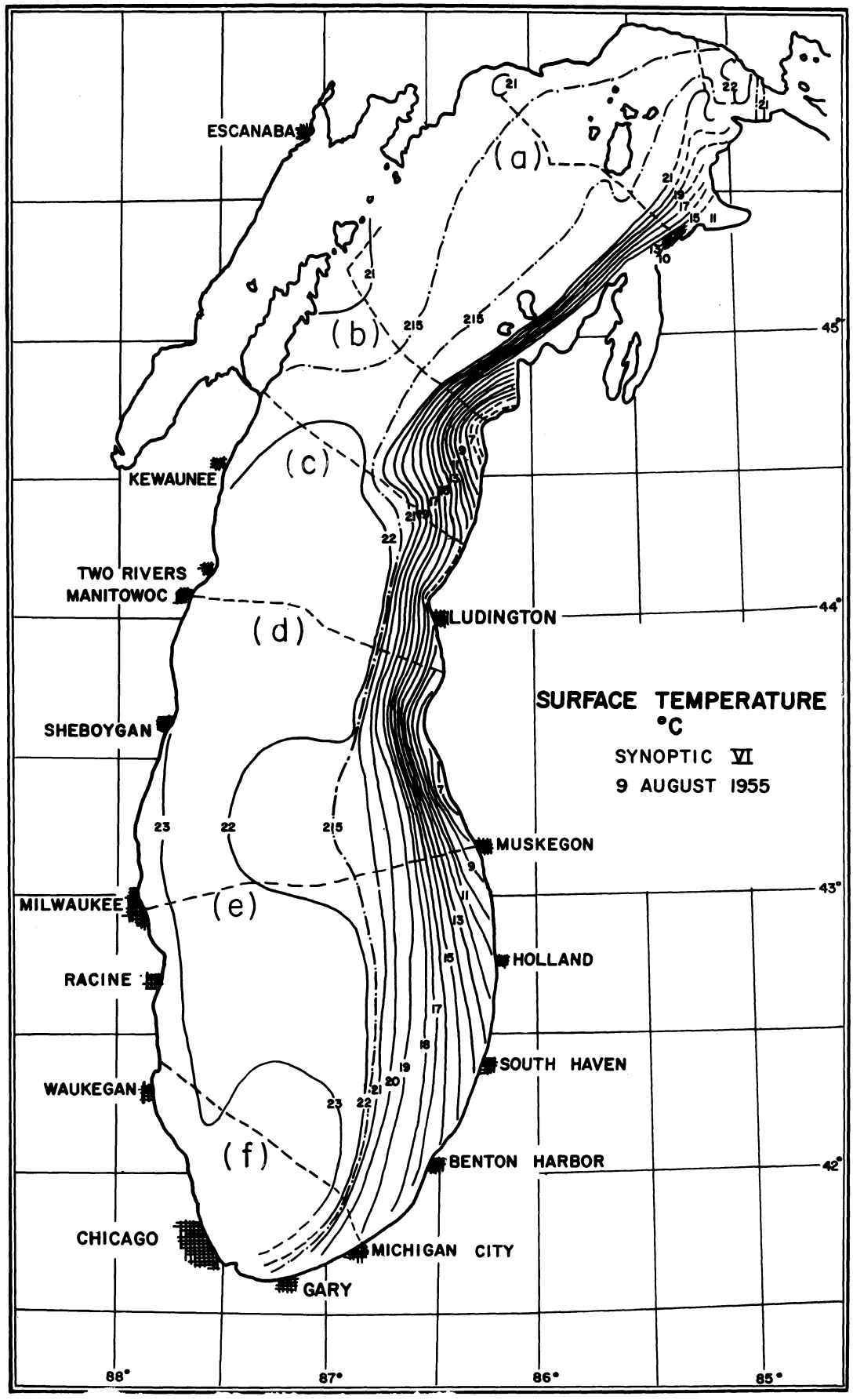

Fig. 34. Lake Michigan, 9 August 1955. Distribution of surface temperature, °C, derived from transections (a) to (f) illustrated in figs. 35 and 36 (Ayers et al. 1958). The corresponding temperatures at coastal water intakes are indicated by vertical arrows in fig. 33.

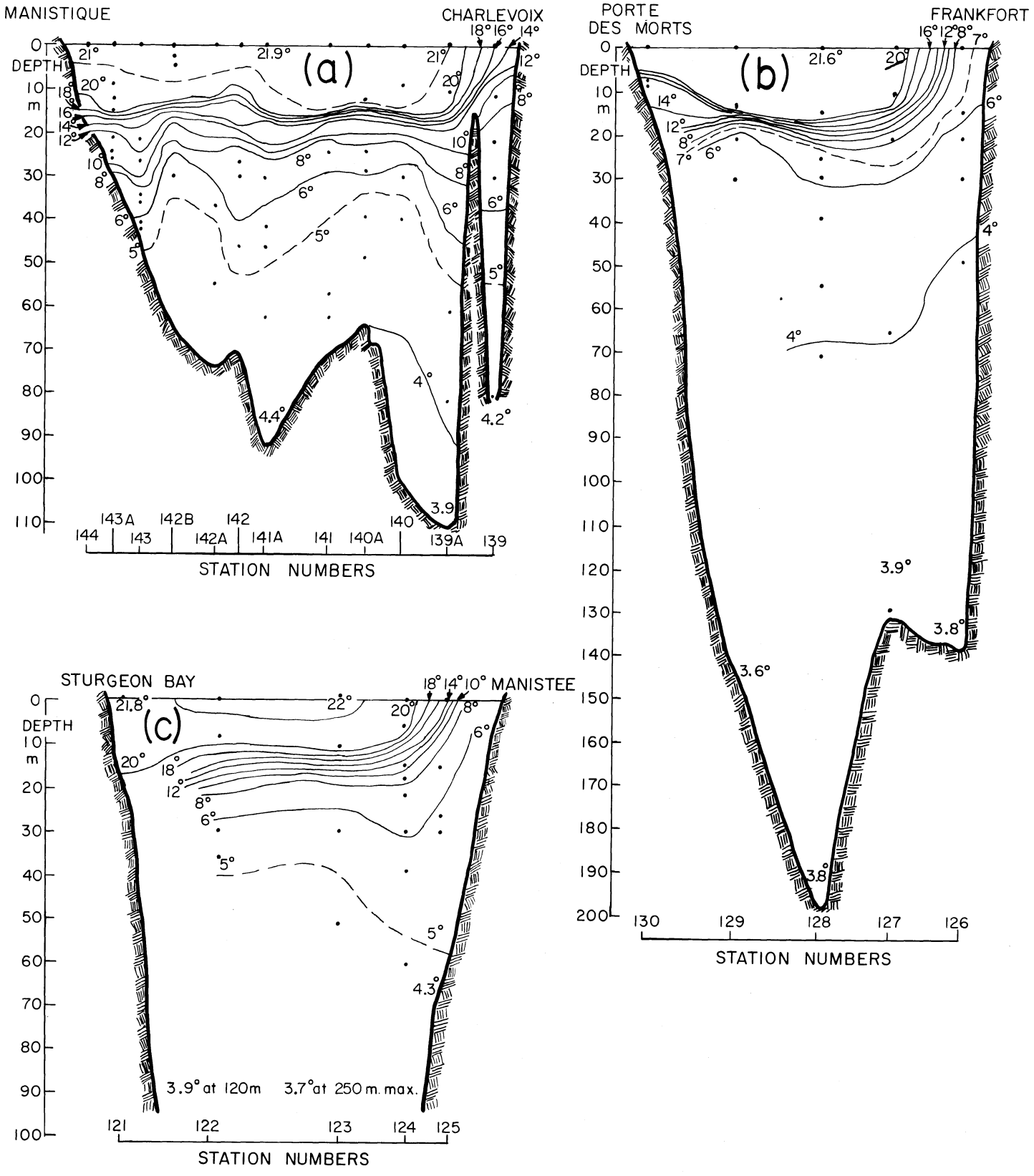

Fig. 35. Lake Michigan, 9 August 1955. Distribution of temperature, °C, observed from moving vessels, in transections (a), (b), and (c), shown in fig. 34 (re-drawn from data in Ayers et al.1958).

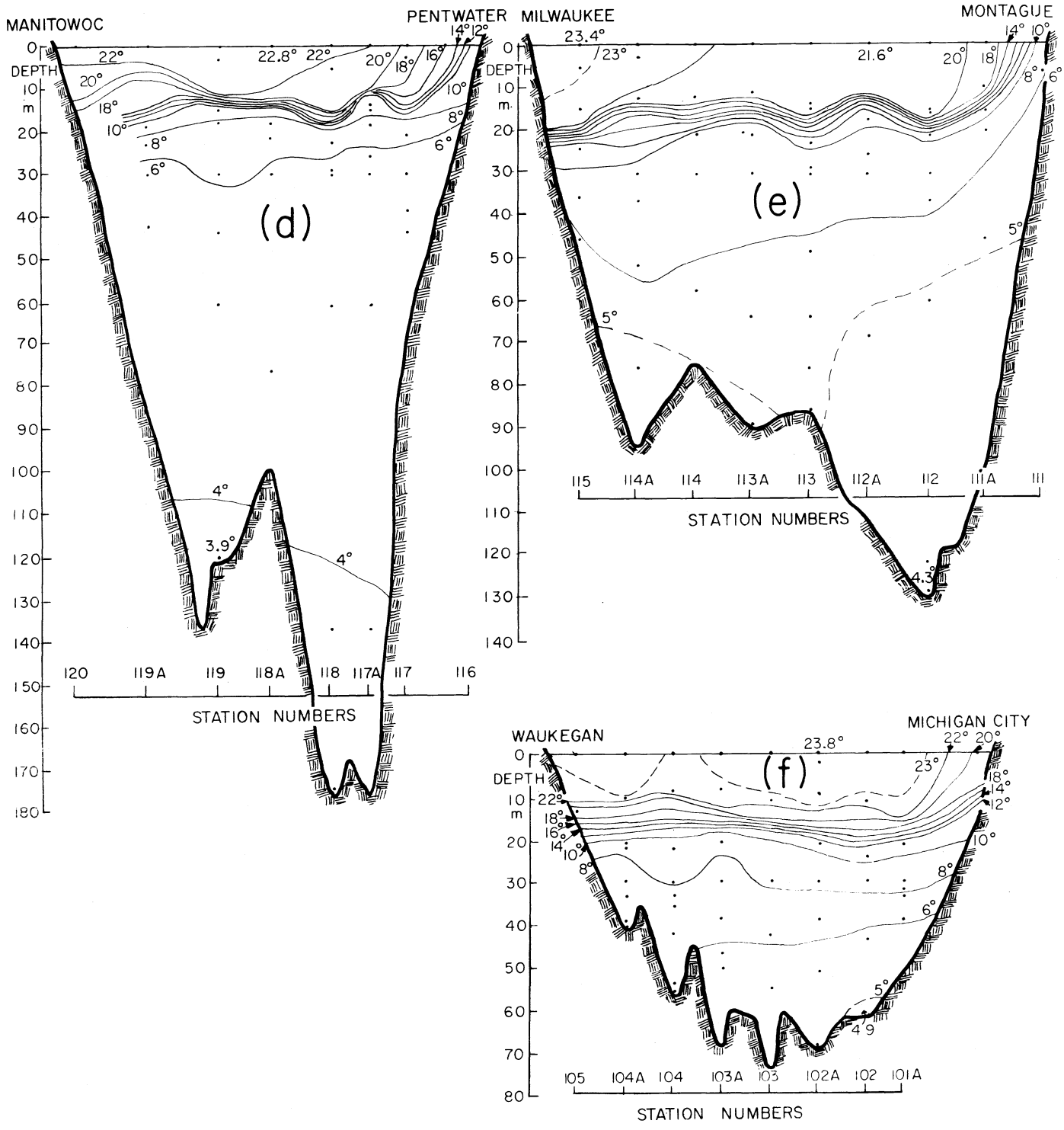

Fig. 36. Lake Michigan, 9 August 1955. Distribution of temperature, °C, observed from moving vessels, in transections (d), (e), and (f), shown in fig. 34 (re-drawn from data in Ayers, et al. 1958).

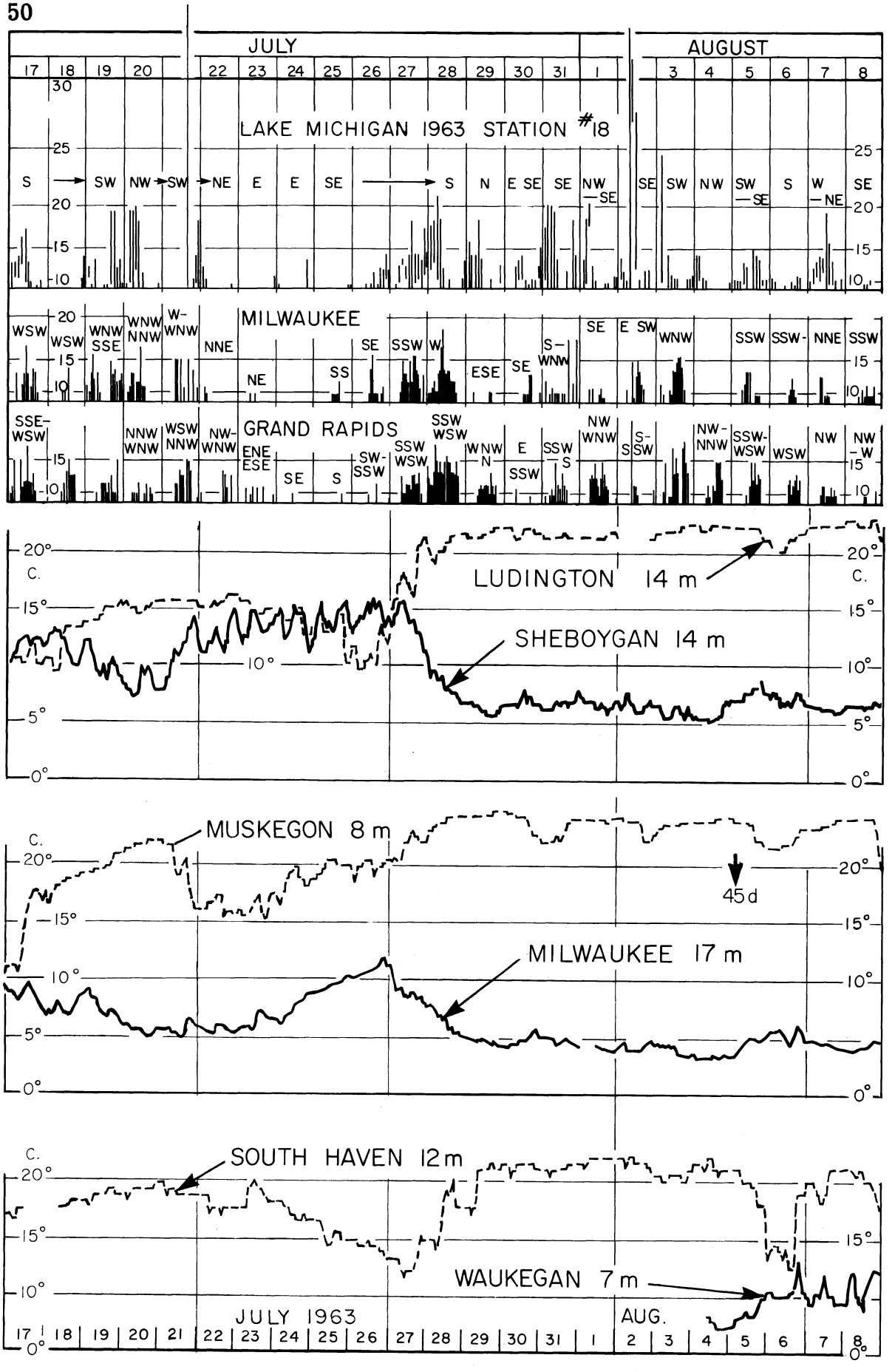

Fig. 37. Lake Michigan, July - August 1963; hourly or hourly mean temperatures, °C, at six municipal water intakes (positions shown in fig. 34) compared with hourly wind speed at land stations (Milwaukee and

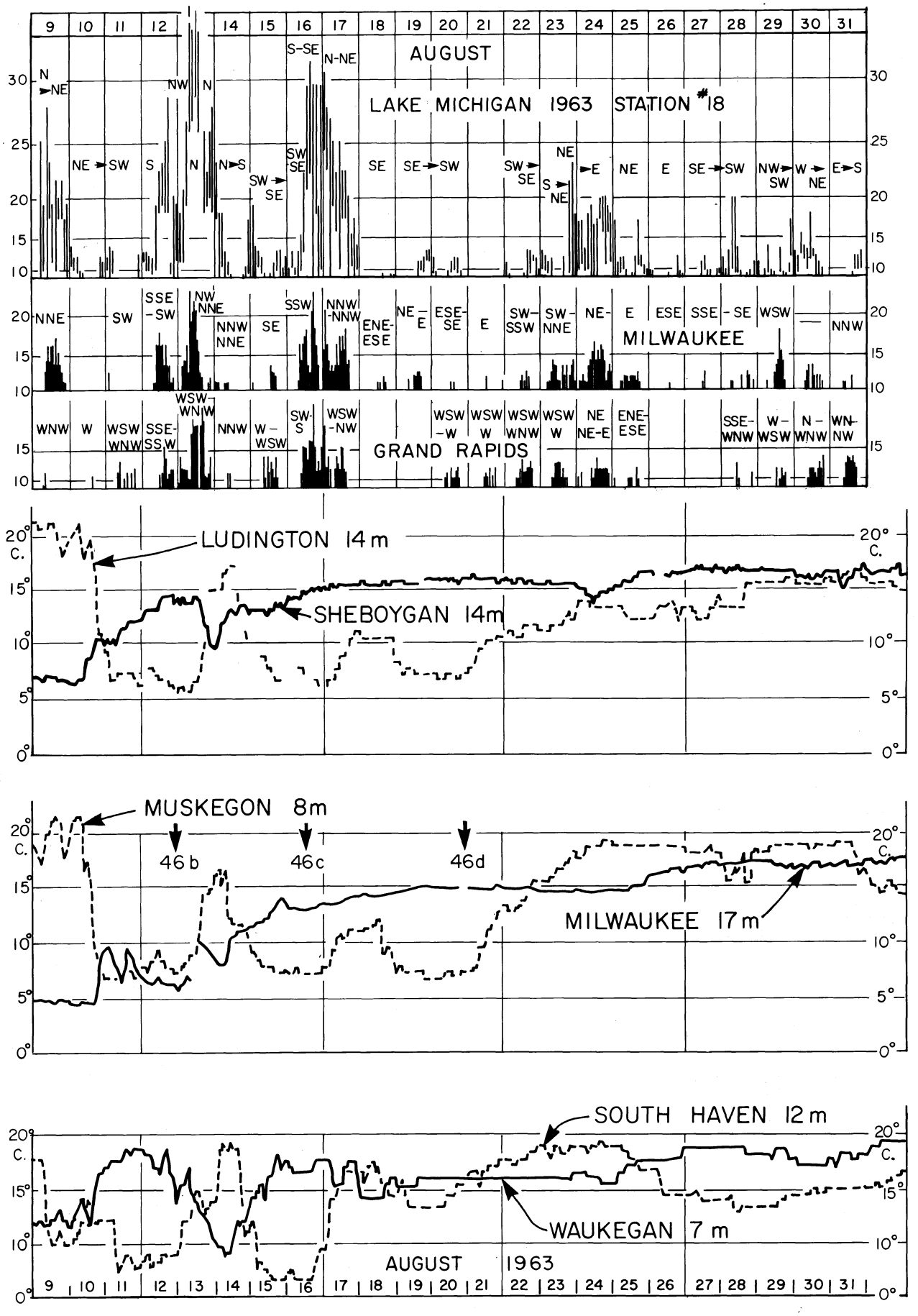

Fig. 37, continued:
Grand Rapids), and at a lake buoy station (station 18, fig. 65), for which 2-hourly ranges of wind speed are shown. General wind directions are also indicated.

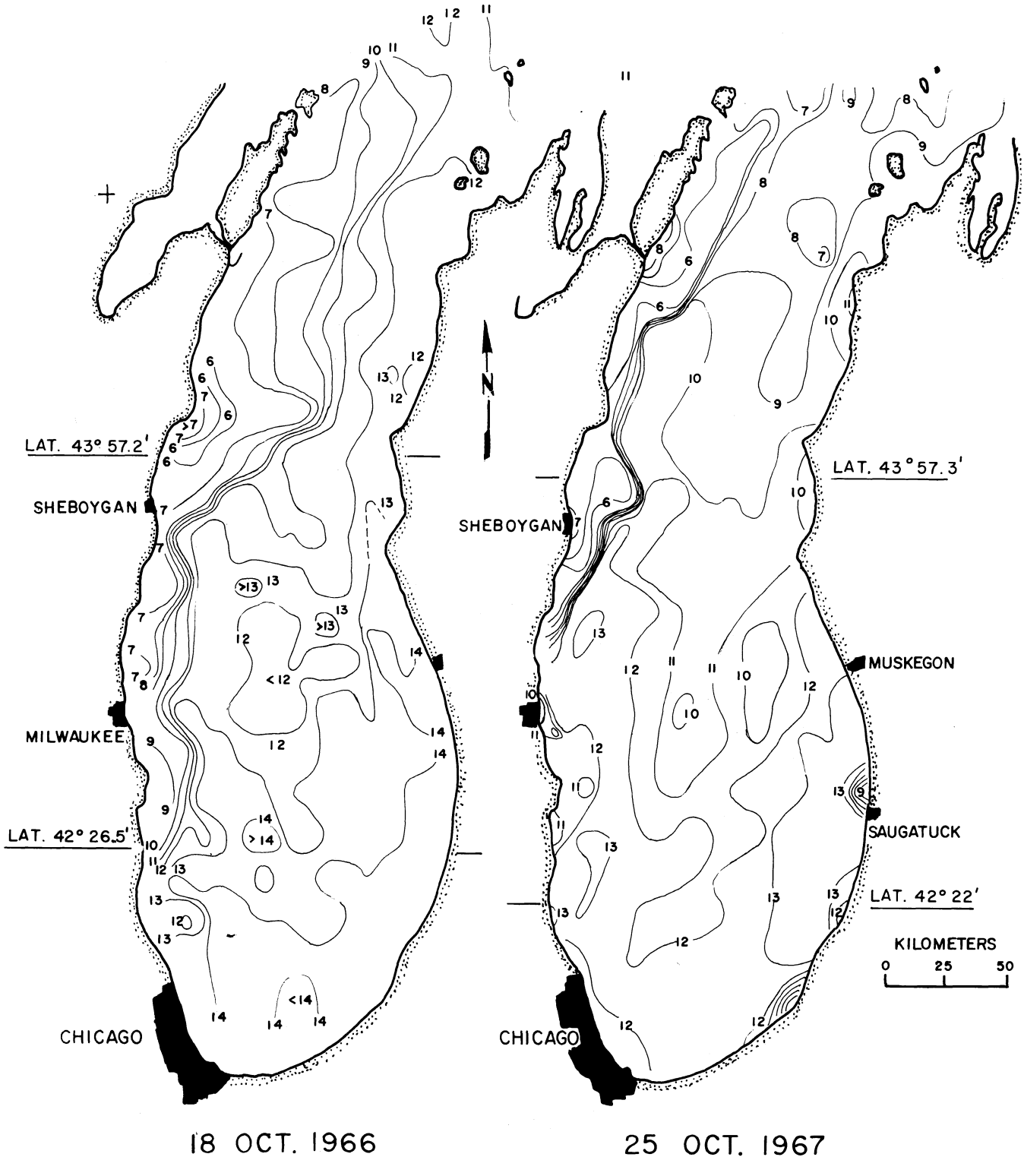

Fig. 38. Lake Michigan: Distribution of surface temperature (°C, 1 min averaged output of an infrared airborne radiation thermometer) on 18 October 1966 and 25 October 1967 (re-drawn from Noble and Wilkerson 1970).

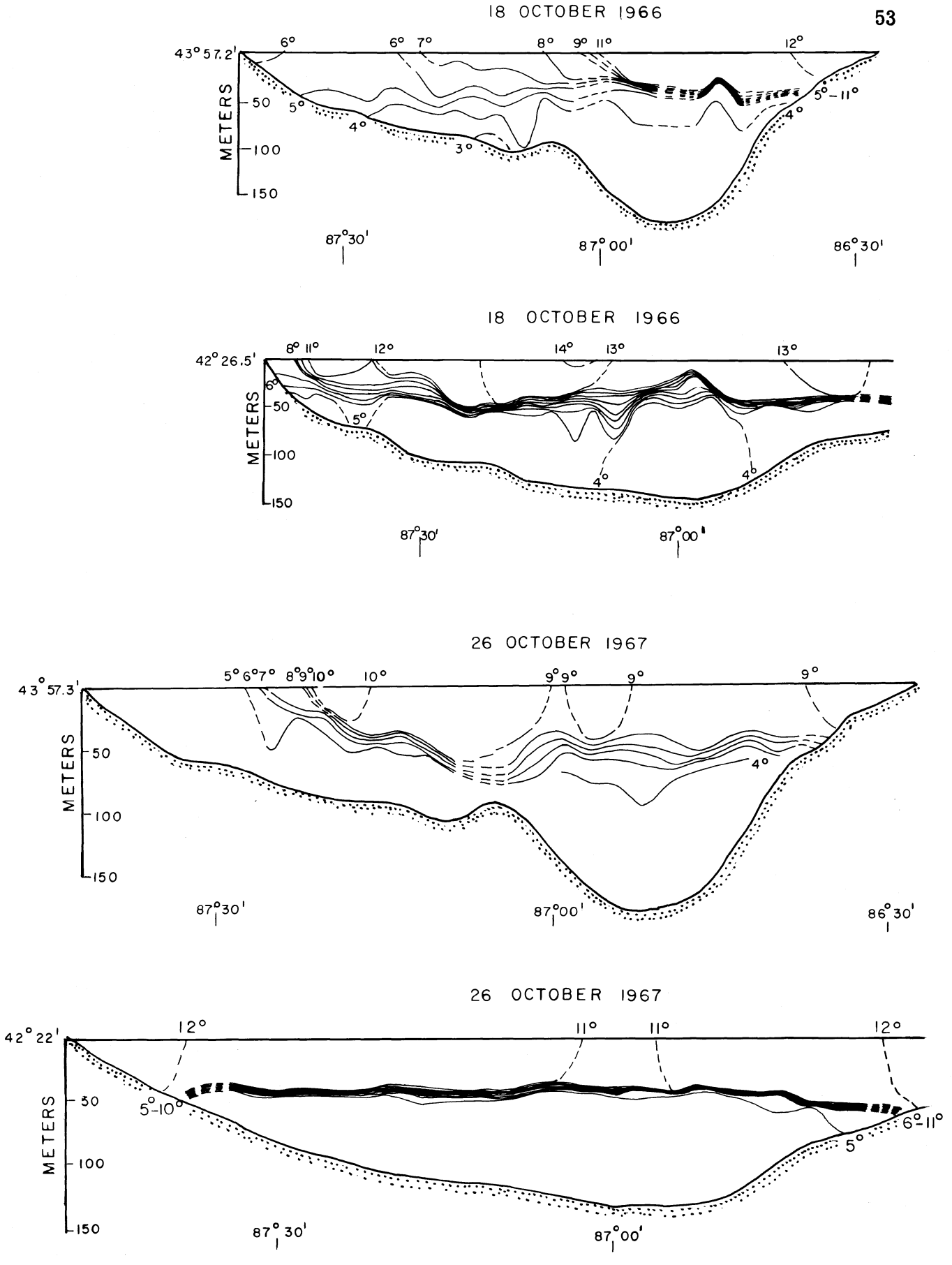

Fig. 39. Lake Michigan: Distribution of temperature, °C, observed from moving vessels, in the latitudinal transections indicated in fig. 38, 18 October 1966 and 26 October 1967 (re-drawn from Noble and Wilkerson 1970).

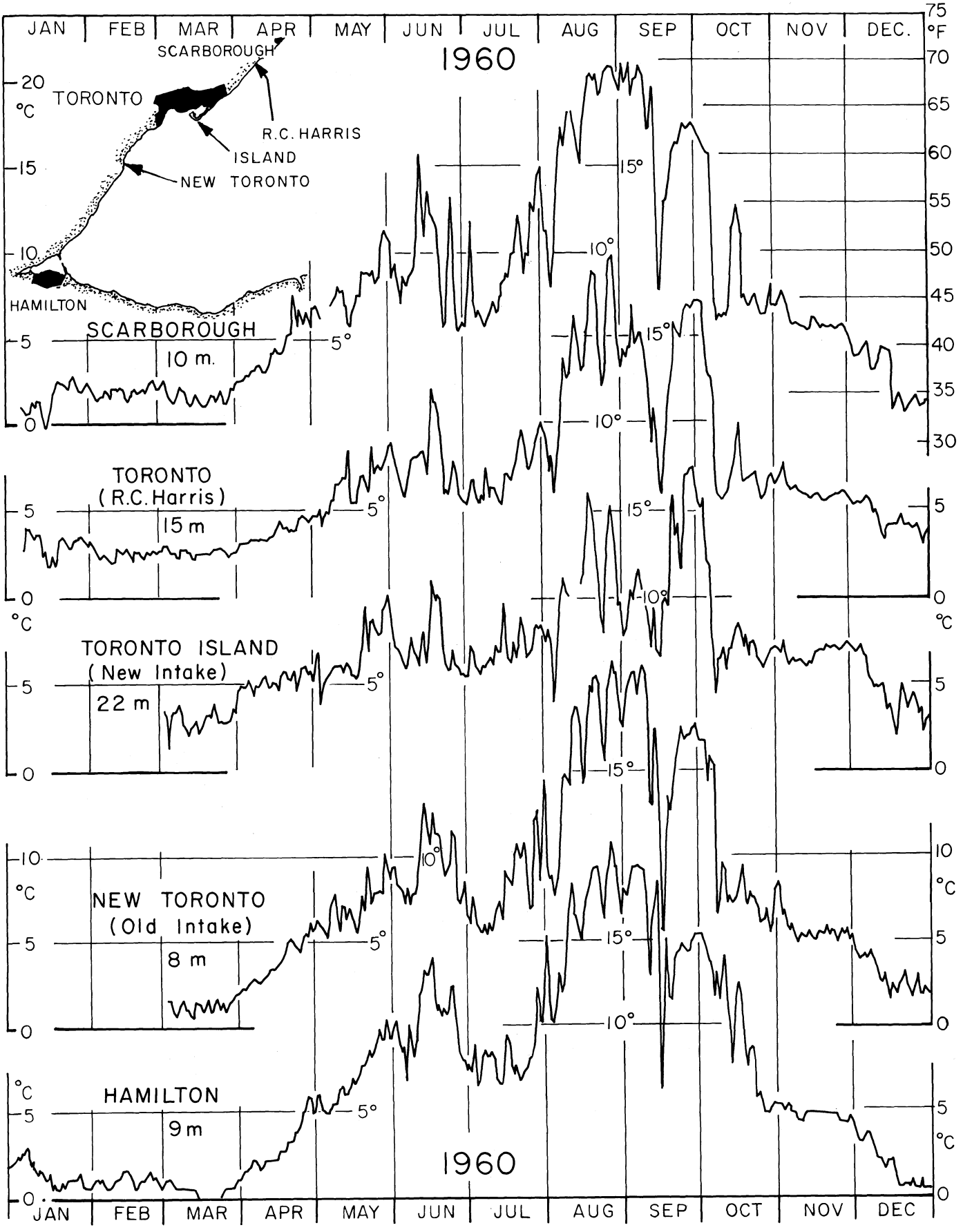

Fig. 40. Lake Ontario 1960: Daily temperature readings at municipal water intakes at the western end of the basin.

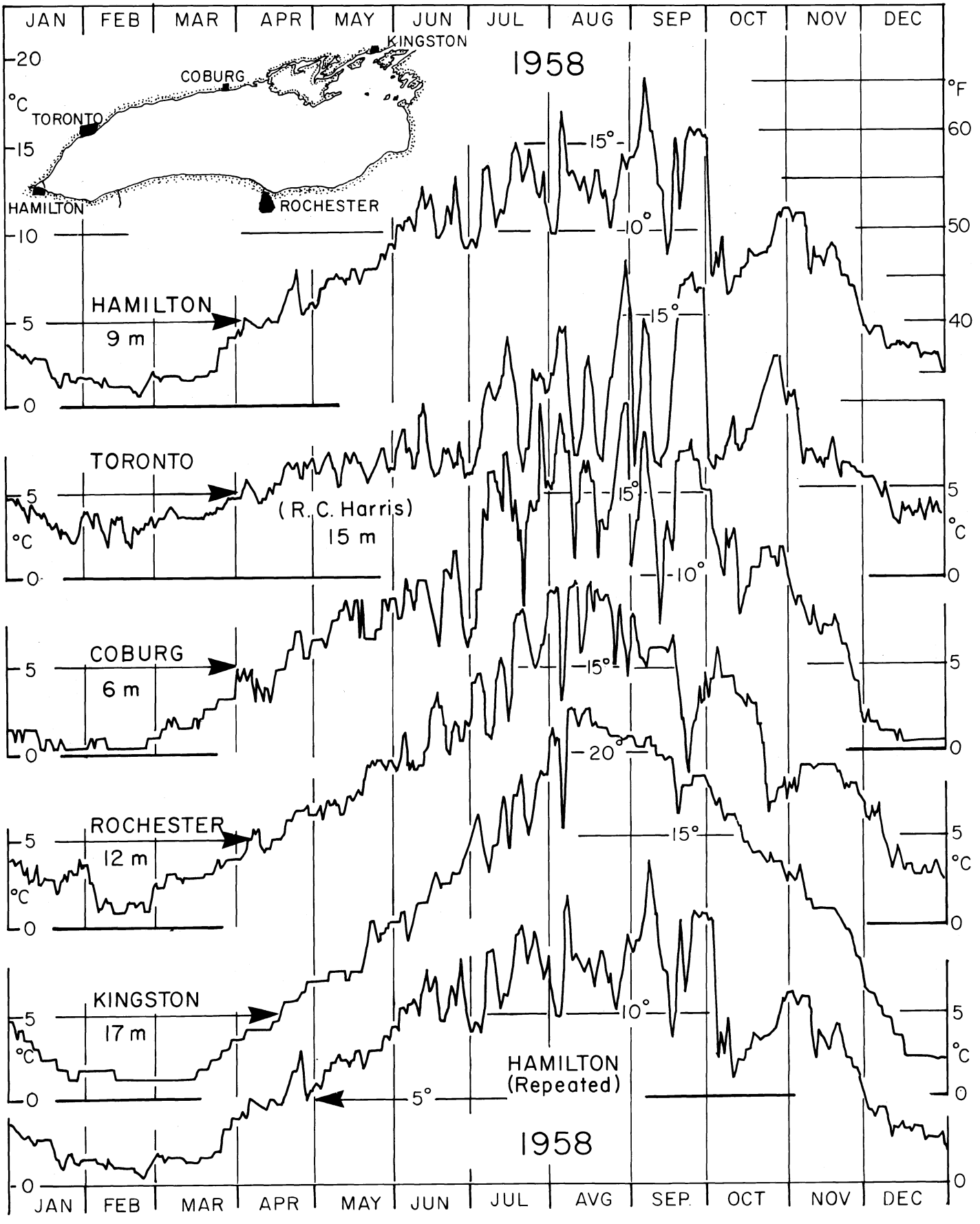

Fig. 41. Lake Ontario 1958: Daily temperature readings at municipal water intakes distributed around the basin.

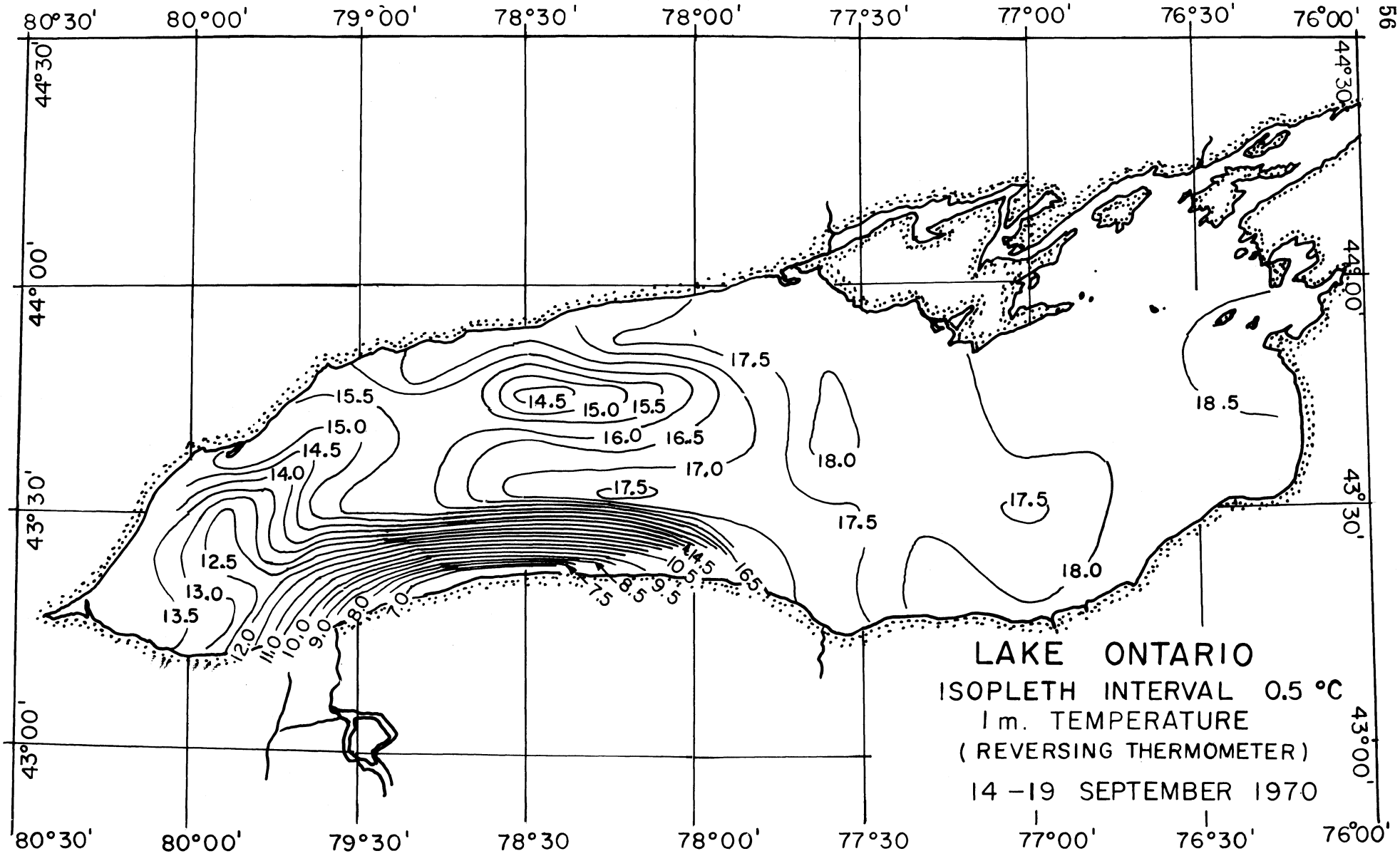

Fig. 42. Lake Ontario, 14-19 September 1970: distribution of temperature, °C, at 1 m depth (from Preliminary Charts of Surface Distribution, prepared and distributed by the Canada Centre for Inland Waters, Burlington, Ontario).

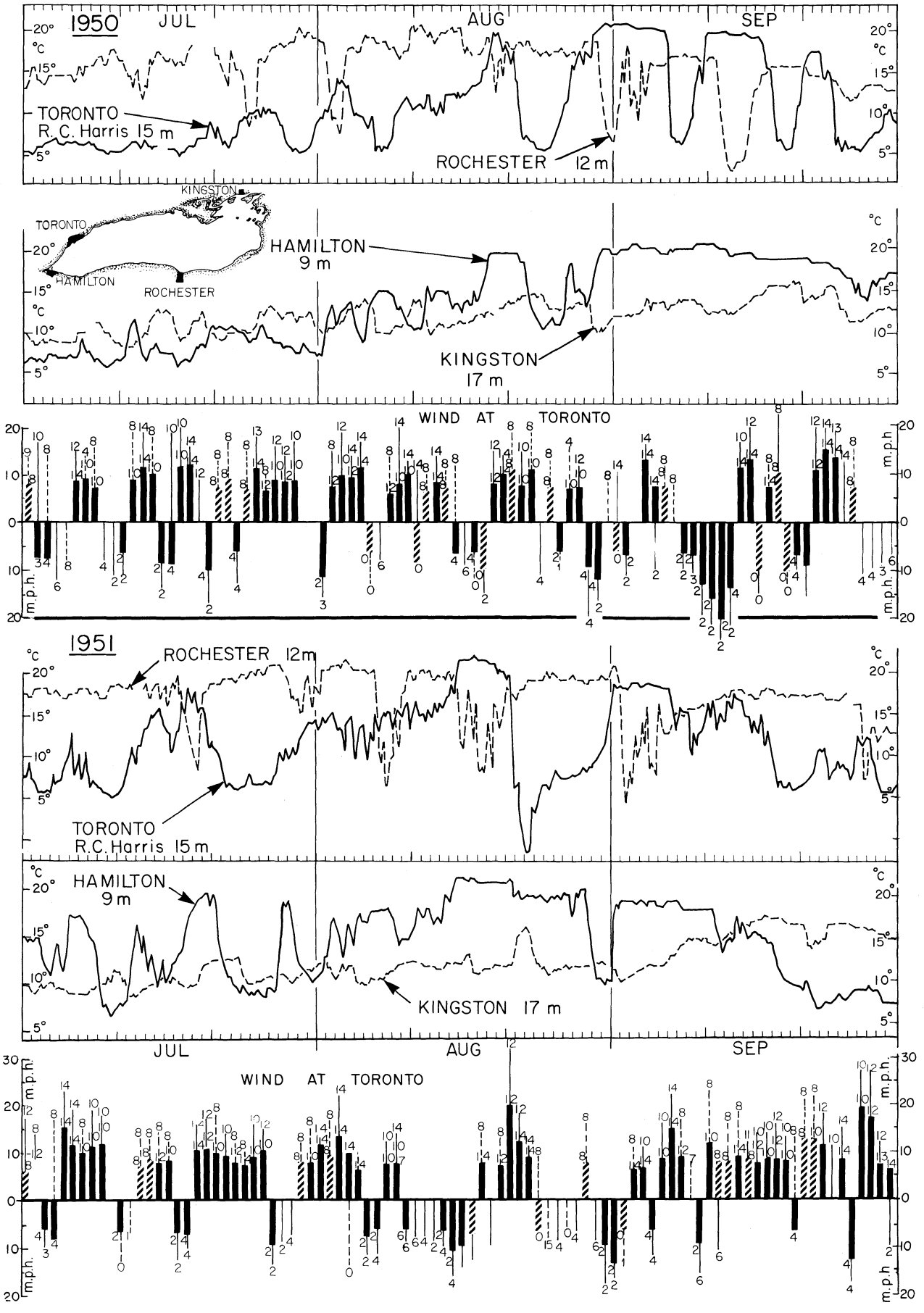

Fig. 43. Lake Ontario 1950, 1951. Temperatures at municipal water intakes compared with wind speed and direction at Toronto. For details see page opposite fig. 30.

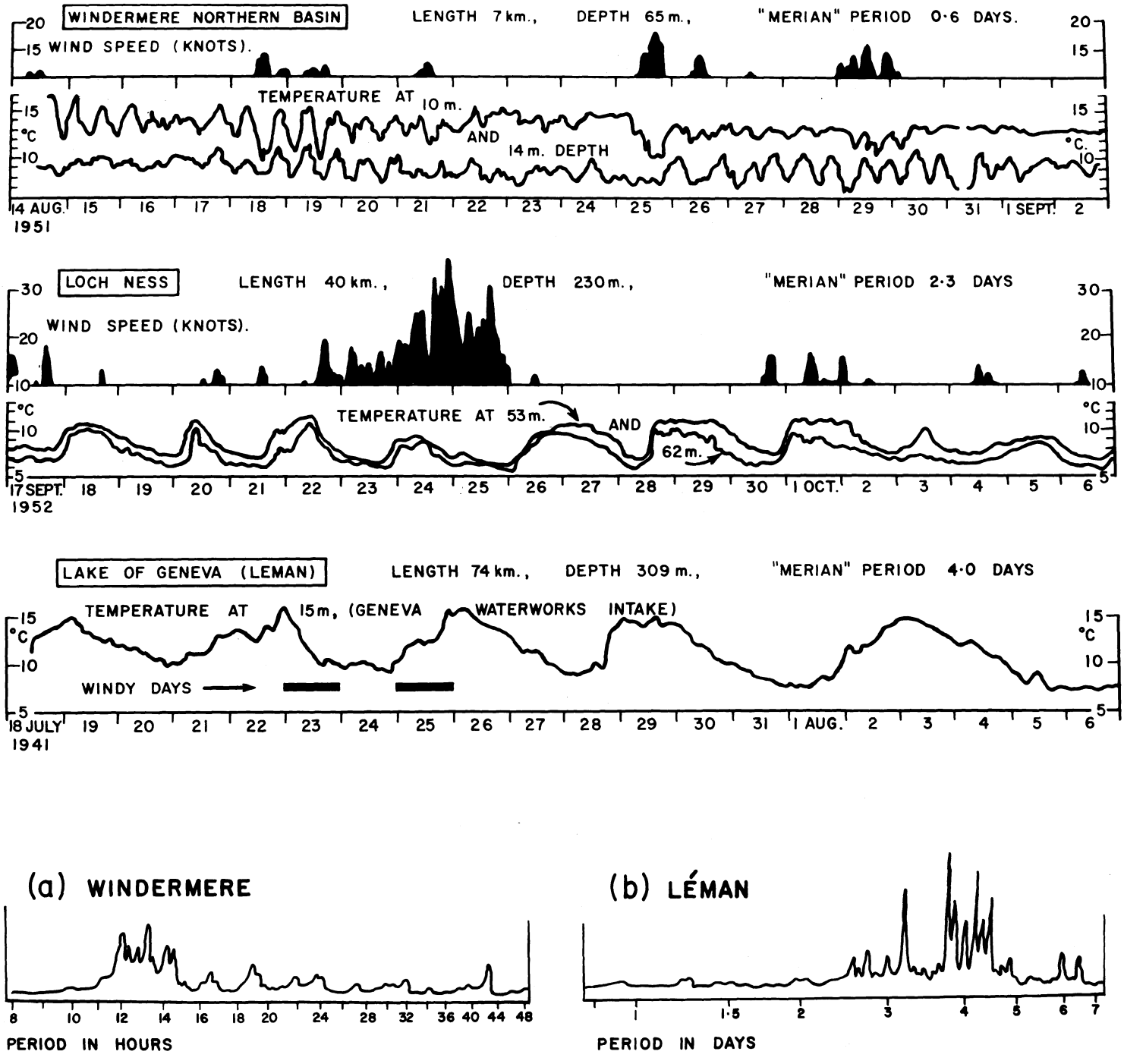

Fig. 44. Oscillations in temperature, °C, at fixed depths in three lake basins varying in length from 7 to 74 km. Also indicated are hourly mean wind speeds (black areas) and the("Merian") period of a uninodal internal seiche in a two-layer rectangular model fitted to basin dimensions and to the density distribution at the time. The upper part of the figure is from Mortimer (1954) . The lower portions (from Mortimer 1953) are frequency spectra derived from (a) a Windermere, northern basin, temperature record at 14 m depth, 14 August - 18 October 1951, and (b) a Lac Lèman temperature record from the Geneva municipal water intake, 15 m depth, 14 July - 21 August for the years 1941-44.

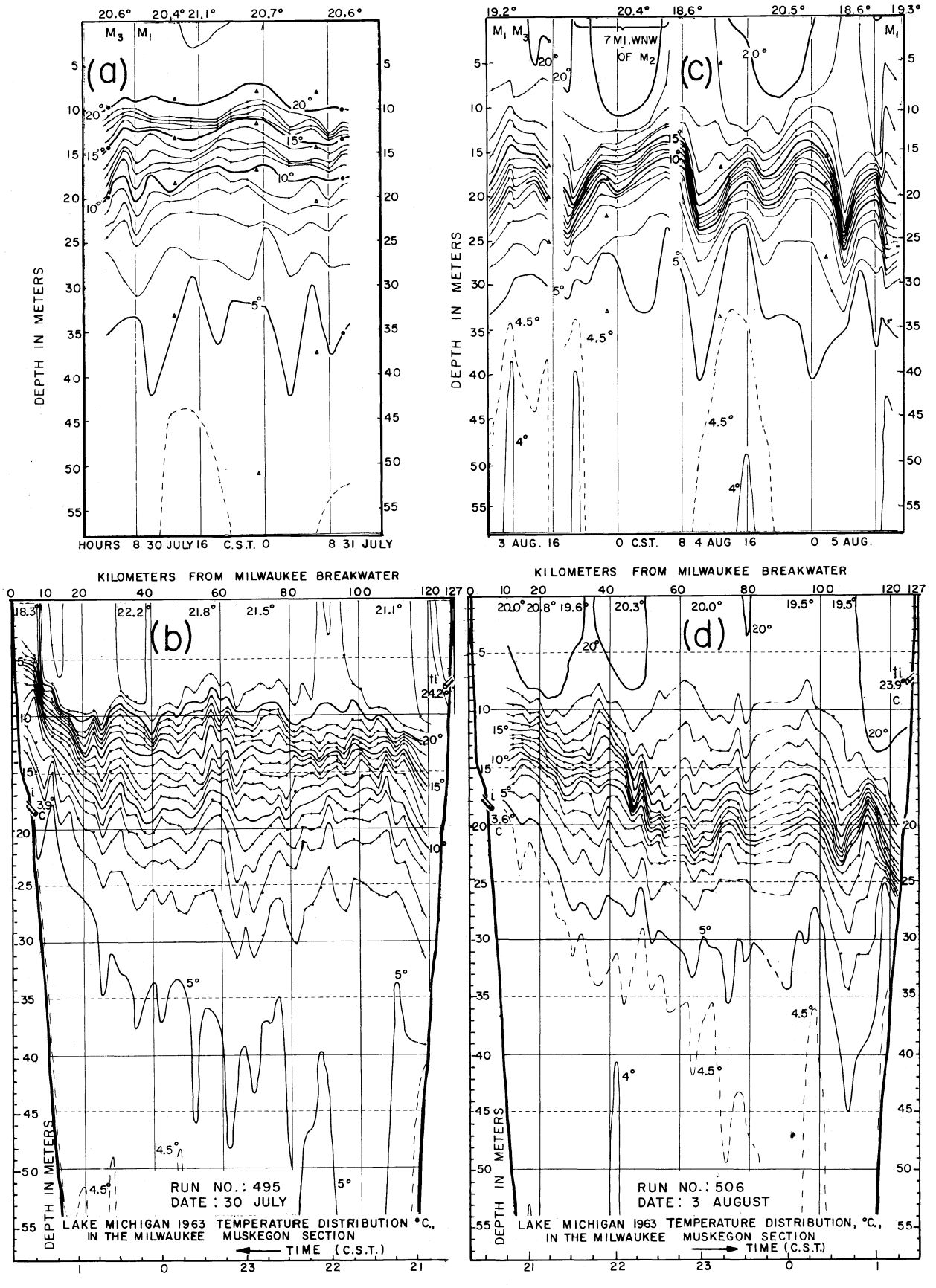

Fig. 45. Lake Michigan 1963: (a) and (c), changes in the depth distribution of temperature, °C, observed from a vessel anchor at station M_2, 30-31 July and 3-5 August; (b) and (d), distribution of temperature, °C, observed from a ferry, Milwaukee-Muskegon transection on 30 July and 3 August. Positions of M_2 and the transection are shown in fig. 65 (from Mortimer 1968).

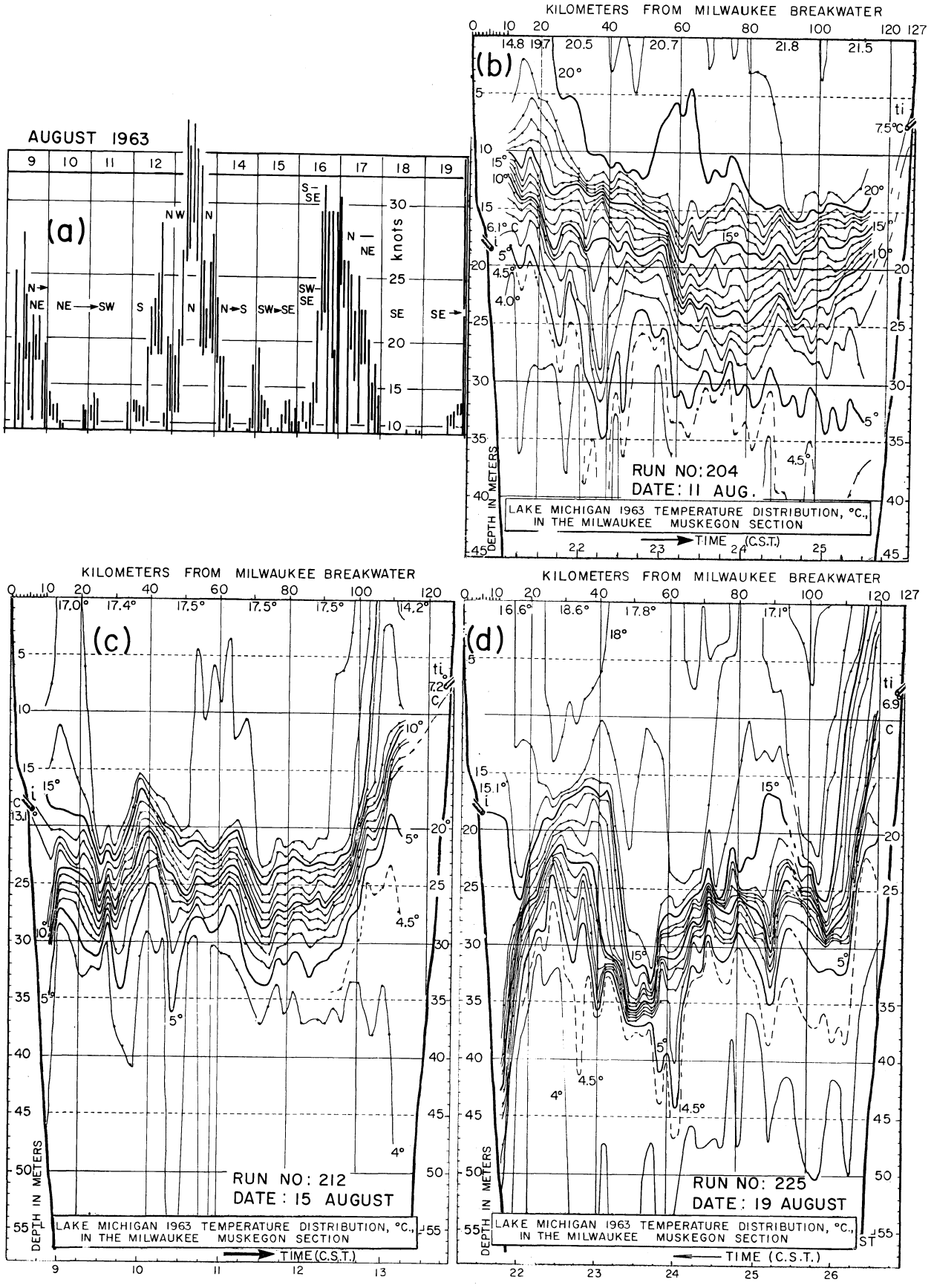

Fig. 46. Lake Michigan 1963: (a) 2-hourly ranges of wind speed at buoy station 18 (position in fig. 65); (b), (c), and (d) distribution of temperature, °C. observed from a ferry, Milwaukee-Muskegon transection on 11, 15, and 19 August (from Mortimer 1968).

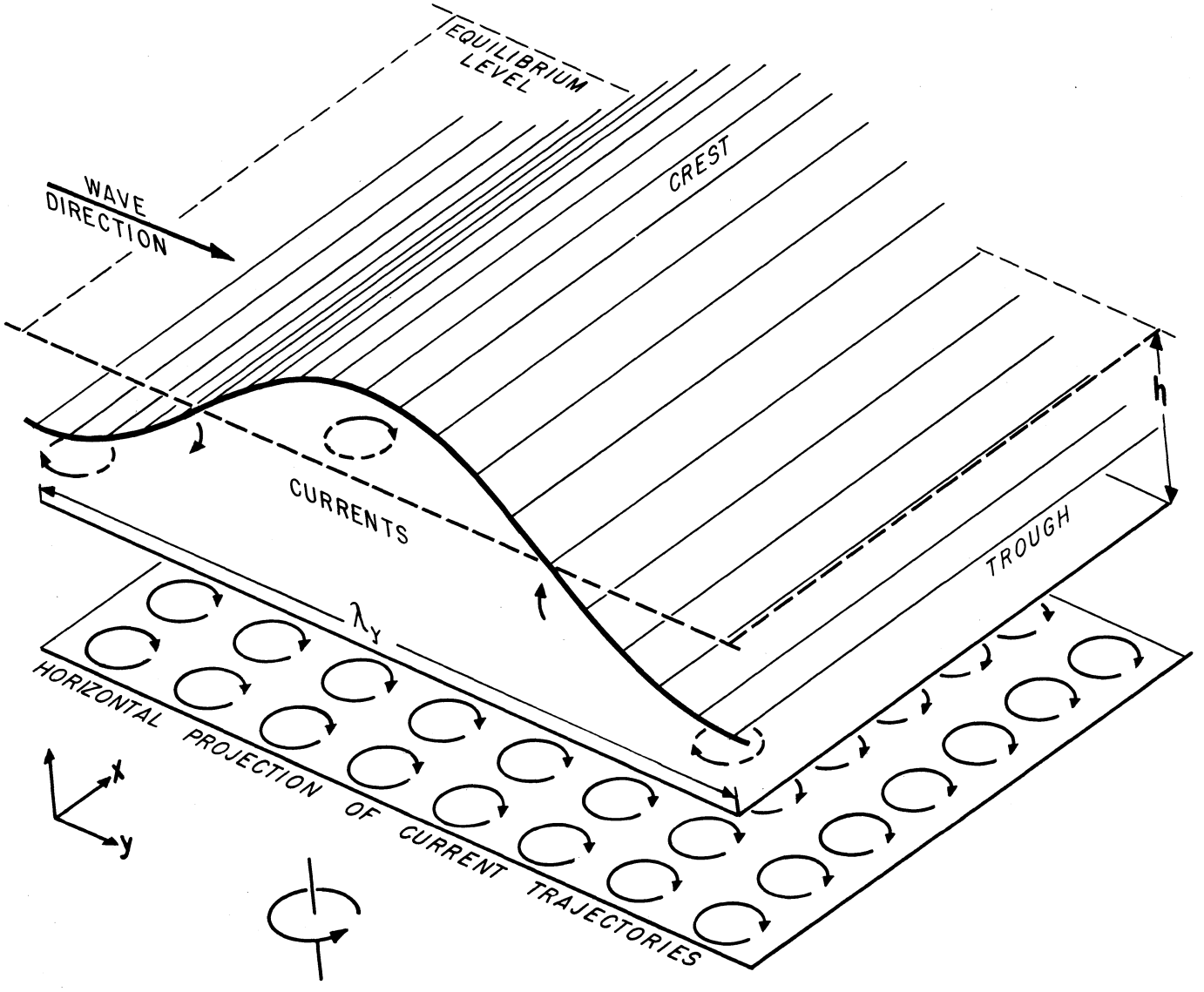

Fig. 47. One wavelength, λ_h, of a Sverdrup wave in a model ocean of uniform depth and infinite extent, rotating counter-clockwise about a vertical axis (adapted from Mortimer 1968). There is no restriction on the direction of wave progress. The wave-associated current trajectories are shown projected onto a horizontal plane. In this case they are ellipses, traversed once per wave cycle. The ellipse becomes more circular as the waveperiod approaches the inertial period. Under the wavecrest, the current vector points in the direction of wave progress.

Note: Current trajectories or vectors are also shown projected onto a horizontal plane in later figures (48, 49, 53 to 57, 80, 81, 87), all of which illustrate uniform-depth models, rotating counter-clockwise about a vertical axis. The elevation topography in these figures may be envisaged either as that of the water surface or as that of the interface in a two-layer model, in which case any current vectors shown are those in the lower layer.

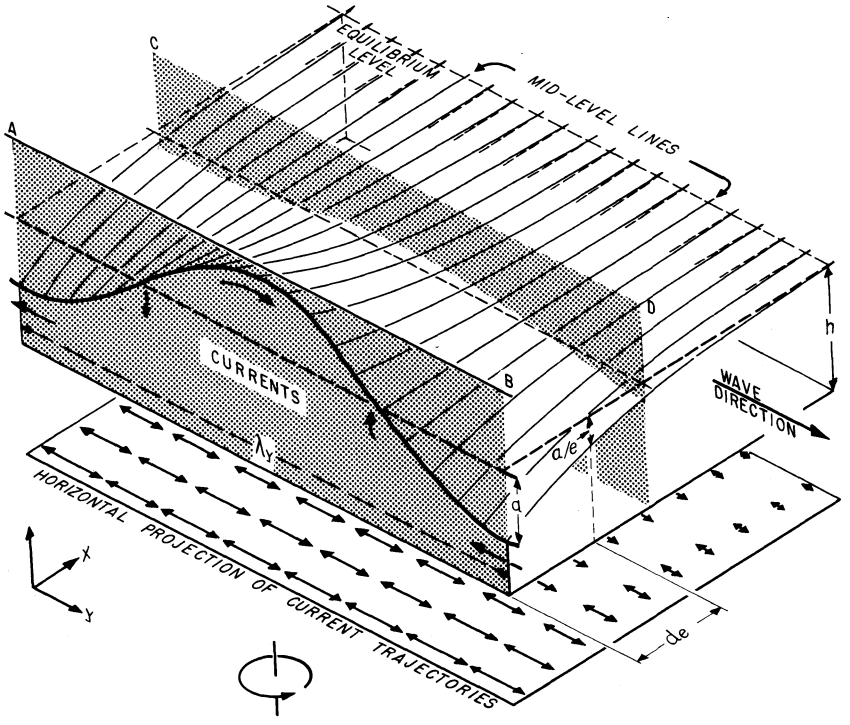

Fig. 48. One wavelength, λ_y, of a Kelvin wave traveling along one side (AB) of a semi-infinite ocean (or of a very wide channel, only one side of which is shown) of uniform depth and rotating counter-clockwise about a vertical axis (adapted from Mortimer 1968). The note in the legend of fig. 47 applies. The amplitudes of wave elevation ("a" at AB) and current decrease exponentially in a direction normal to AB, falling to 1/2 of the "onshore" amplitude at a distance d_e "offshore". Currents are always and everywhere parallel to AB. Therefore, a second vertical side, for example CD parallel to AB, can be inserted without disturbing the wave, to form the fig. 49 model of a Kelvin wave traveling along a narrow channel.

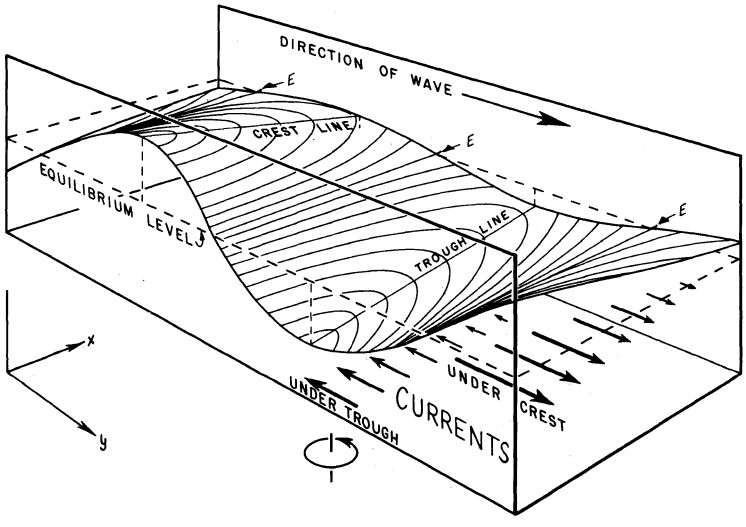

Fig. 49. Portion of a Kelvin wave traveling along a narrow channel (adapted from Mortimer 1963); see legend of fig. 48 and the note in the legend of fig. 47.

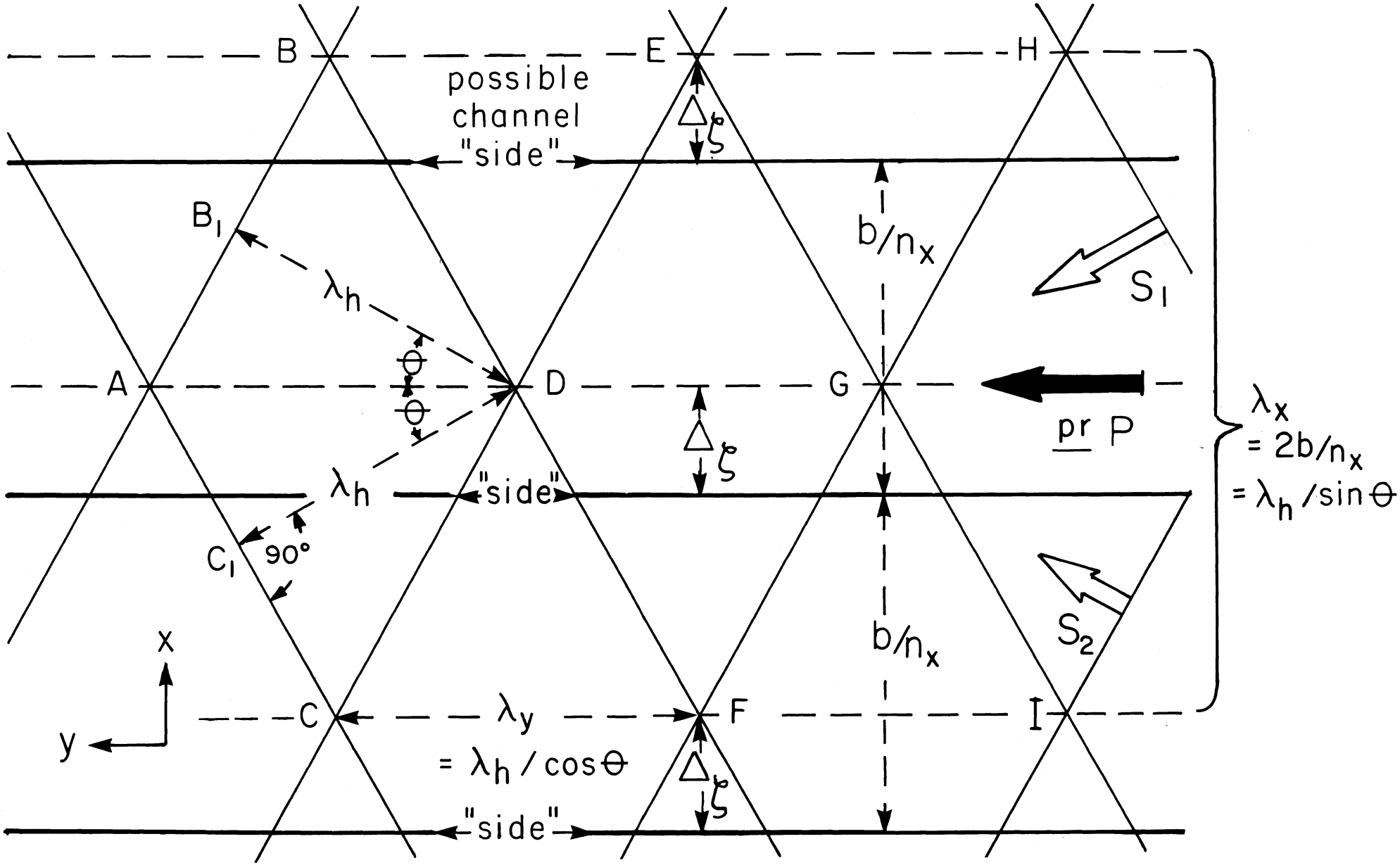

Fig. 50. Geometric relationships in a combination of two Sverdrup waves (S_1, S_2) of equal wavelength (λ_h), amplitude, and period, traveling in directions which form an angle 2θ. Letters A-I indicate points of S_1, S_2 wavecrest intersection. As explained in the text and illustrated in fig. 51, the combination produces a progressive Poincaré wave of wavelength $\lambda_y = \lambda_h/\cos\theta$. This P wave is progressive in the y-direction(which bisects the angle 2θ) and is standing in the x-direction. The "channel sides", shown at intervals of b/n_x, correspond to those shown as lines A and B in fig. 51. For further explanation, including a definition of $\Delta\zeta$, consult the text.

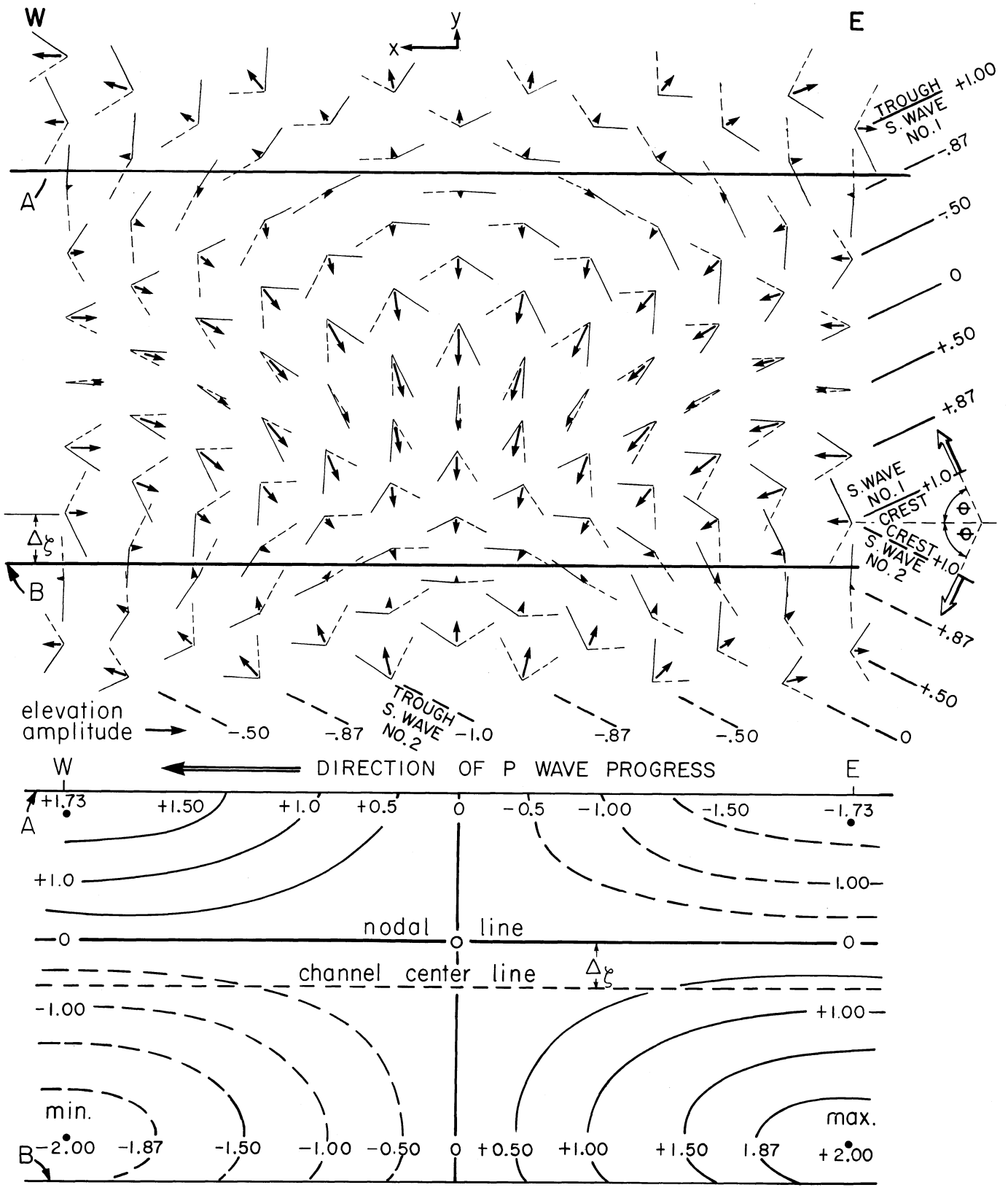

Fig. 51. A progressive Poincaré wave, shown as a combination of current vectors (upper portion) and elevations (lower portion) of two Sverdrup waves (S_1, S_2 of equal amplitude, period and wavelength, λ_h) traveling in directions which form an angle 2θ. The S wave vectors, at intervals of $\lambda_h/12$ (thin lines, unbroken for S_1, broken for S_2) combine to produce the current field (thick arrows as vector means) of the progressive P wave traveling in a direction which bisects 2θ, and with A and B as lines (possible "channel sides") along which the x-component of current falls to zero. For further explanation, including definition of Δ_ζ, see text.

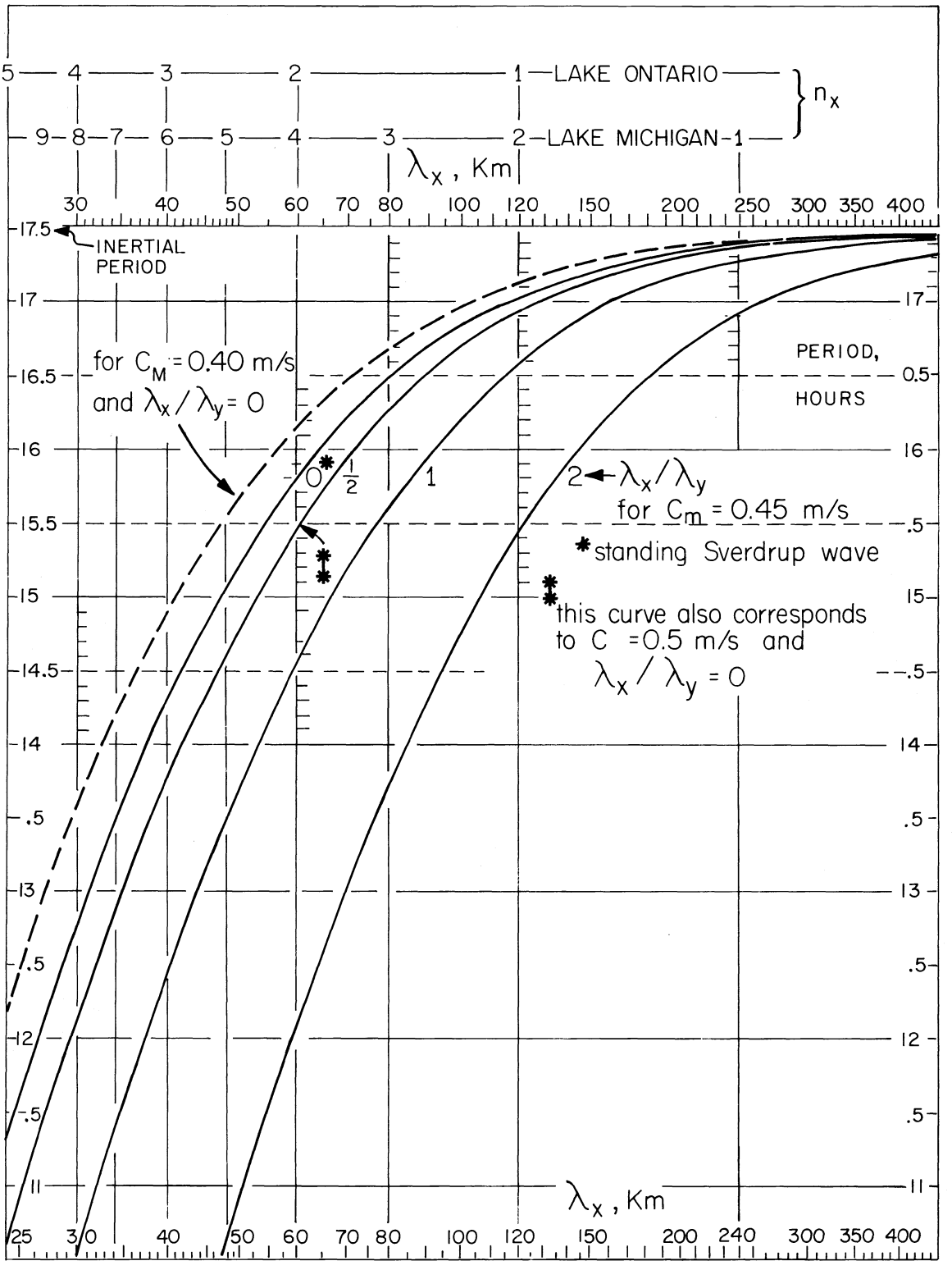

Fig. 52. Period/wavelength relationships for Poincaré waves in the case: c_m, 0.45 m/sec; inertial period, 17.5 hr; λ_x/λ_y ratio, 0, 1/2, 1 and 2. (Curves are also included for c_m values of 0.4 and 0.5 m/sec, both at $\lambda_x/\lambda_y = 0$.) Taking "channel widths" of 120 and 60 km, respectively, as values representative of Lakes Michigan and Ontario, values of λ_x corresponding to various values of n_x for each basin model are indicated by vertical lines.

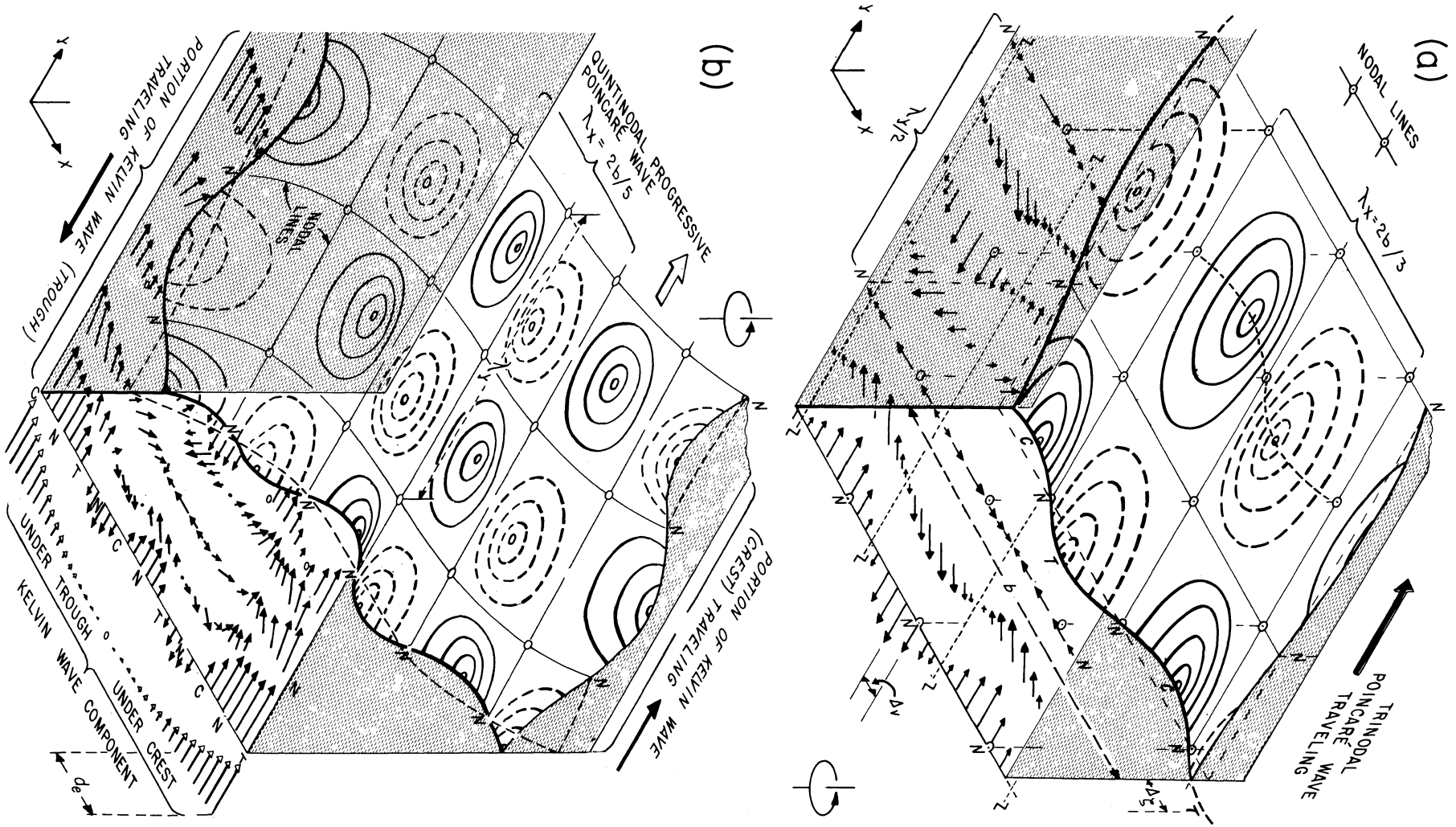

Fig. 53. Distribution, along a channel of width b, of wave elevation and current vectors in Poincaré waves of $\lambda_x/\lambda_y = 1/2$: (a) a progressive P wave of transverse nodality $n_x = 3$; and (b) a progressive P wave of $n_x = 5$, combined with a pair of Kelvin waves traveling in opposing directions along the channel sides (at distance d_e from the channel side, the K wave amplitude is 1/e of that at the side). The note in the legend of fig. 47 applies. The following letters refer to the P wave: N, nodal lines, longitudinal or transverse; C and T, crests and troughs; Z lines of zero current, whose position is governed by the Δ_v shift of eq. 31. Note also the elevation shift, Δ_ζ, governed by eq. 30.

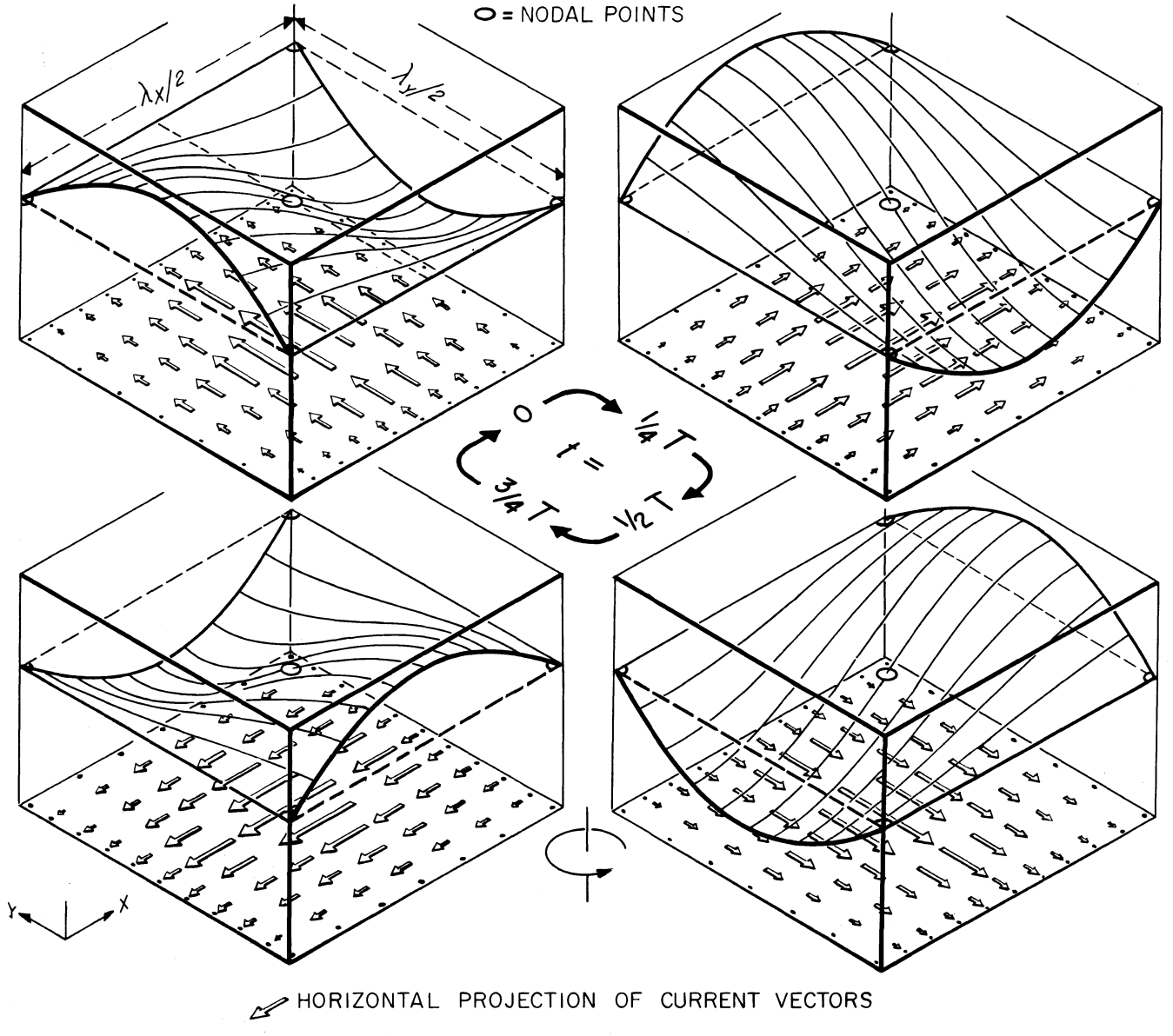

Fig. 54. An approximate model of wave elevation and current vectors at quarter-cycle stages in a standing Poincaré wave cell (period, T, very close to the inertial period; $\lambda_x/\lambda_y = 1$; adapted from Mortimer 1968). The note in the legend of fig. 47 applies.

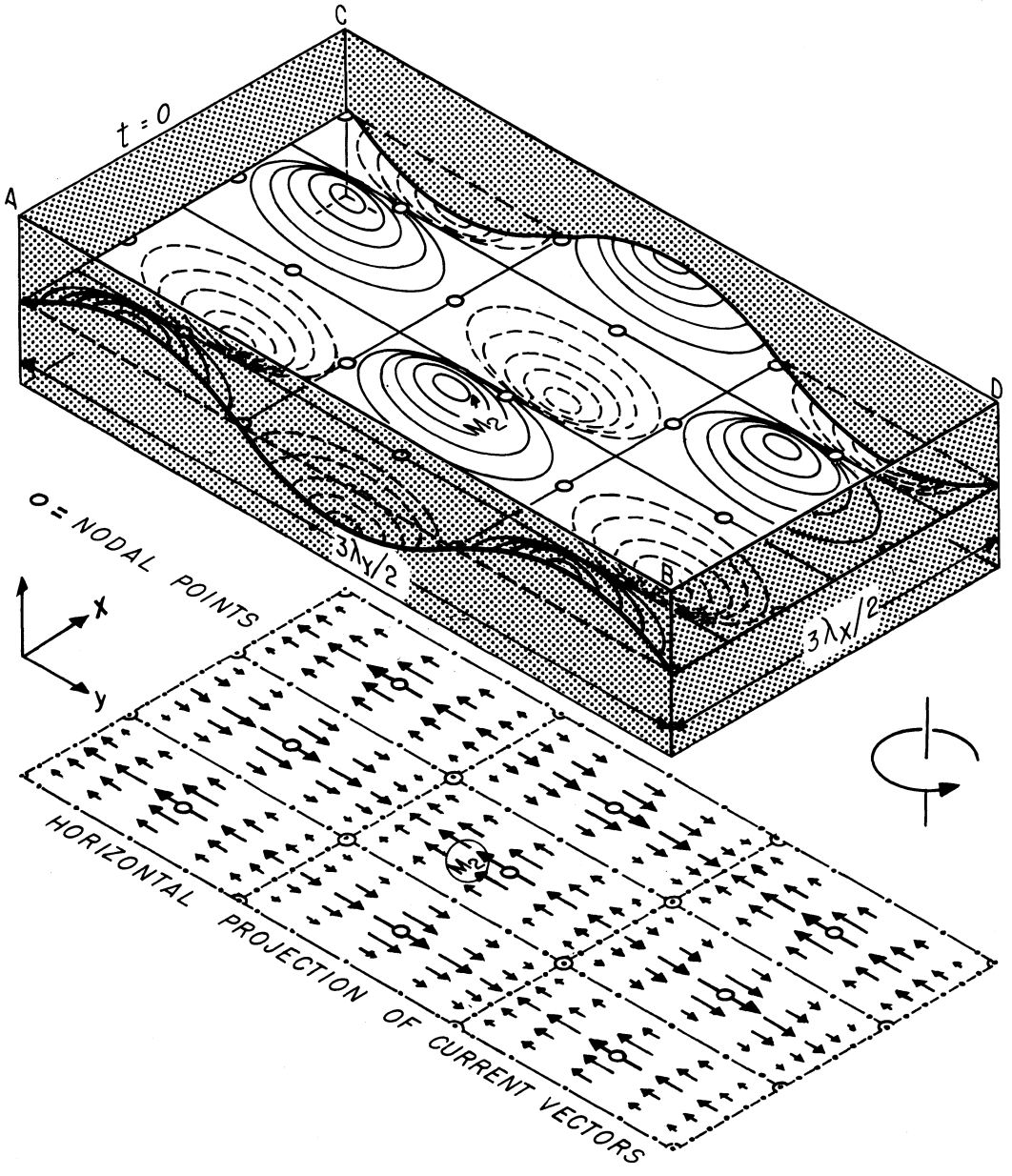

Fig. 55. An approximate model of wave elevation and current vectors in a 3x3 cell array of a standing Poincaré wave (period, T, very close to the inertial period; $\lambda_x/\lambda_y = 1/2$; transverse nodality 3; longitudinal "nodality" 3, see text; phase t = 0; adapted from Mortimer 1968). This model represents a component of a complete solution for the basin, see text. The note in the legend of fig. 47 applies.

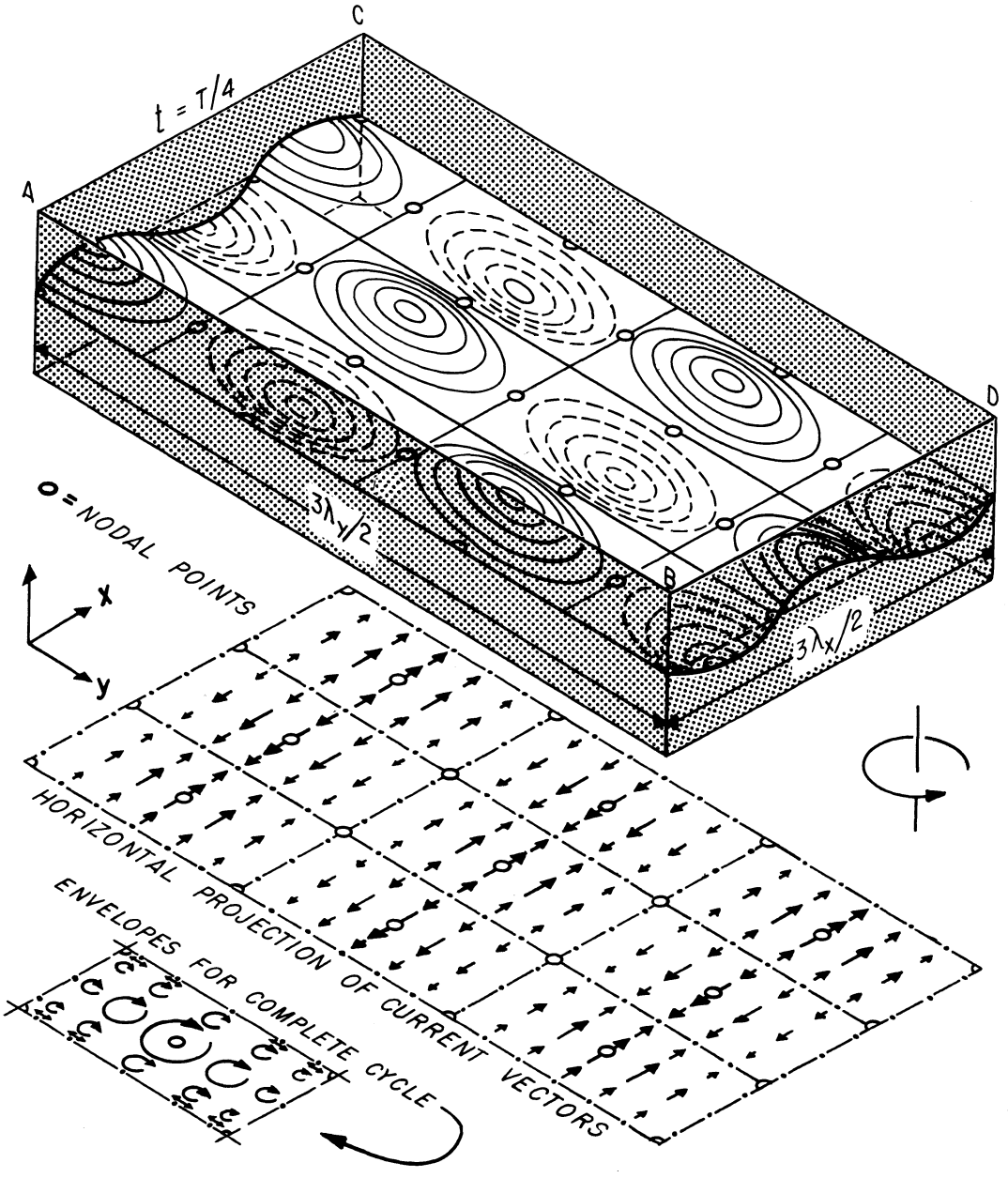

Fig. 56. Particulars as in fig. 55, but for phase t = T/4.

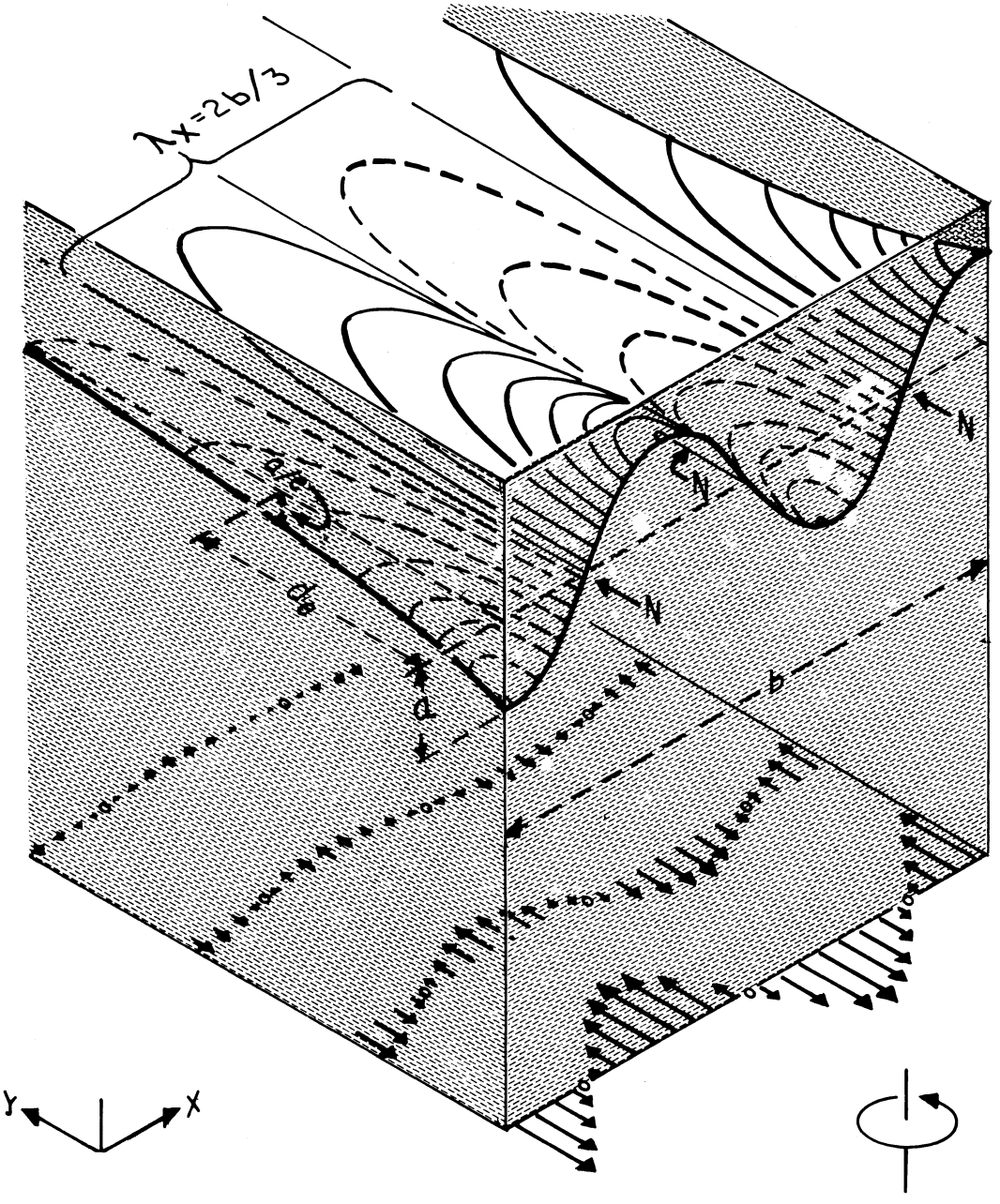

Fig. 57. Exponential Poincaré wave solution of transverse nodality $n_x = 3$, at a transverse boundary in a basin (or gulf) of width b. (The note in the legend of fig. 47 applies.) The waveform is standing in the x-direction; the amplitude, a at the transverse boundary (y = 0), decreases exponentially in the y-direction; d_e is the distance at which amplitude has fallen to a/e. N indicates a nodal line.

The existence of current components, here illustrated normal to the transverse boundary, demonstrates that the single exponential Poincaré wave is not itself a possible solution in the basin (or gulf) model. For this model, the complete solution is a combination of a set of P waves ($n_x = 1$ to ∞) and a pair of K waves, all of the same frequency, coincident with one of the basin eigenfrequencies, as explained in the text.

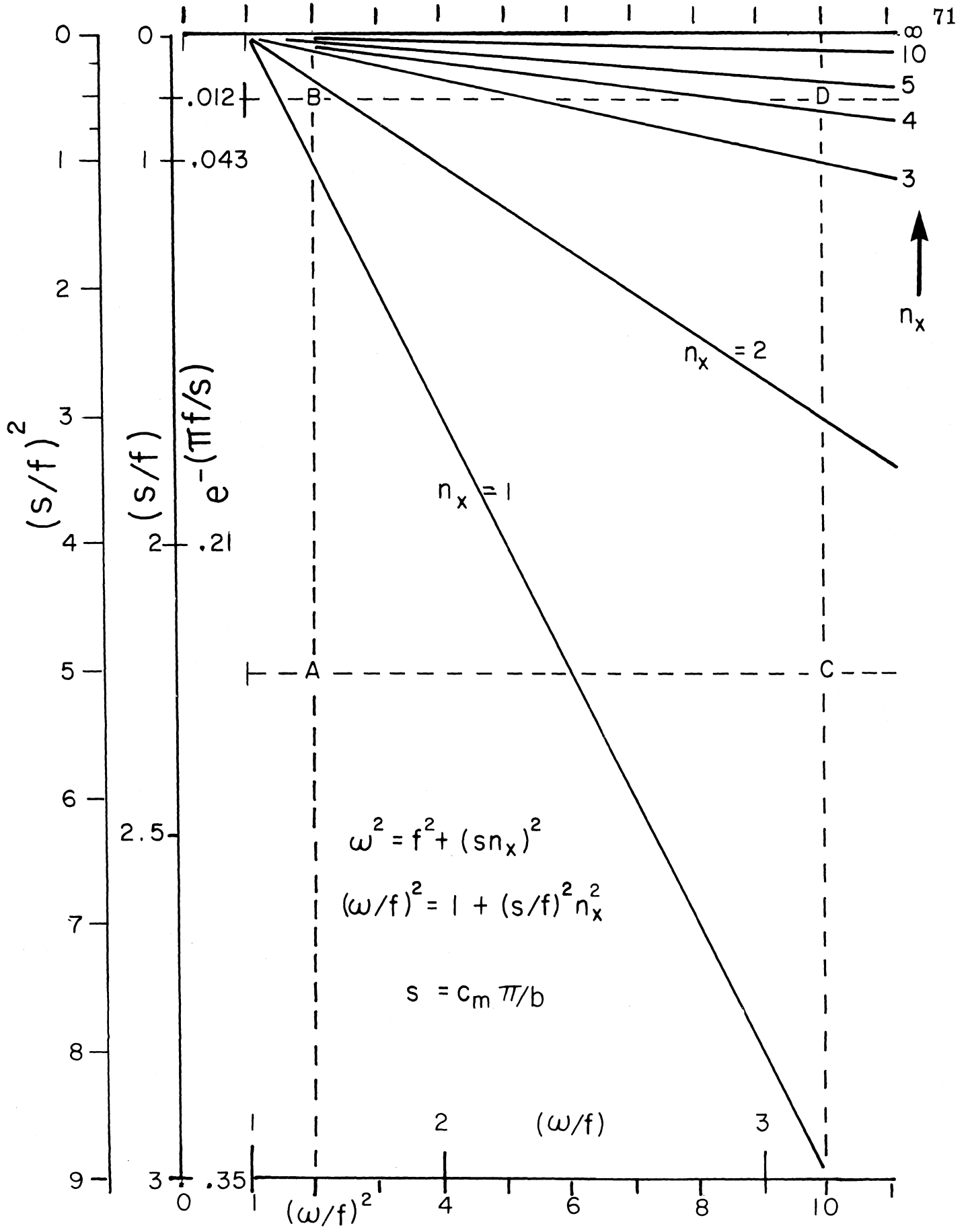

Fig. 58. Graphs of $\omega^2 = f^2 + (s\,n_x)^2$ over ranges 0 to 10 of $(s/f)^2$ and $(\omega/f)^2$, and for n_x = 1, 2, 3, 4, 5, 10 and infinity. For each value of n_x, ω defines the frequency of the corresponding standing Sverdrup wave in a channel of width $c_m\pi/s$; f is the inertial frequency; and $(s\,n_x)$ defines the frequencies of a corresponding set of transverse seiches in the channel without rotation.

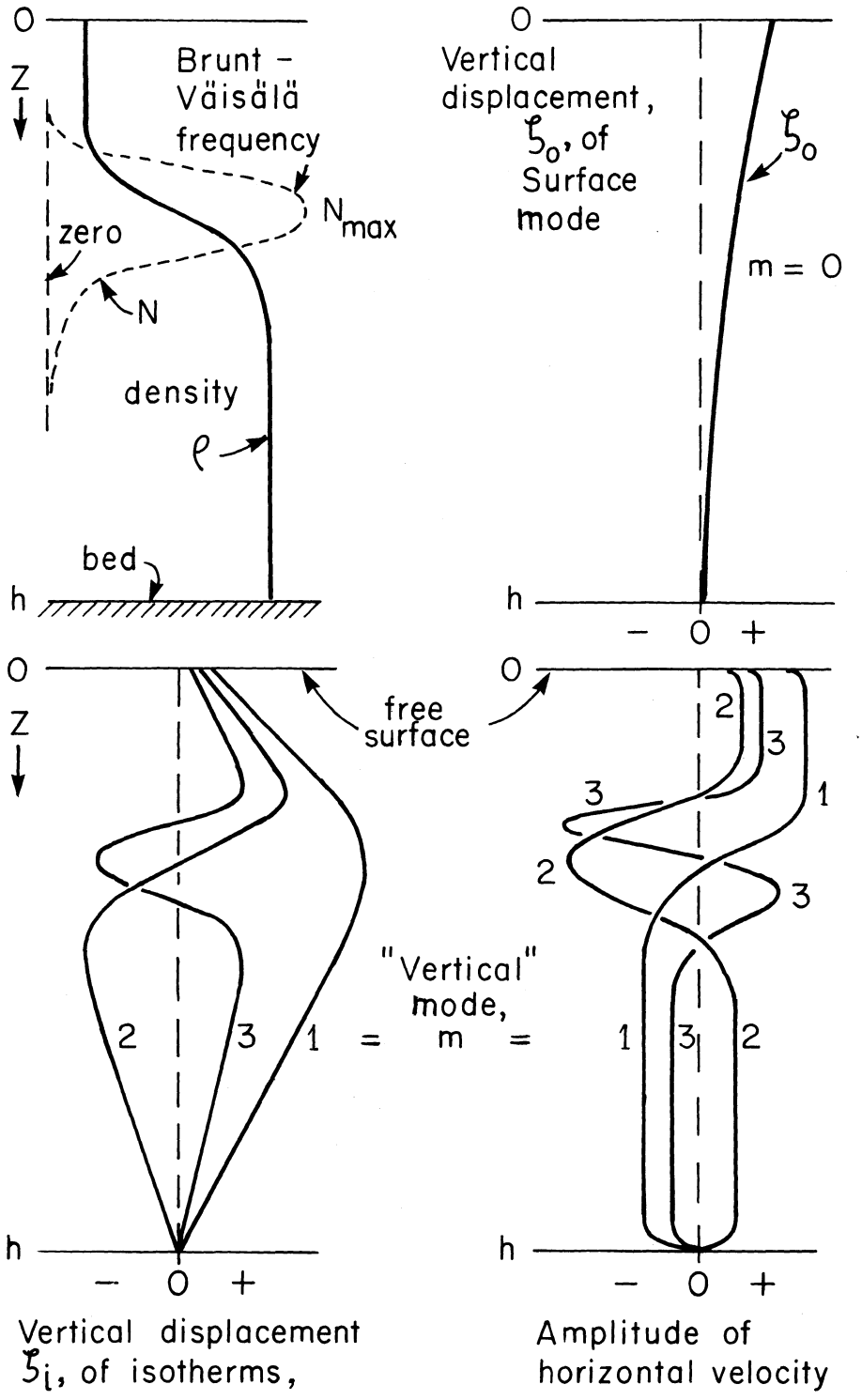

Fig. 59. Vertical dependence—for internal waves of vertical modes m = 1, 2, 3, and for the given vertical distribution of ρ and N—of (vertical) displacement of isotherms (ζ_i) and (horizontal) amplitude of water velocity. Also shown is the vertical displacement (ζ_0) corresponding to the surface mode.

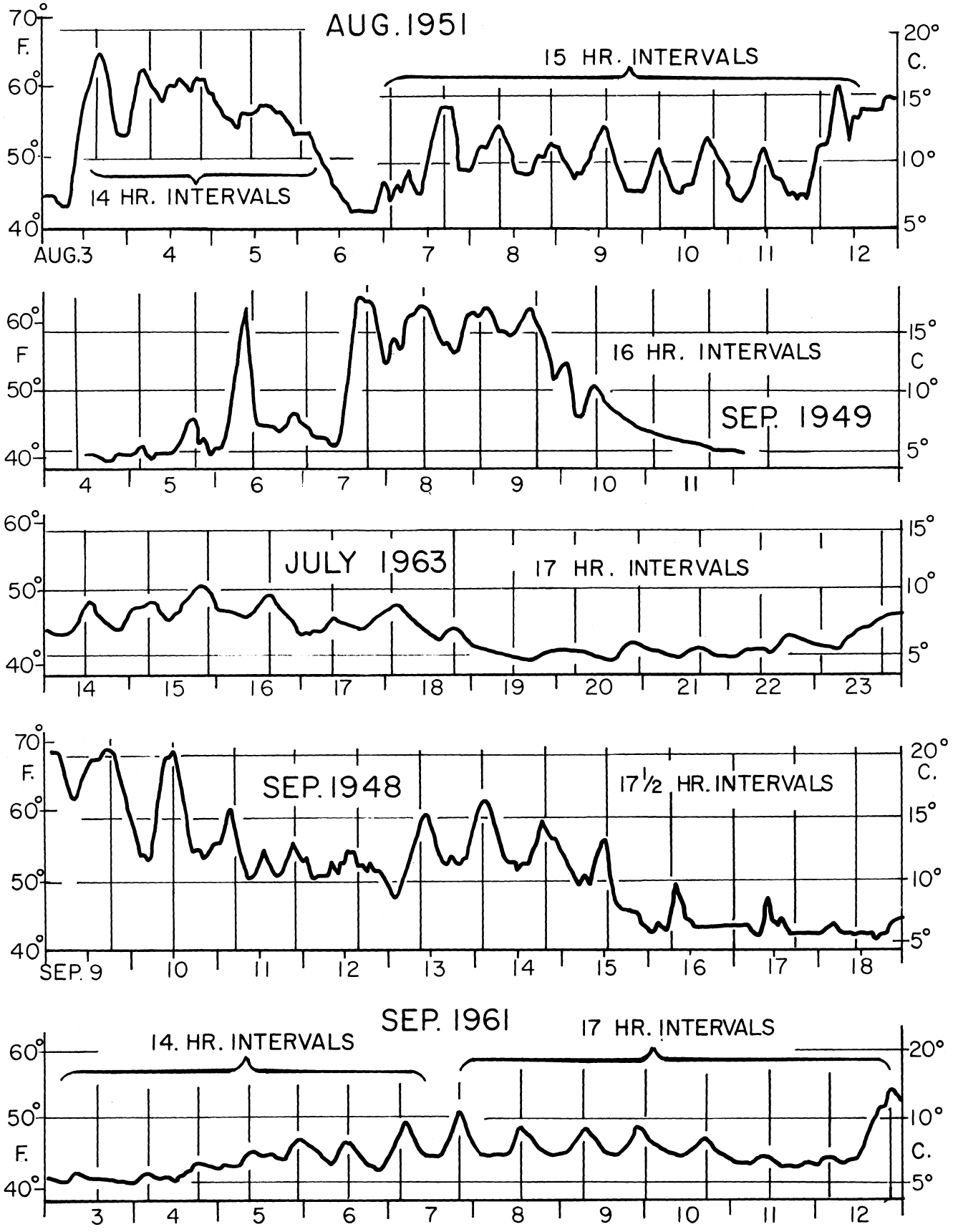

Fig. 60. Lake Michigan: "periodic" fluctuations in temperature (hourly means or hourly readings) at the municipal filtration plant intake at Milwaukee, Wis., during selected episodes. The mean periodicity assigned to each episode is estimated as a "best fit" by eye.

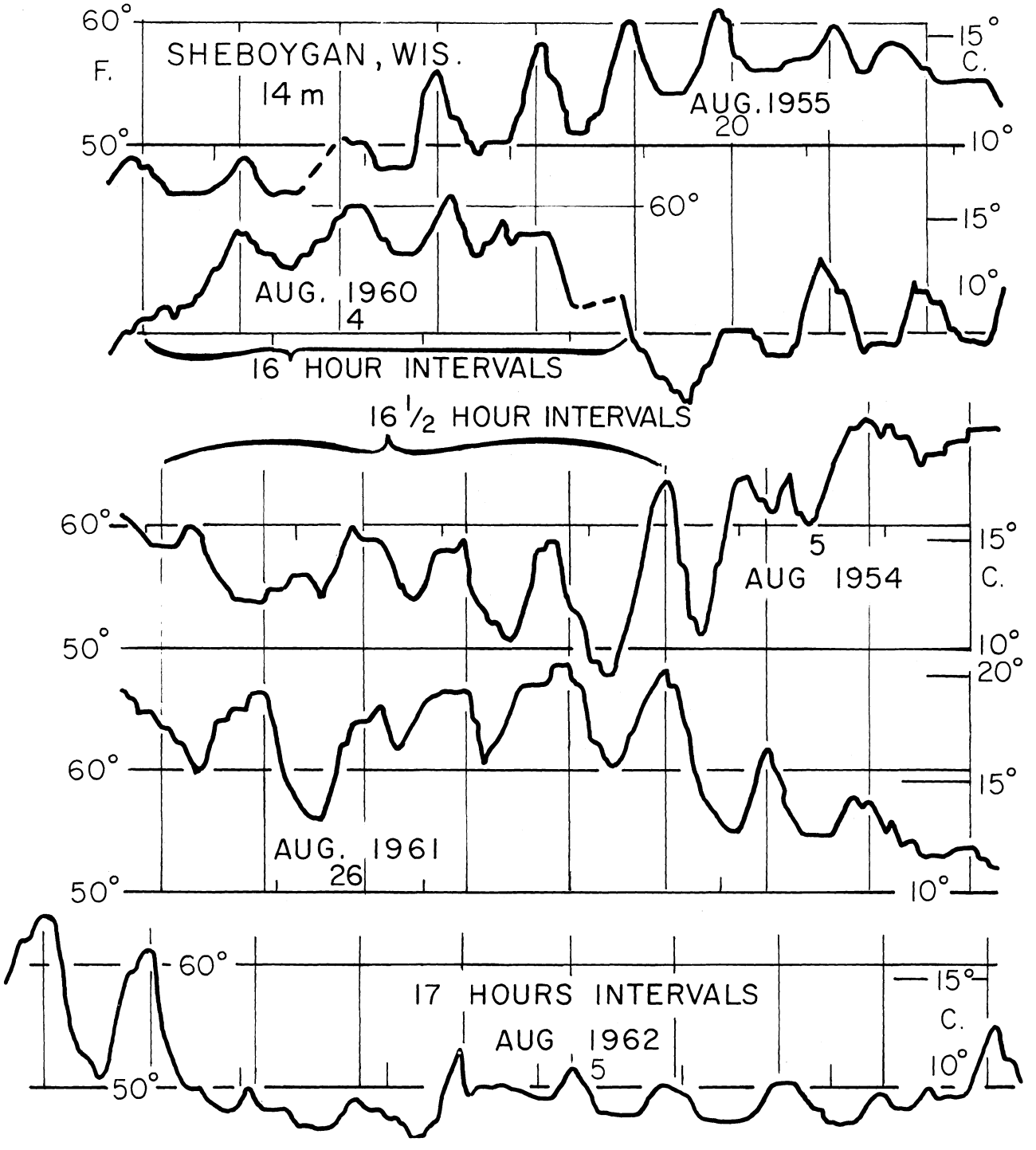

Fig. 61. Lake Michigan: "periodic" fluctuations in temperature (hourly readings) at the water intake of the municipal filtration plant at Sheboygan, Wis., during selected episodes, to each of which an estimated mean periodicity is assigned. (The episodes selected were those showing the clearest periodic behavior in fig. 5 of Mortimer, 1963, but the assignment of an 18 hr period to one episode in that figure is not justified.)

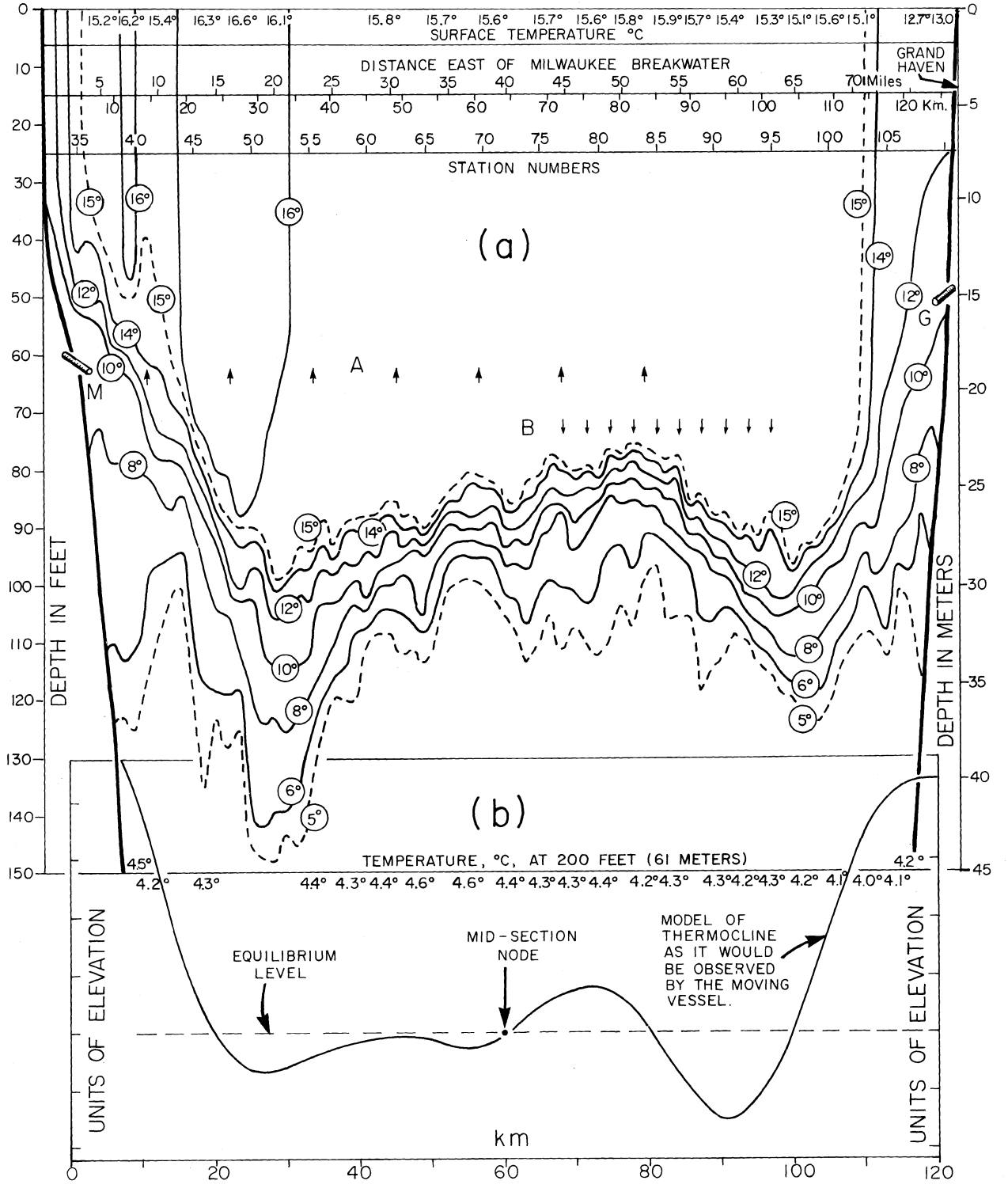

Fig. 62. (a) Lake Michigan, 26 September 1962. Distribution of temperature °C, observed from R. V. "Cisco" in the transection Milwaukee, Wis., to Grand Haven, Mich. Bathythermograph casts at approximately 1 mi intervals (1st, 1 mi off Milwaukee 0724 EST; last, 1 mi off Grand Haven, 1506 EST); surface temperatures from the ship's intake thermograph; (from Mortimer 1963).

(b) A model thermocline, developed in fig. 74 and fitted to the observed thermocline in (a) above with the assumptions listed on p. 71 of the text. The model takes account of the relative phases of the vessel passage and of postulated internal wave components.

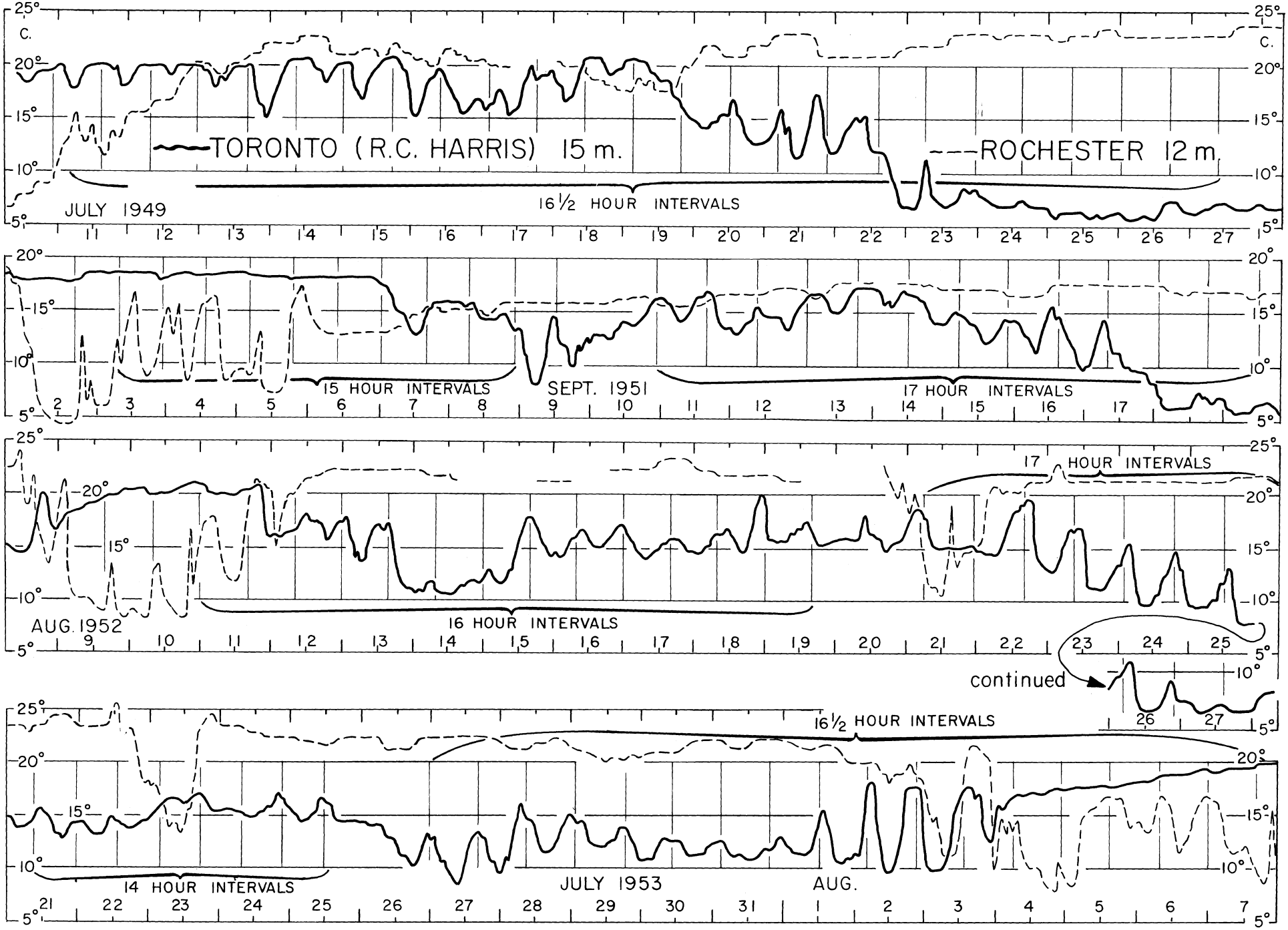

Fig. 63. Lake Ontario. "Periodic" fluctuations in temperature (hourly readings or hourly means) at water intakes of the municipal filtration plants at Toronto, Ont. and Rochester, N.Y. Further details in legend to fig. 60.

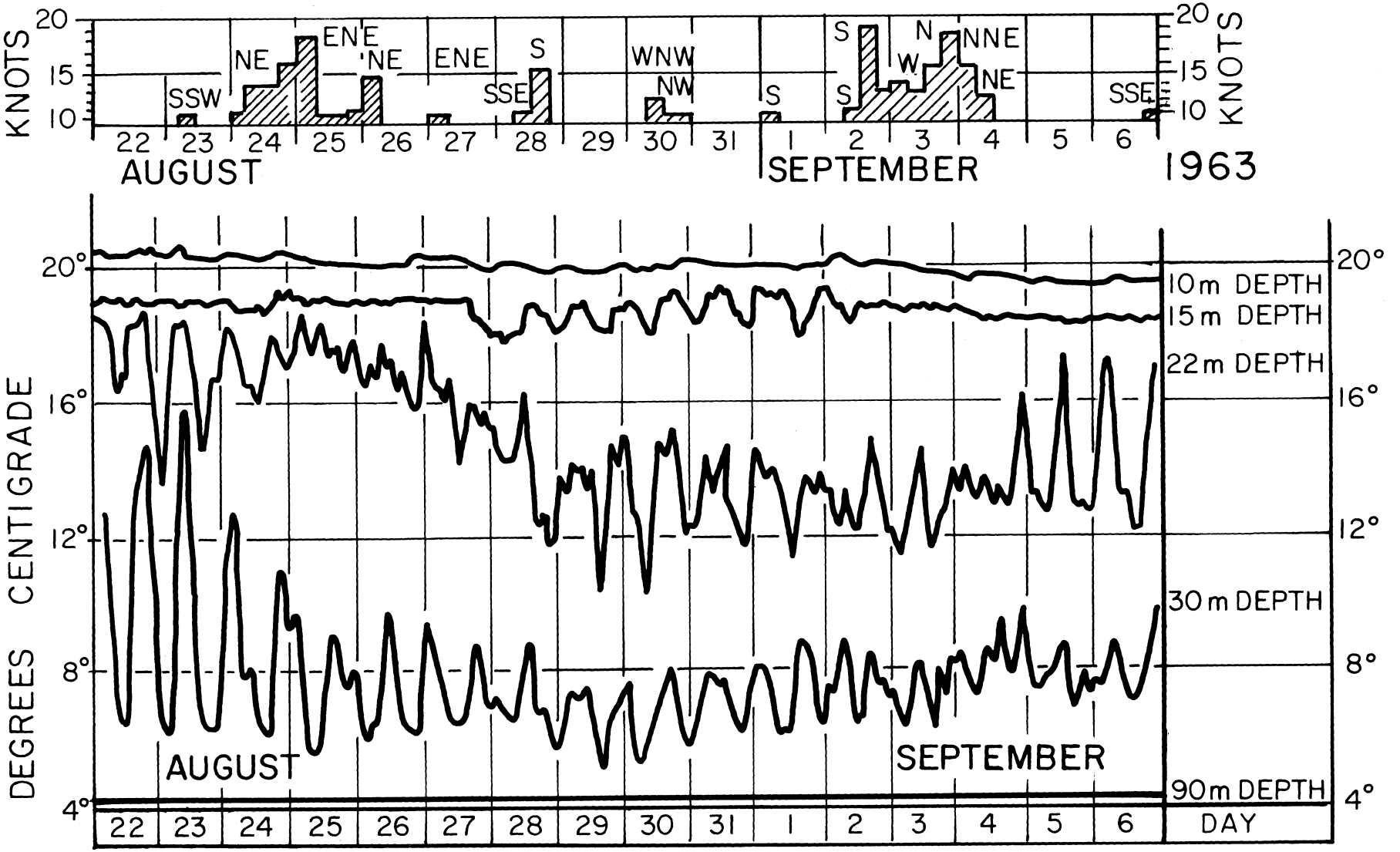

Fig. 64. Lake Michigan, 22 August to 6 September 1963. Temperature fluctuations (re-arranged from fig. 7-34 in U.S. Dept. Int. 1967) at five depths at station 9 (position shown in fig. 65) compared with 6-hourly mean wind speeds at 3 m above the water, also at station 8 (Basic Data Report, "Lake Michigan Winds," U.S. Dept. Int. FWPCA, Great Lakes Regional Office, Chicago). Only wind speeds of more than 10 knots are shown, plotted on a $(\text{speed})^2$ scale.

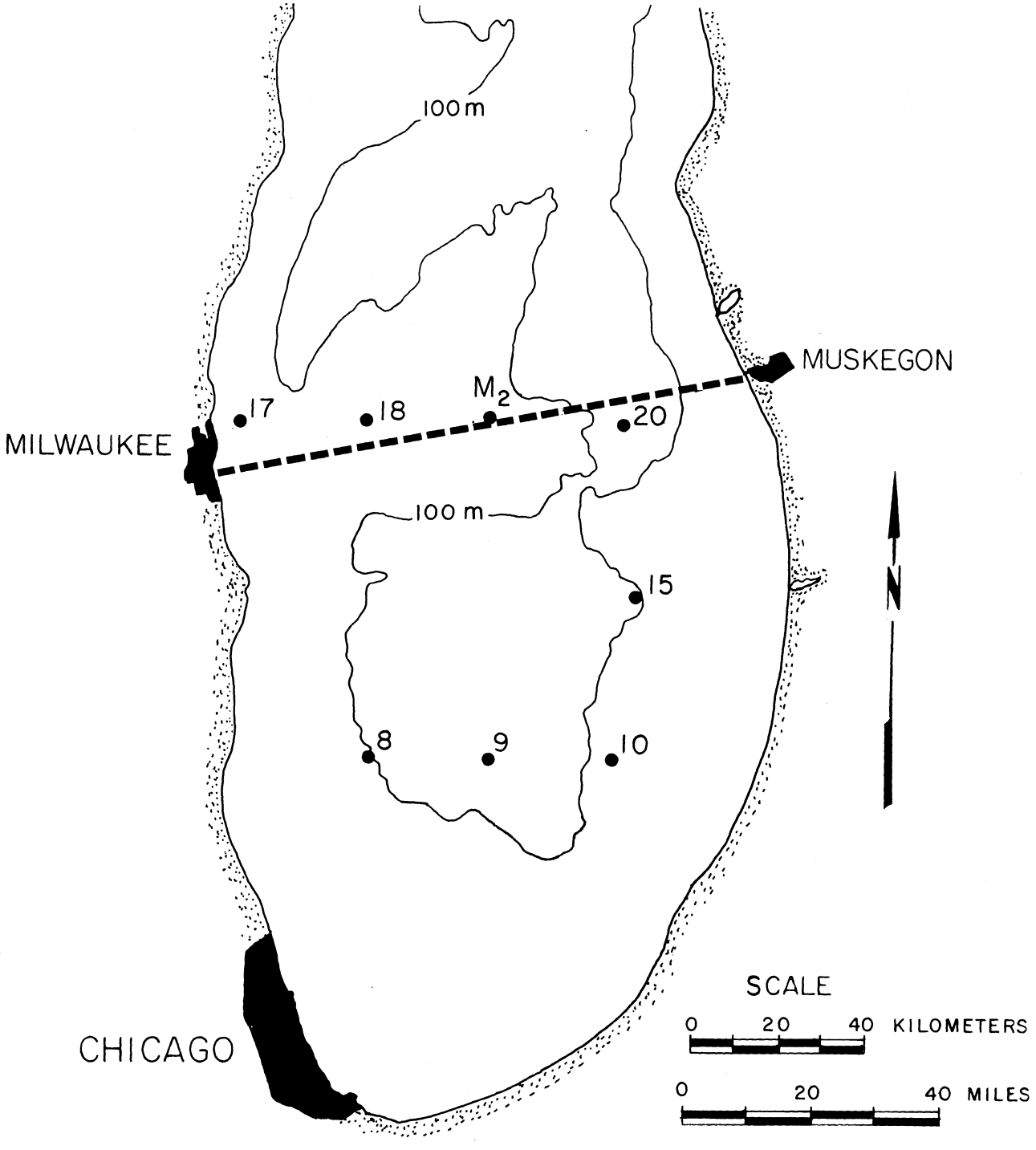

Fig. 65. Lake Michigan, southern half; positions of the Milwaukee-Muskegon railroad ferry track and of the fixed stations mentioned in the text.

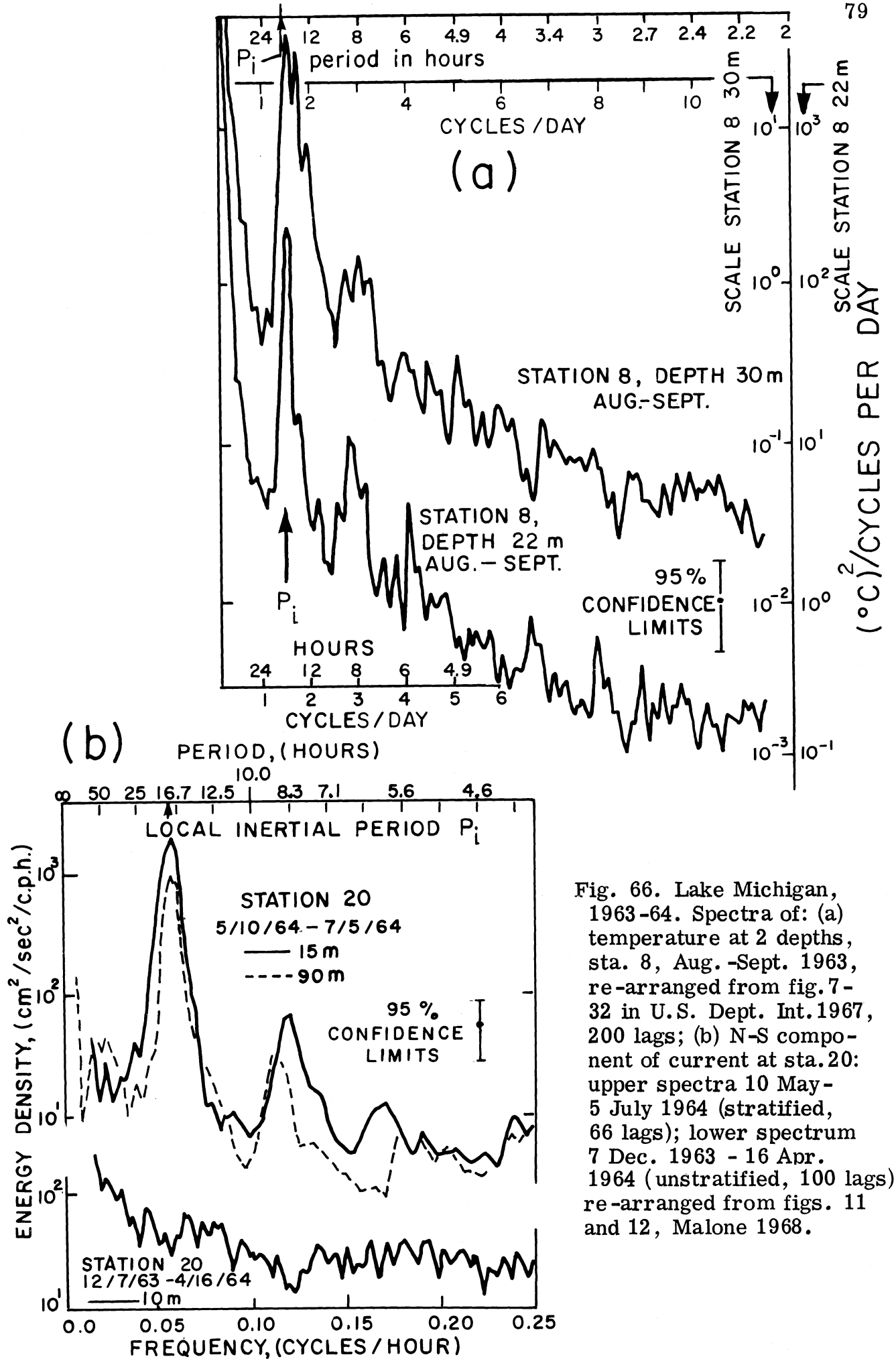

Fig. 66. Lake Michigan, 1963-64. Spectra of: (a) temperature at 2 depths, sta. 8, Aug.-Sept. 1963, re-arranged from fig. 7-32 in U.S. Dept. Int. 1967, 200 lags; (b) N-S component of current at sta. 20: upper spectra 10 May-5 July 1964 (stratified, 66 lags); lower spectrum 7 Dec. 1963 - 16 Apr. 1964 (unstratified, 100 lags), re-arranged from figs. 11 and 12, Malone 1968.

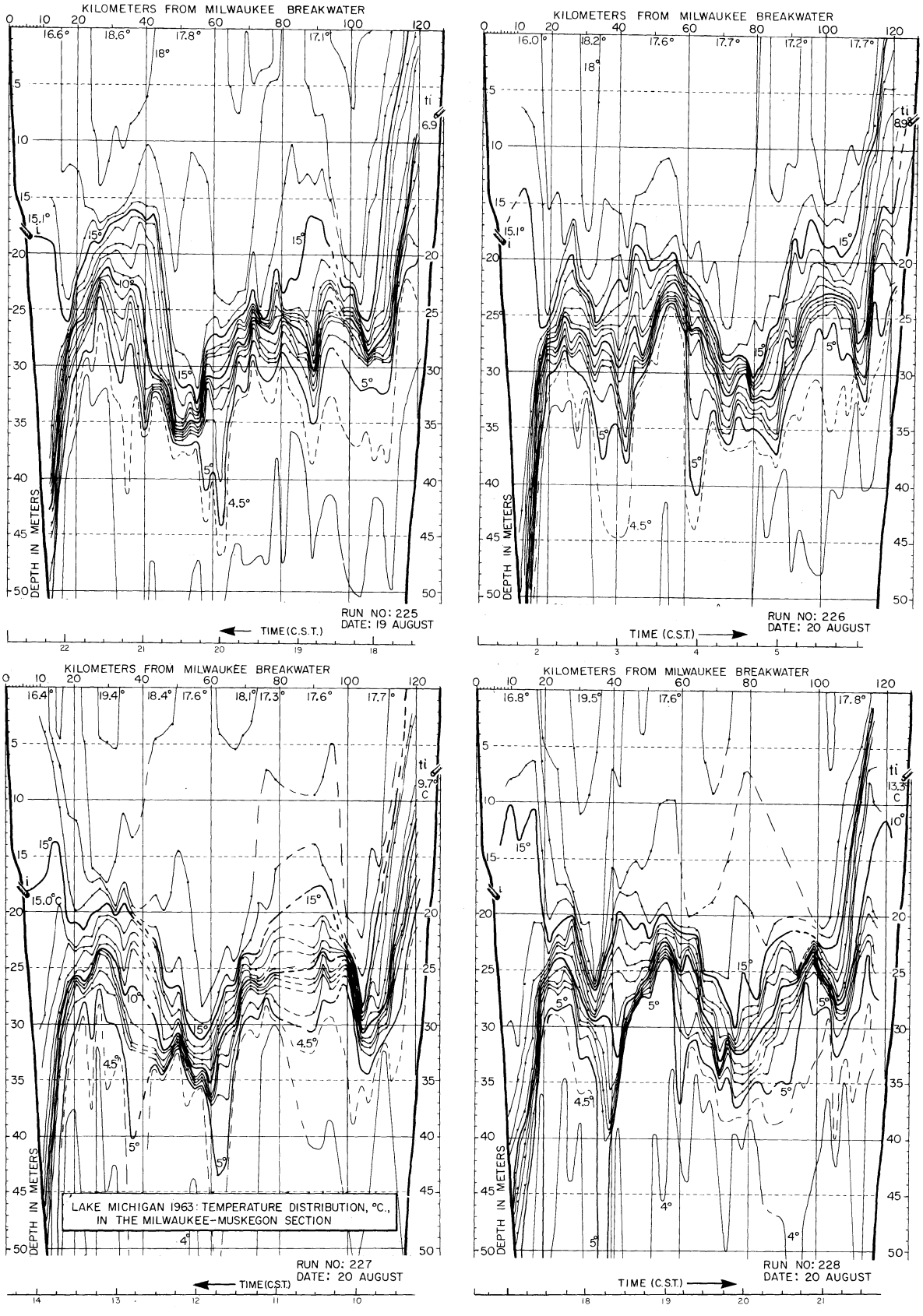

Fig. 67. Lake Michigan, 19-20 August 1963. Distribution of temperature, °C, in the Milwaukee-Muskegon transection, observed on four consecutive ferry crossings (from Mortimer 1968).

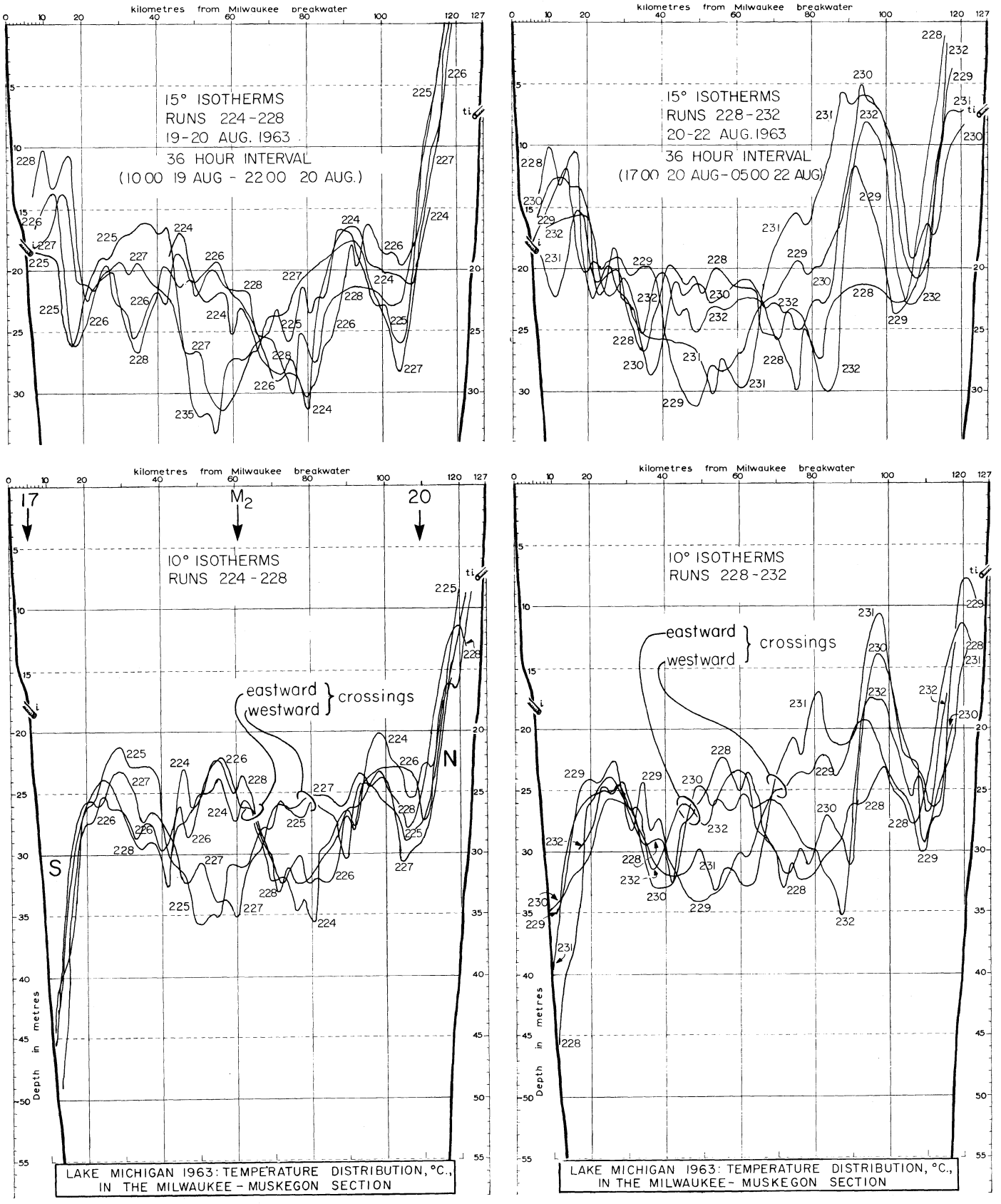

Fig. 68. Lake Michigan, 19-22 August 1963. Distribution of the 10° and 15° isotherms, observed from a ferry, Milwaukee-Muskegon transection, superimposed for two groups of five consecutive ferry crossings.

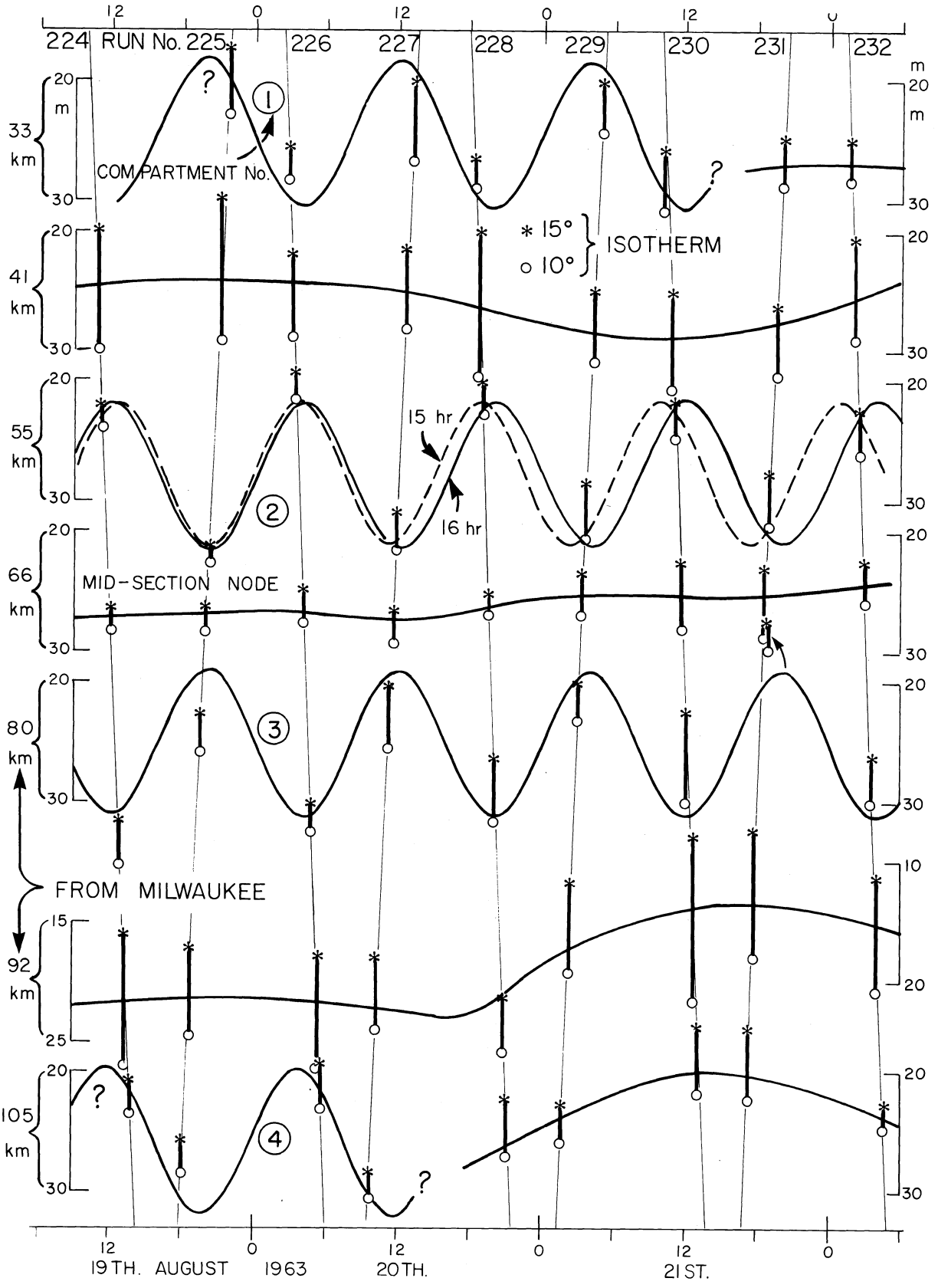

Fig. 69. Lake Michigan, 19-20 August 1963: oscillations in depth of the thermocline (defined as lying between the 10° and 15°C isotherms) at selected distances from Milwaukee, observed on nine consecutive ferry runs (thin lines) across the Milwaukee-Muskegon transection. Where appropriate, a sinusoid corresponding to a 16 hr period (also to a 15 hr period, broken line, at the 55 km station) is fitted to the observations.

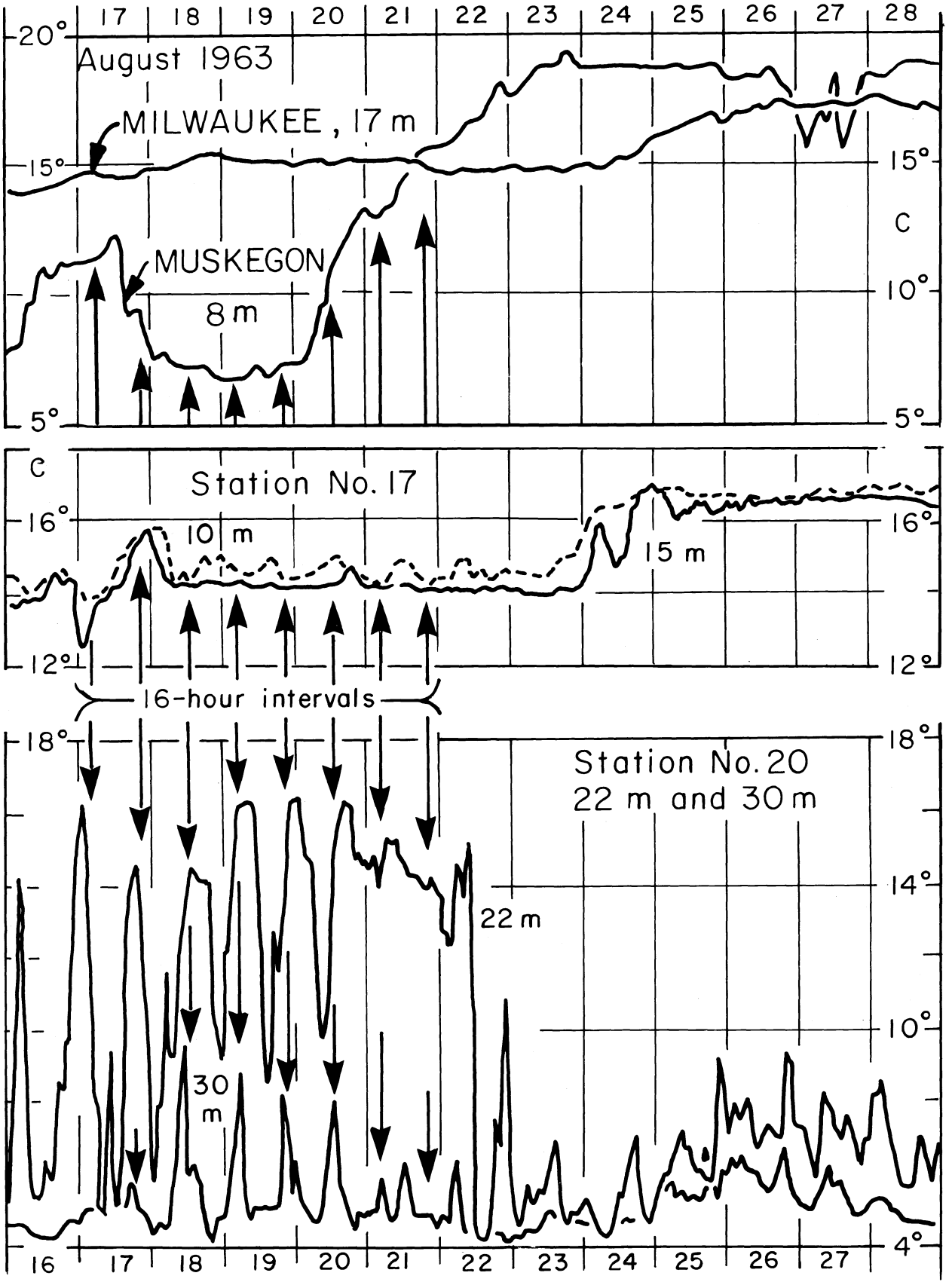

Fig. 70. Lake Michigan, 16-28 August 1963. Temperature, °C, at municipal water intakes at Milwaukee, Wis., and Muskegon, Mich., and at U.S. Dept. Int. (1967) stations 17 (10 and 15 m) and 20 (22 and 30 m).

Fig. 71 (opposite page) "Thermocline depth" as observed from a vessel during a 6 hr crossing of a model basin, in which a uninodal internal seiche of 16 hr period is in progress. Thin lines display the (sinusoidal) thermocline topography at each hour of the 16 hr cycle (0 hr corresponds to WHT, defined as the maximum elevation on the left-hand or "western" side); and thick unbroken lines in sections (a) to (h) represent thermocline depth as observed on eastward crossings starting at the hours 0 to 7, respectively. Thick broken lines show observed thermocline depth on the return westward crossings, assuming a 2 hr delay between arrival at and departure from the E side. Observed thermocline depths, corresponding to (W) starting hours 8 to 15, can be obtained by inverting sections (a) to (h), but not their scales, about their 12 hr axes. Observed thermocline topographies for all 15 eastward passages are superimposed in (i).

Legends for later figures

Fig. 72. "Thermocline depth" as observed from a vessel during a 6 hr crossing of a model basin of 120 km width, in which internal seiches of (a) nodality I and III and (b) nodality V are in progress. Vessel timing corresponds to that in fig. 71, with the starting time from the W side at 2 hr before WHT (see fig. 71 legend). Unbroken and broken lines represent eastward and westward crossings, respectively; and the three seiches are assumed to be of equal period (16 hr), of equal amplitude, and in phase at the E and W sides of the basin. Sections (c) to (f) illustrate the seiche combinations as indicated. The dotted line in (c) represents the I + III combination, but with the phase of III reversed.

Fig. 73. (a) to (d): "Thermocline depth" as observed from a vessel during a 6 hr crossing of a model basin of 120 km width, in which internal seiches (I, III, and V, see fig. 72) of 16 hr period are combined in varying proportions. Vessel timing corresponds to that fig. 71, with a starting time from the W side of 4 hr before WHT; (e) portion of fig. 68, showing observed depth of the 10°C isotherm in Lake Michigan, during five consecutive ferry crossings, 19-20 August 1963.

Fig. 74. "Thermocline depth" as observed from a vessel during a 10 hr crossing (W to E starting at WHT) of a model basin of 120 km width, in which internal seiches of equal periods (16 hr), equal amplitudes and of nodality I, III, and V are in progress, singly (upper three sections) or combined (lower two sections). The combination (I + III + V) is compared, as a model in fig. 62b, with the Lake Michigan observations illustrated in fig. 62a.

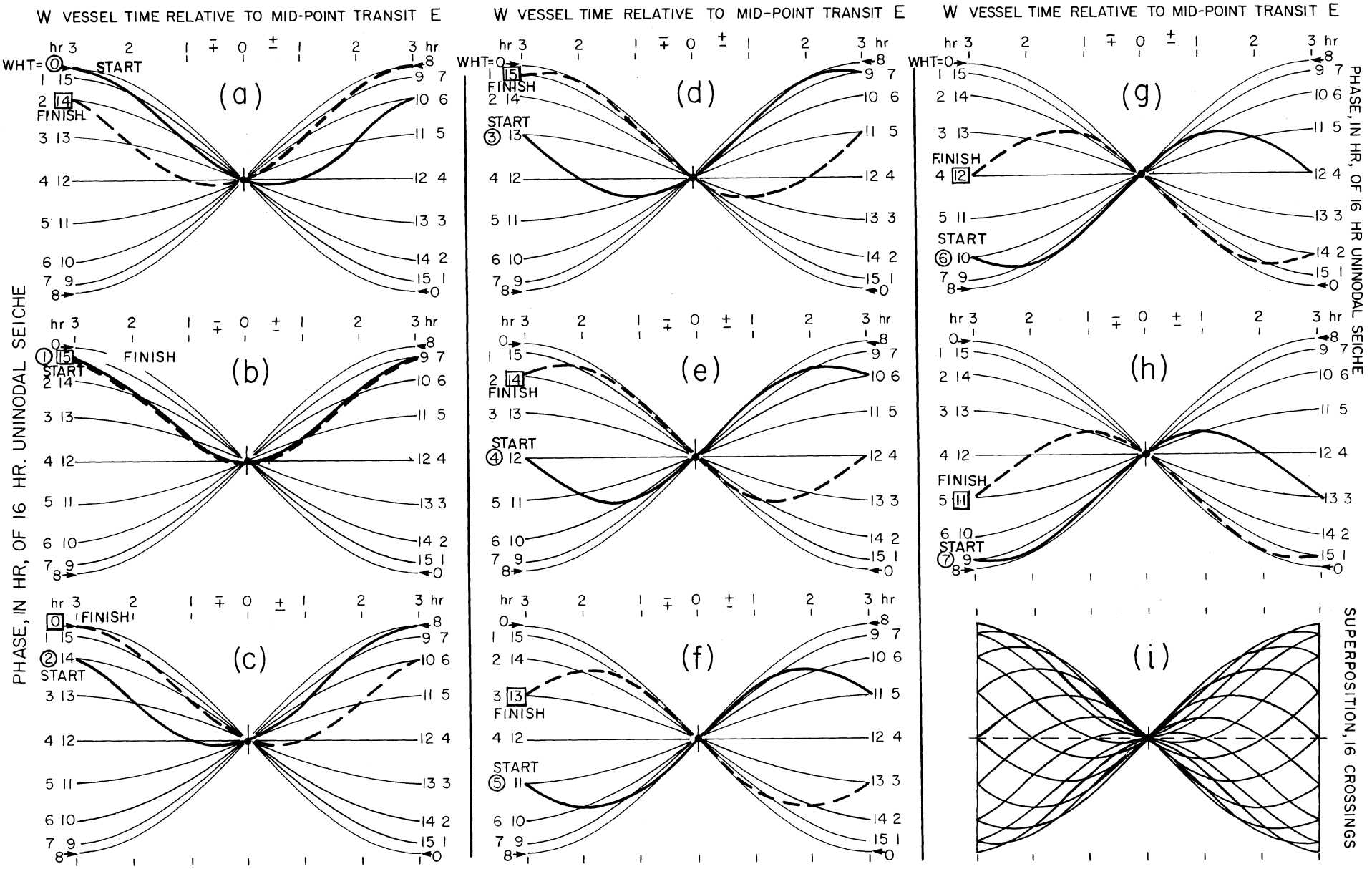

Fig. 71. See opposite page.

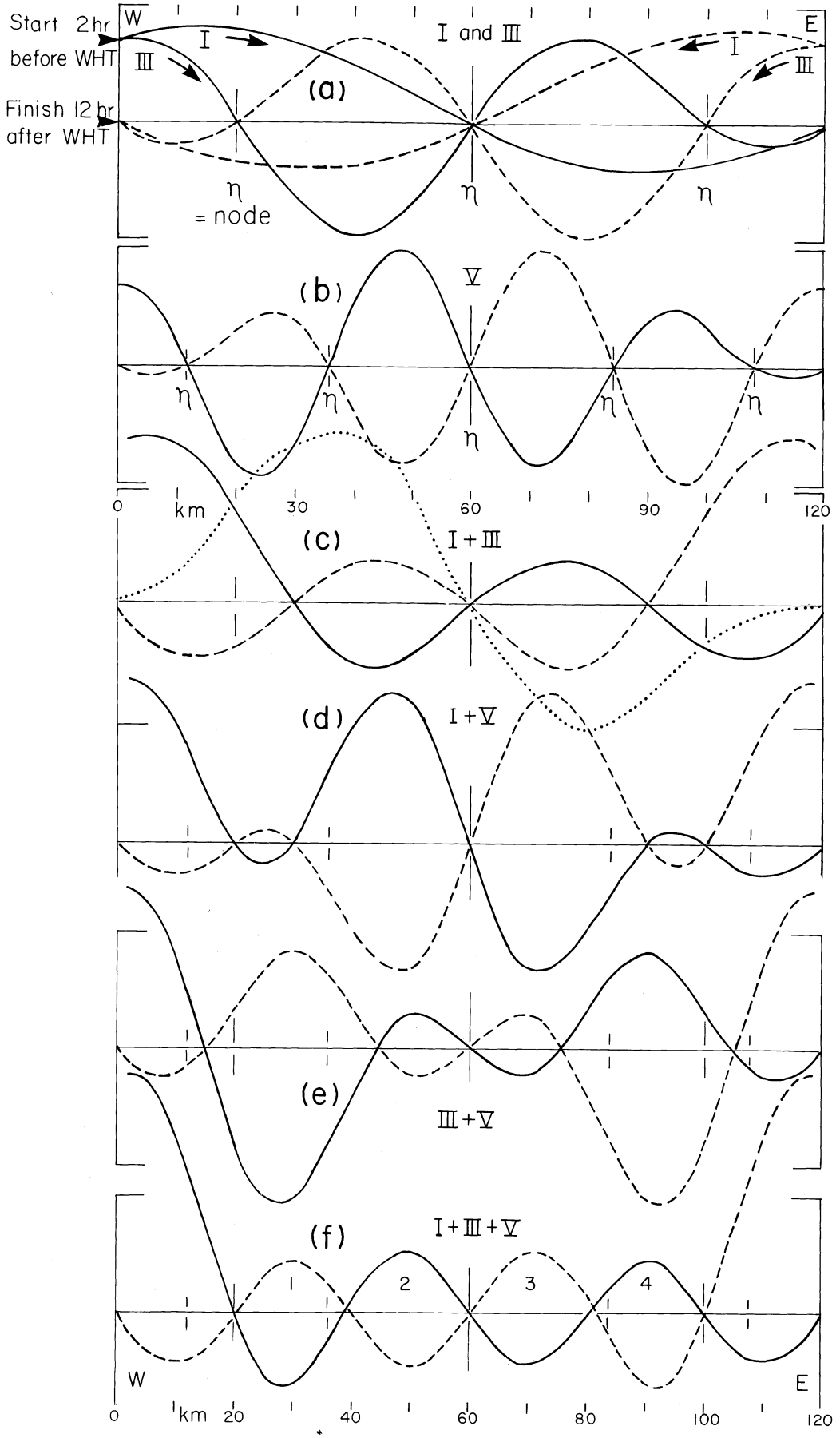

Fig. 72. "Thermocline depth" as observed from a vessel during a 6 hr crossing of a model basin of 120 km width. For full legend, see page opposite fig. 71.

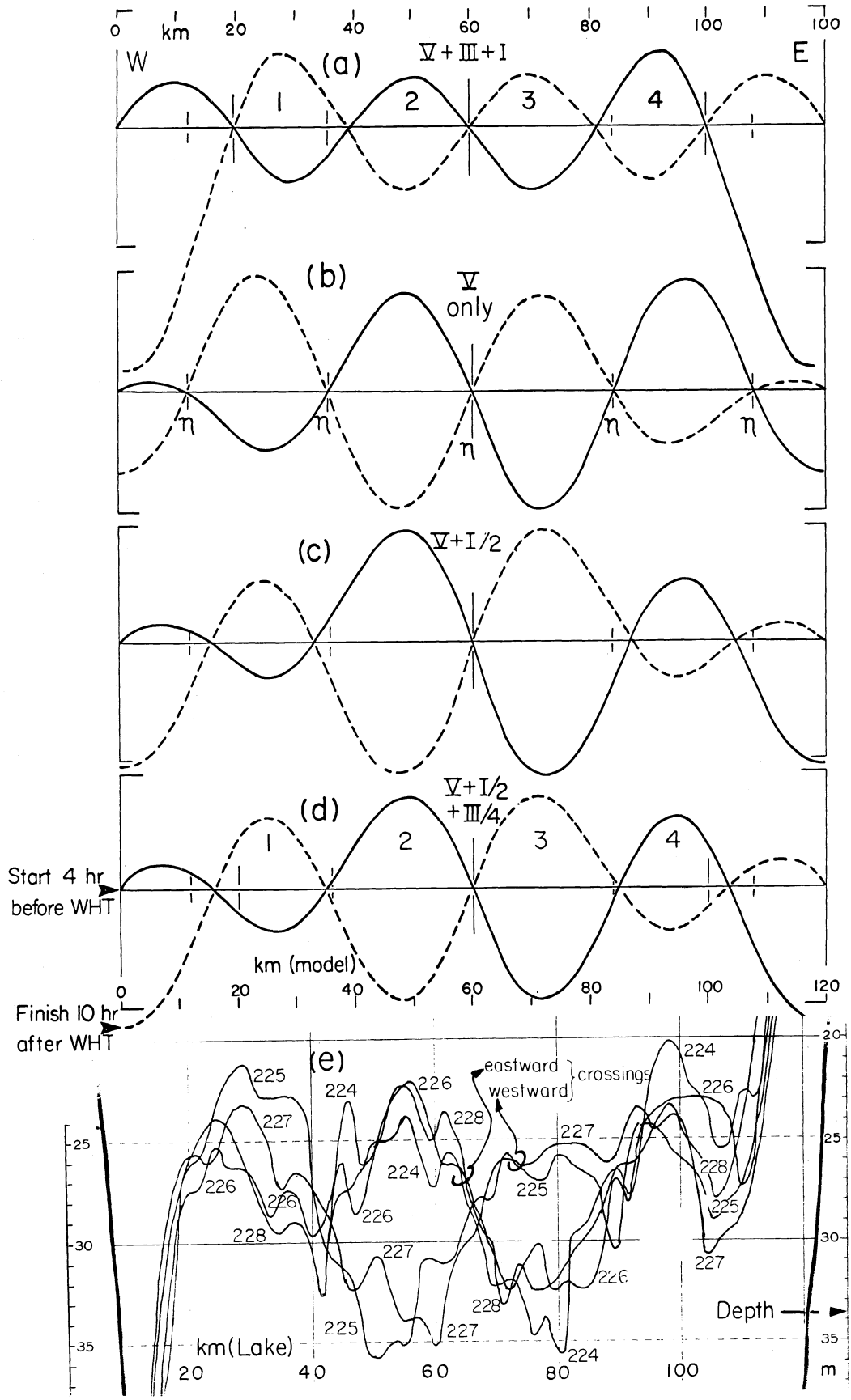

Fig. 73. "Thermocline depth, (a) to (d), as observed from a vessel during a 6 hr crossing of a model basin of 120 km width, compared with (e) observations of depth of the 10° isotherm (fig. 68). For full legend, see page opposite fig. 71.

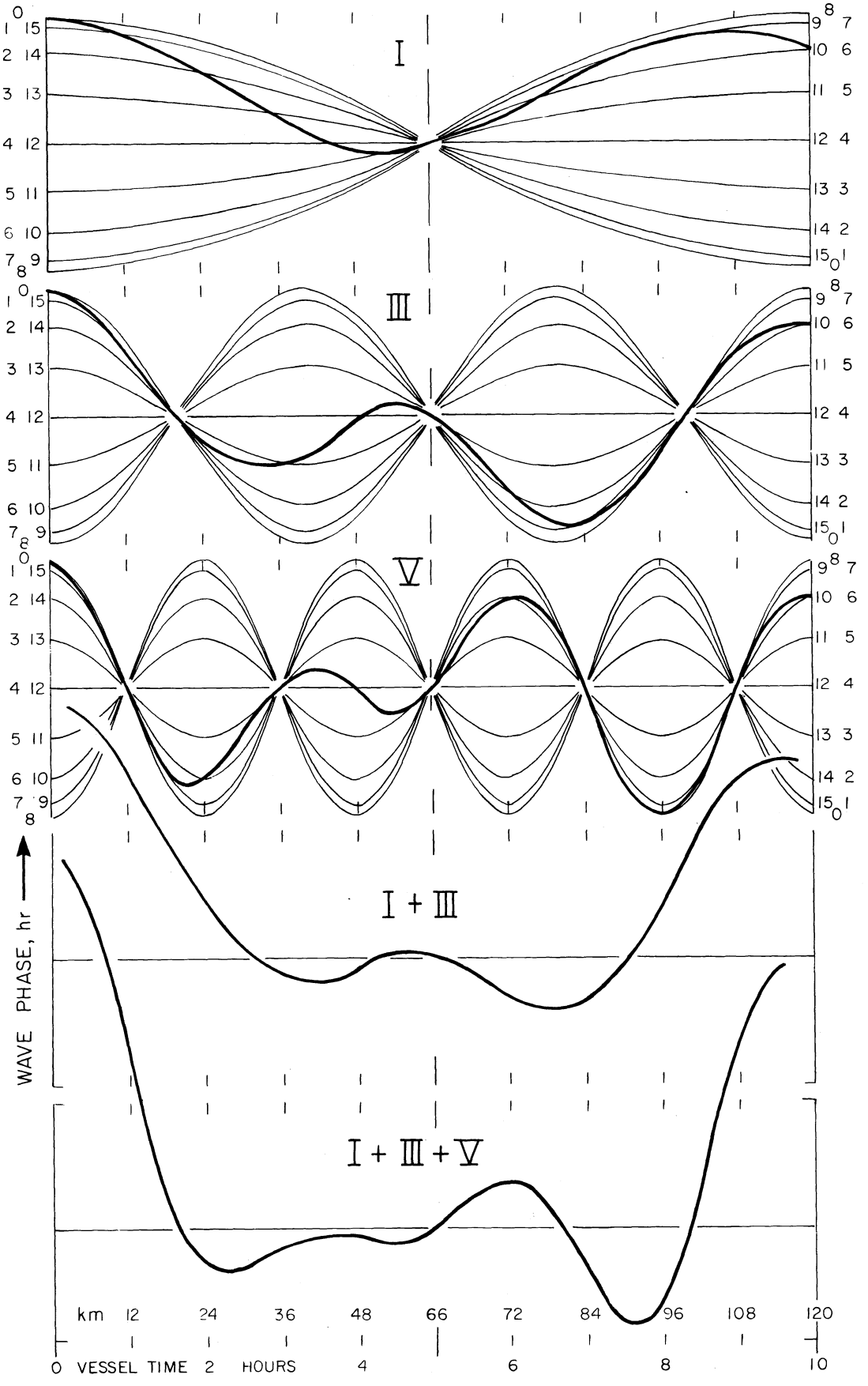

Fig. 74. "Thermocline depth" as observed from a vessel during a 10 hr crossing of a model basin of 120 km width. For full legend see page opposite fig. 71.

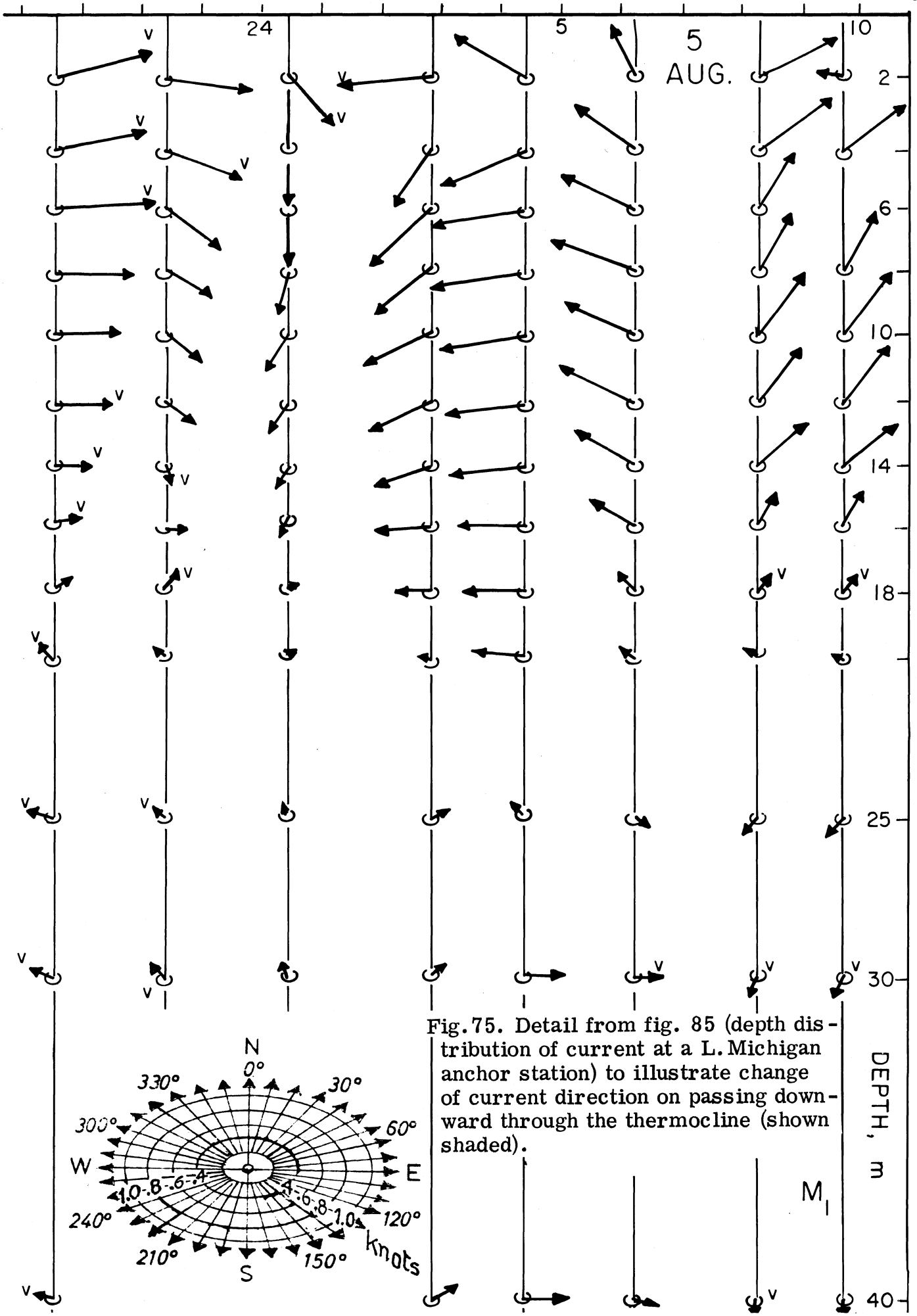

Fig. 75. Detail from fig. 85 (depth distribution of current at a L. Michigan anchor station) to illustrate change of current direction on passing downward through the thermocline (shown shaded).

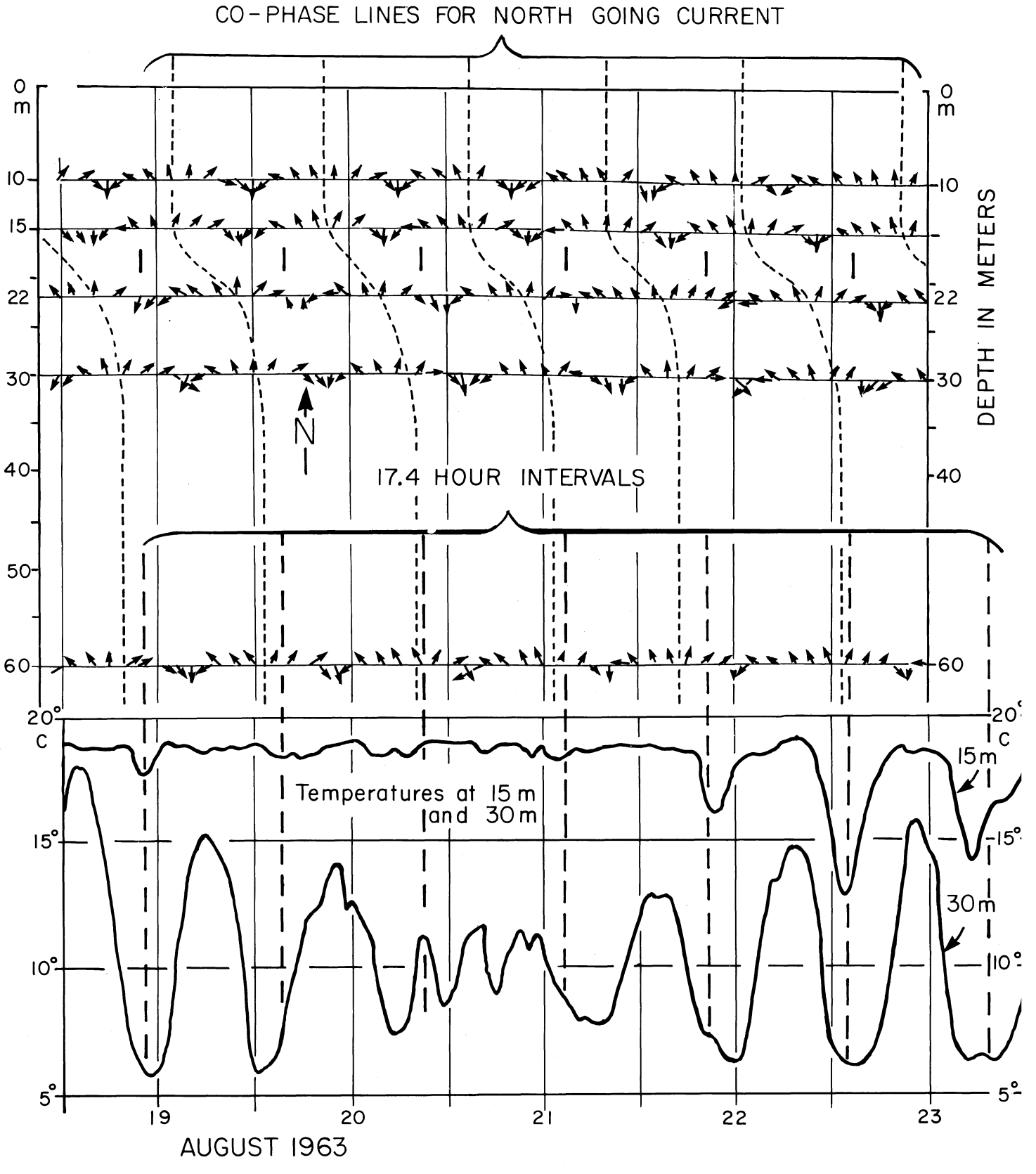

Fig. 76. Lake Michigan, station 8, 19-23 August 1963. Current directions at five depths (10, 15, 22, 30 and 60 m; adapted from U.S. Dept. Int. 1967, fig. 6-3), compared with temperatures at two depths (15 and 22 m, Verber, personal communication).

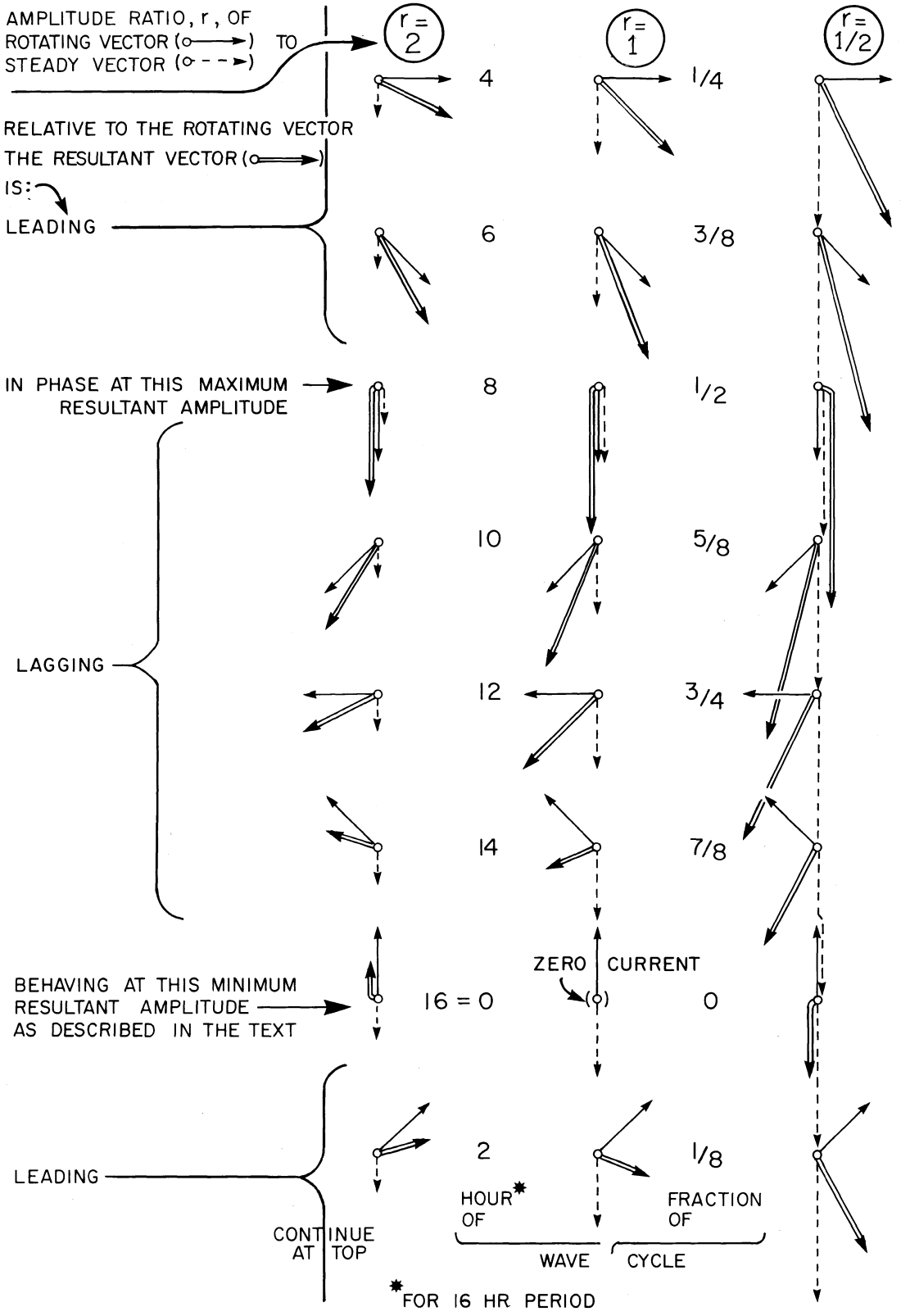

Fig. 77. Vector addition of currents associated with a Poincaré wave of 16 hr period ("rotating vector", thin unbroken arrow) and a steady, uni-directional current ("steady vector", thin broken arrow). The vector sum ("resultant vector", thick arrow) is illustrated at 1/8 wave cycle intervals and for three vector amplitude ratios, r (rotating/steady), of 2, 1 and 1/2. The figure is further explained in the text.

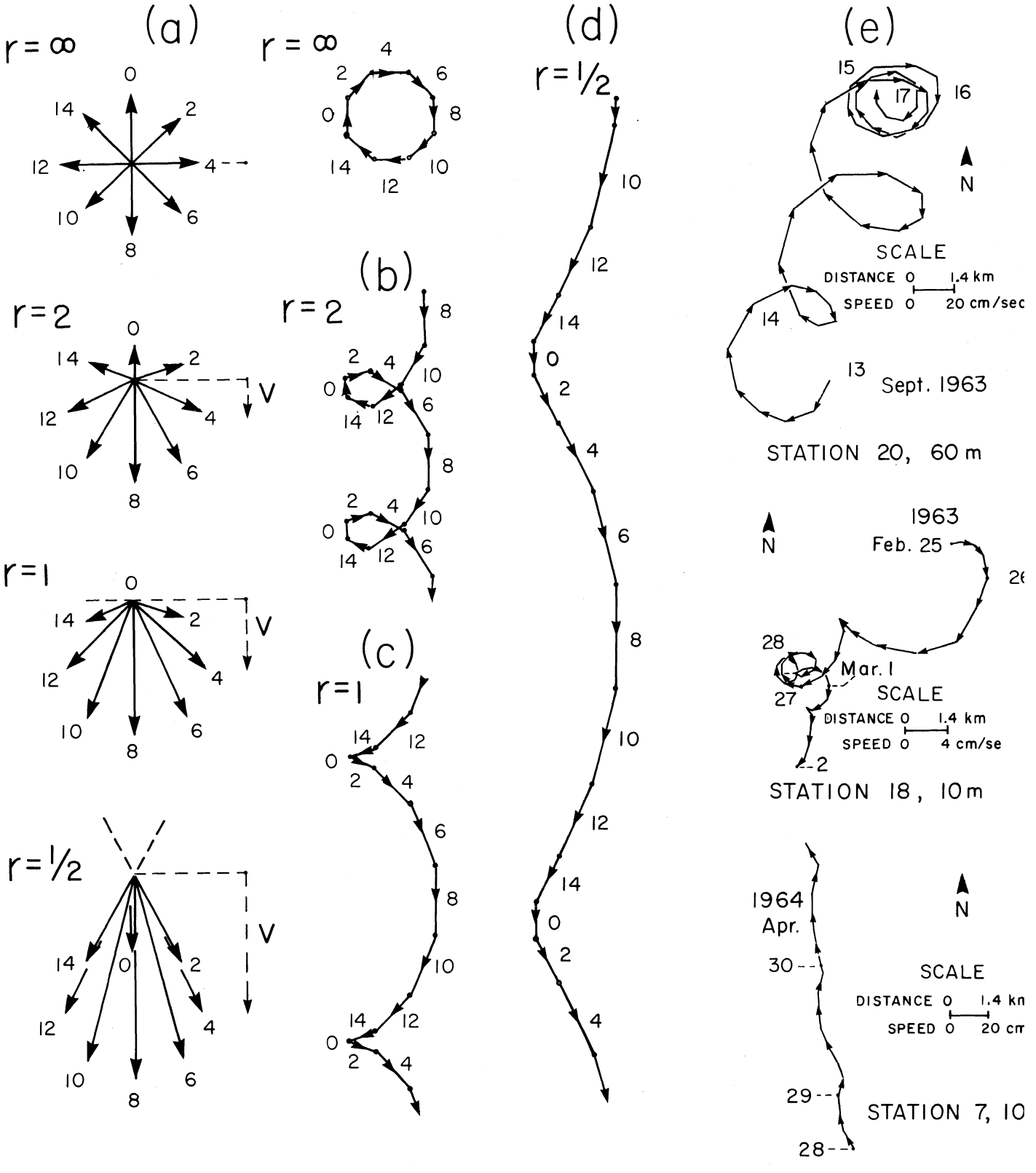

Fig. 78. (a), current "roses" corresponding to vector amplitude ratios (rotating/steady, see legend of fig. 77) r = ∞, 2, 1, and 1/2; (b), (c), and (d), current trajectories corresponding to r = 2, 1, and 1/2, respectively; (e) observed current trajectories in Lake Michigan (progressive vector diagrams from Verber 1966).

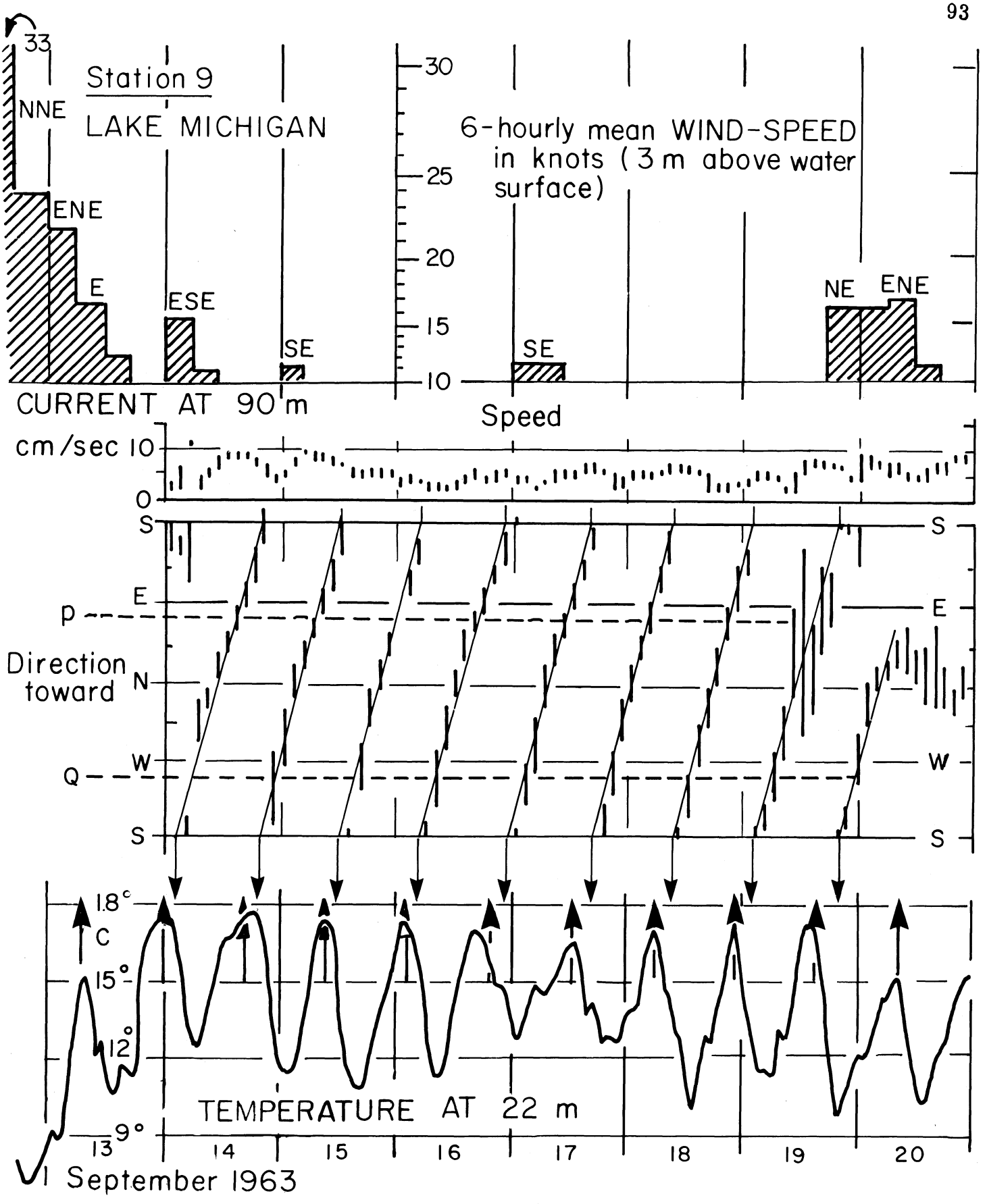

Fig. 79. Lake Michigan, station 9, 13-20 September 1963. Current speed and direction at 90 m (adapted from Verber 1965) compared with temperature at 22 m and with wind speed at that station (Verber, personal communication).

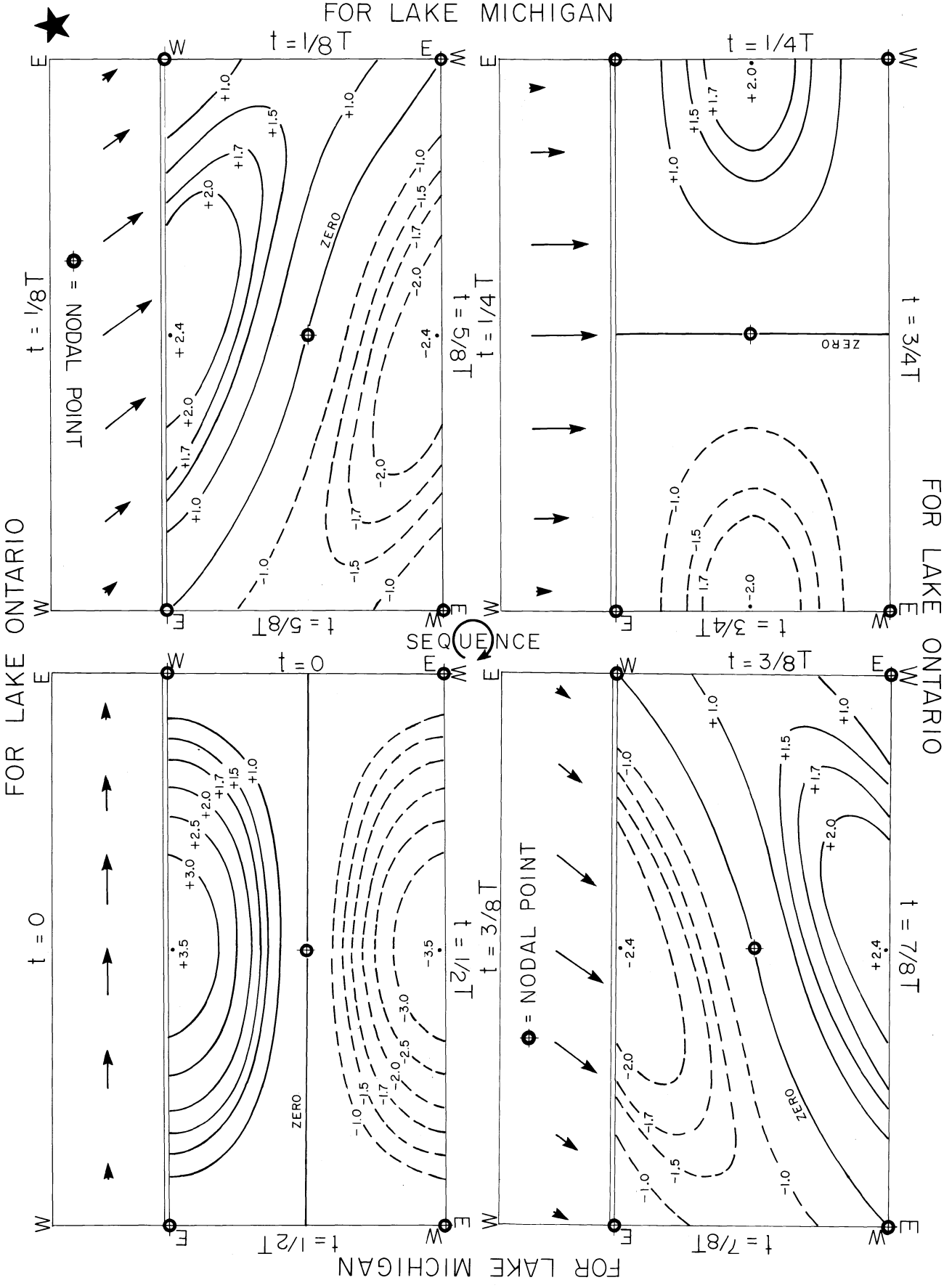

Fig. 80. Legend on opposite page.

Fig. 80 (opposite page)

A standing Poincaré wave, of $\lambda_x/\lambda_y = 1/2$, produced by combination of a pair of fig. 51 progressive P waves of equal period , T, and of equal amplitude (i.e., the amplitude illustrated in fig. 51), traveling in opposite directions along a channel, the sides of which correspond to lines A and B in fig. 51. (The note in the legend to fig. 47 applies.) Here illustrated is the distribution of elevation in one standing P wave cell, i.e., of length $\lambda_y/2$ and width $\lambda_x/2$, at T/8 intervals. Also illustrated are the corresponding current vectors representative of the interior region of the cell (see text). Viewed with the asterisk at top right, the long axis of the cell is orientated E-W as a model for Lake Ontario, and the first four of the eight stages of one oscillation cycle are seen. Rotated through 180°, the figure shows the four succeeding stages. Turned through 90° and 270°, the figure models the corresponding stages for Lake Michigan with the long axis of the cell orientated N-S.

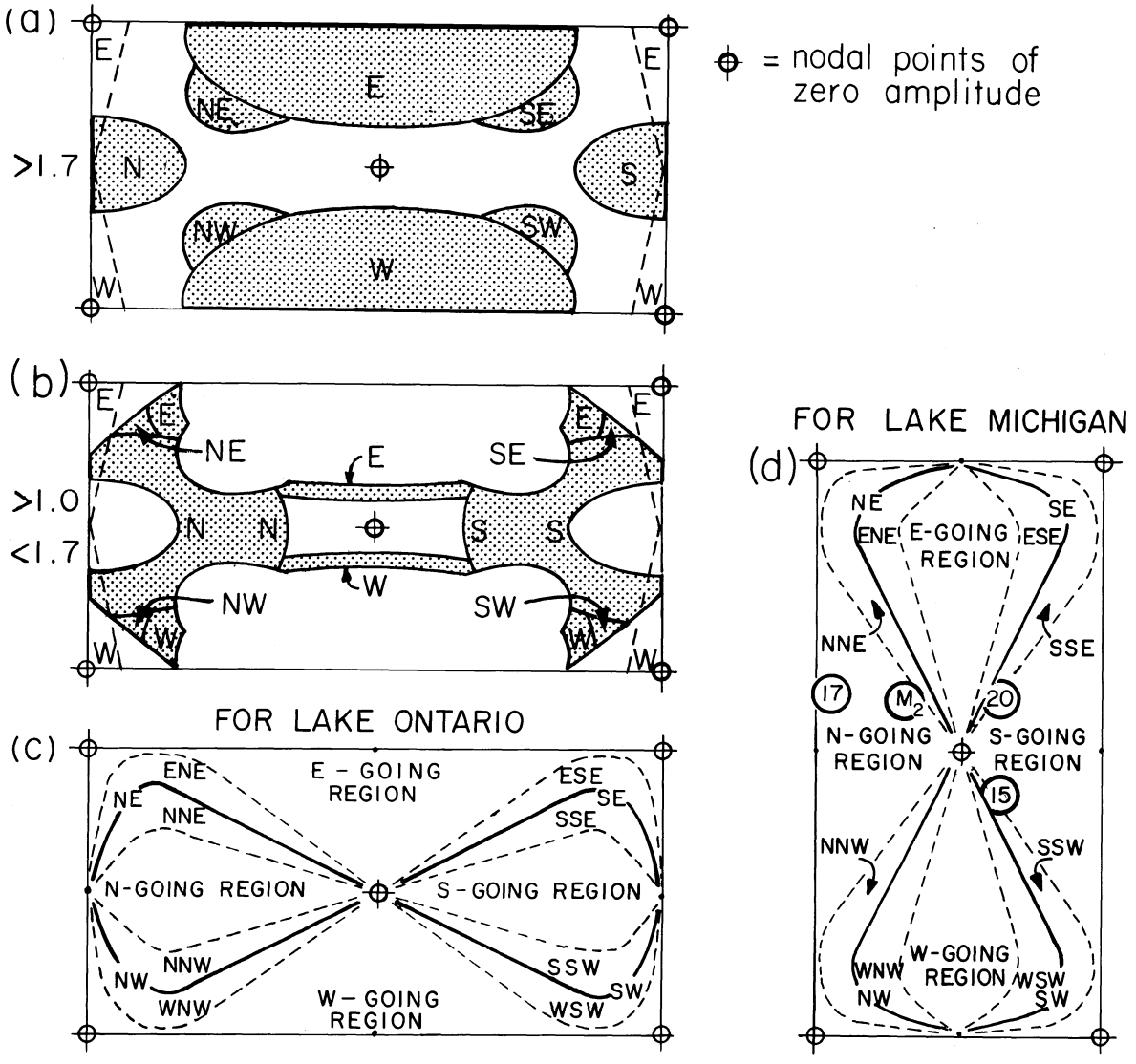

Fig. 81. Distribution, within the fig. 80 standing Poincaré wave cell, of those regions in which the maximum positive elevation (MPE) is: (a) > 1.7; and (b) < 1.7 > 1.0. For each region, and for the whole cell in (c) for Lake Ontario and (d) for Lake Michigan, the direction toward which the current flows at the time of MPE is shown. (The note in the legend of fig. 47 applies.)

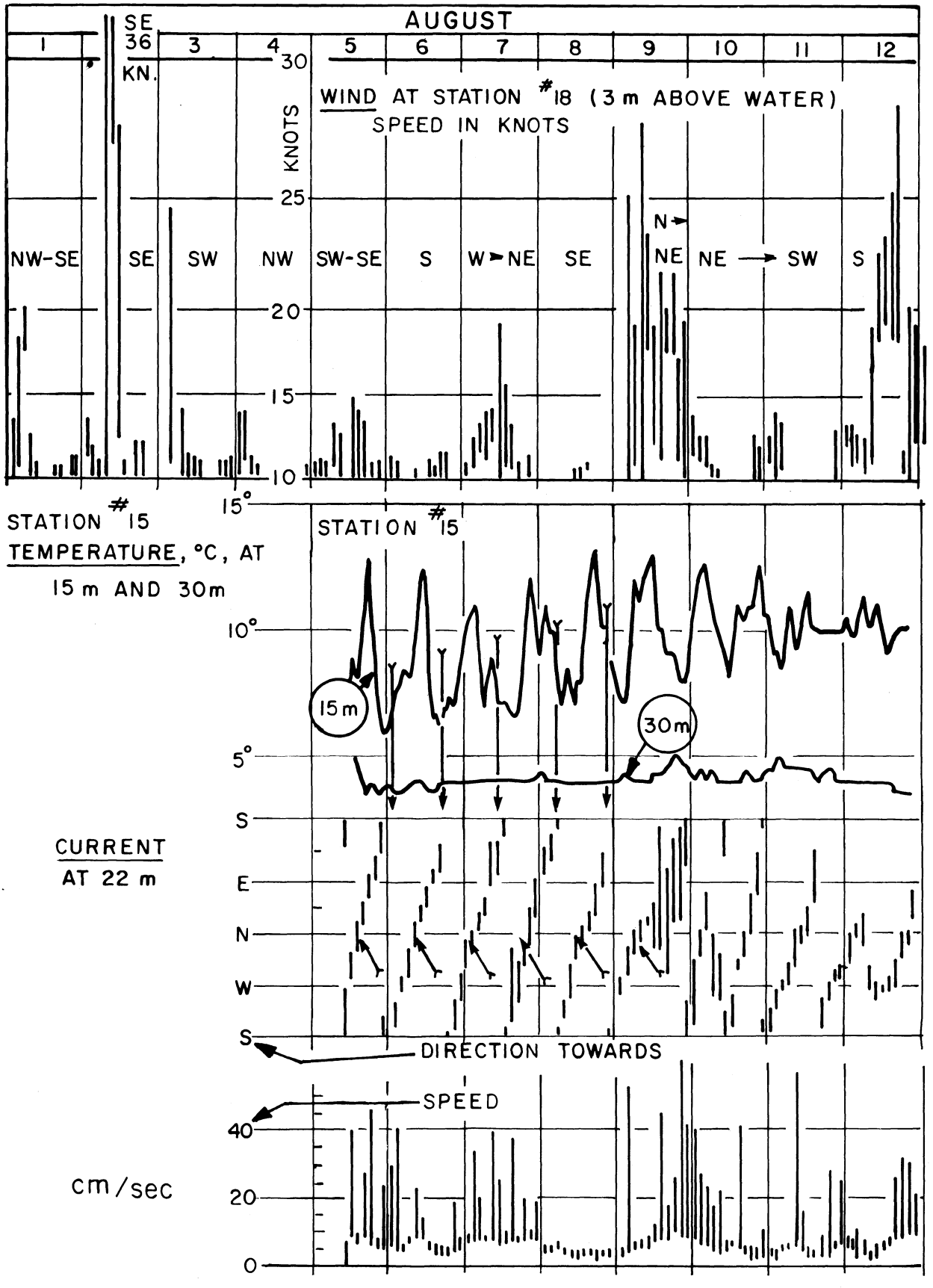

Fig. 82. Lake Michigan, station 15, 1-12 August 1963: see legend of fig. 83, noting different depths of measurements.

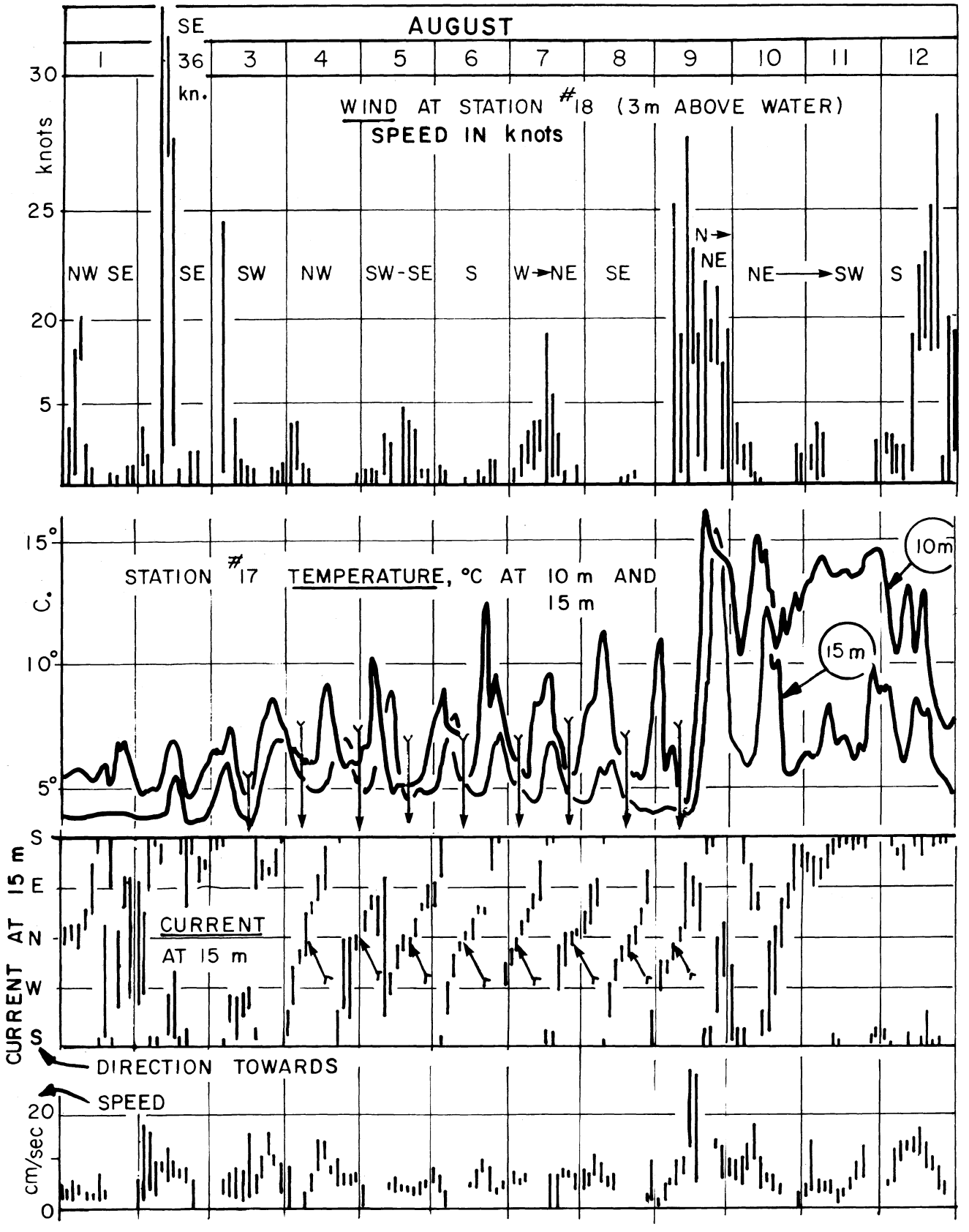

Fig. 83. Lake Michigan, station 17 (U.S. Dept. Int. 1967), 1-12 August 1963: temperature (hourly) at 10 m and 15 m; current speed and direction (2 hourly ranges) at 22 m; wind speed and direction at station 18.

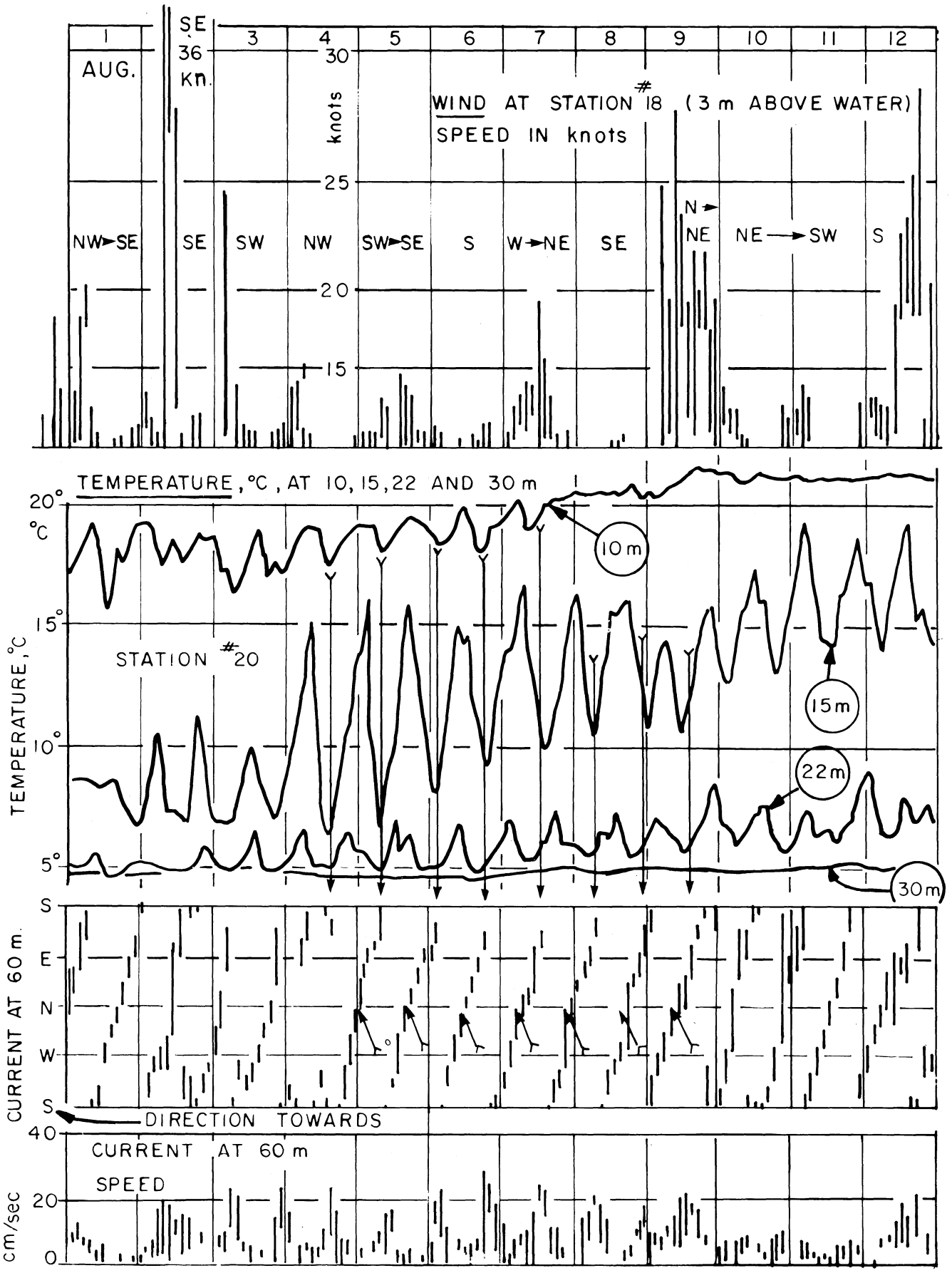

Fig. 84. Lake Michigan, station 20, 1-12 August 1963: see legend of 83, noting different depths of measurements.

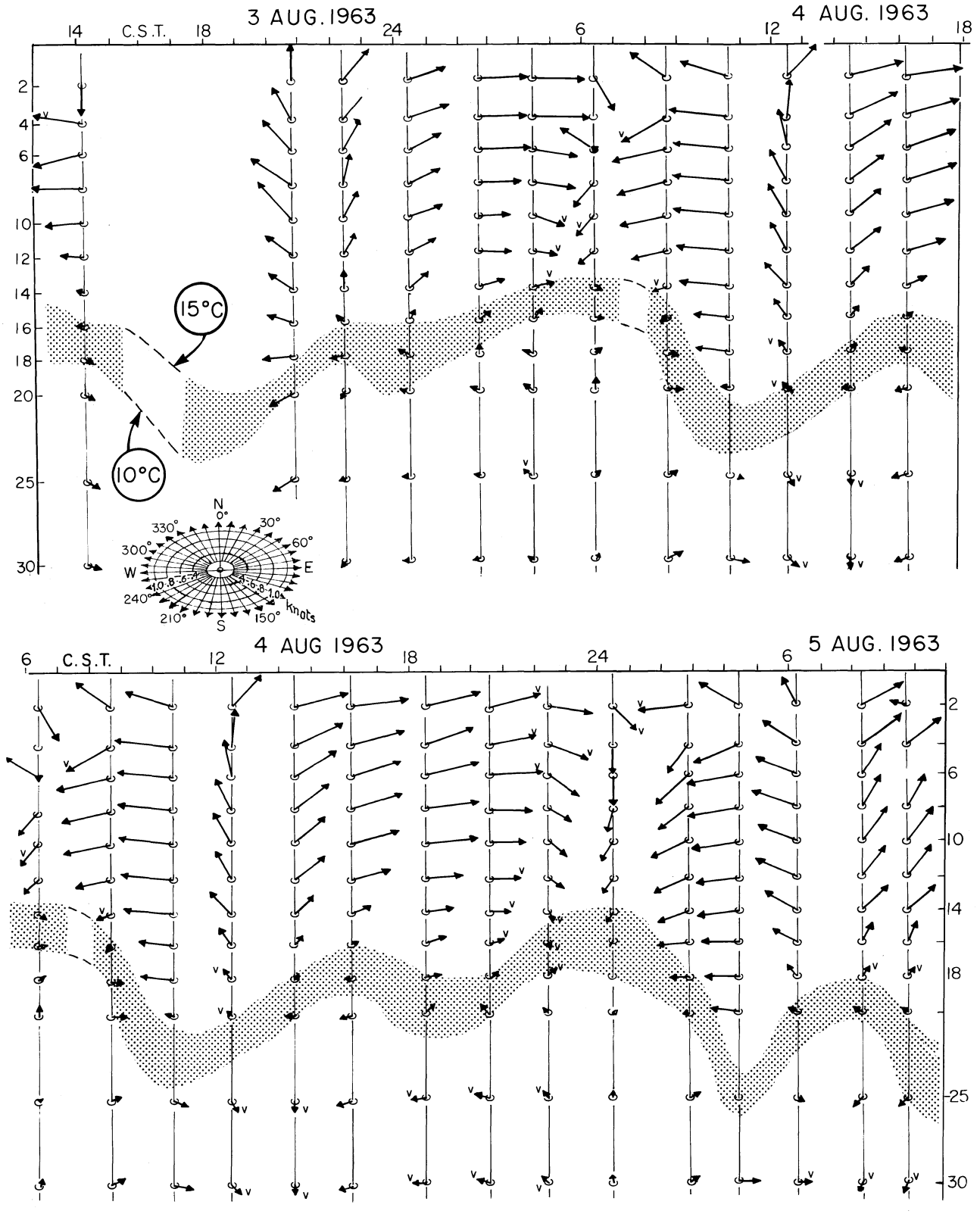

Fig. 85. Lake Michigan, 3-5 August 1963. Distribution of current speed and direction, at roughly 2 hr intervals in the upper 30 m at anchor station M_2 (see fig. 65). Also shown (shaded) is the thermocline layer, defined as bounded by the 10° and 15° isotherms. The figure (re-drawn from Mortimer 1968) is composed of two overlapping portions to shown how current and thermocline patterns follow an approximately 17 hr cycle.

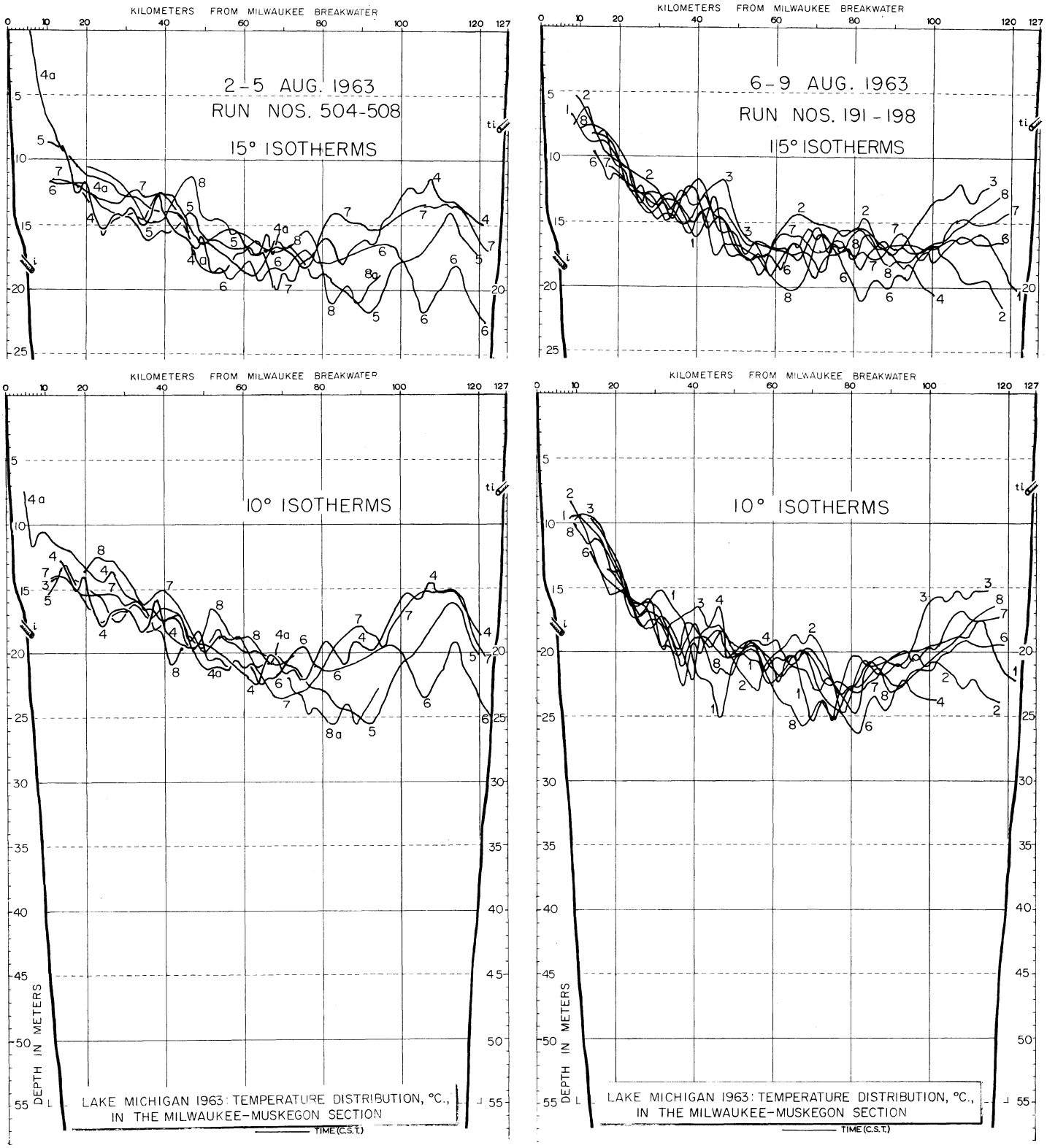

Fig. 86. Lake Michigan, 1963: distribution of the 15° and 10° C isotherms, observed from a ferry, Milwaukee-Muskegon transection, superimposed from two groups of consecutive crossings, 2-5 and 6-9 August.

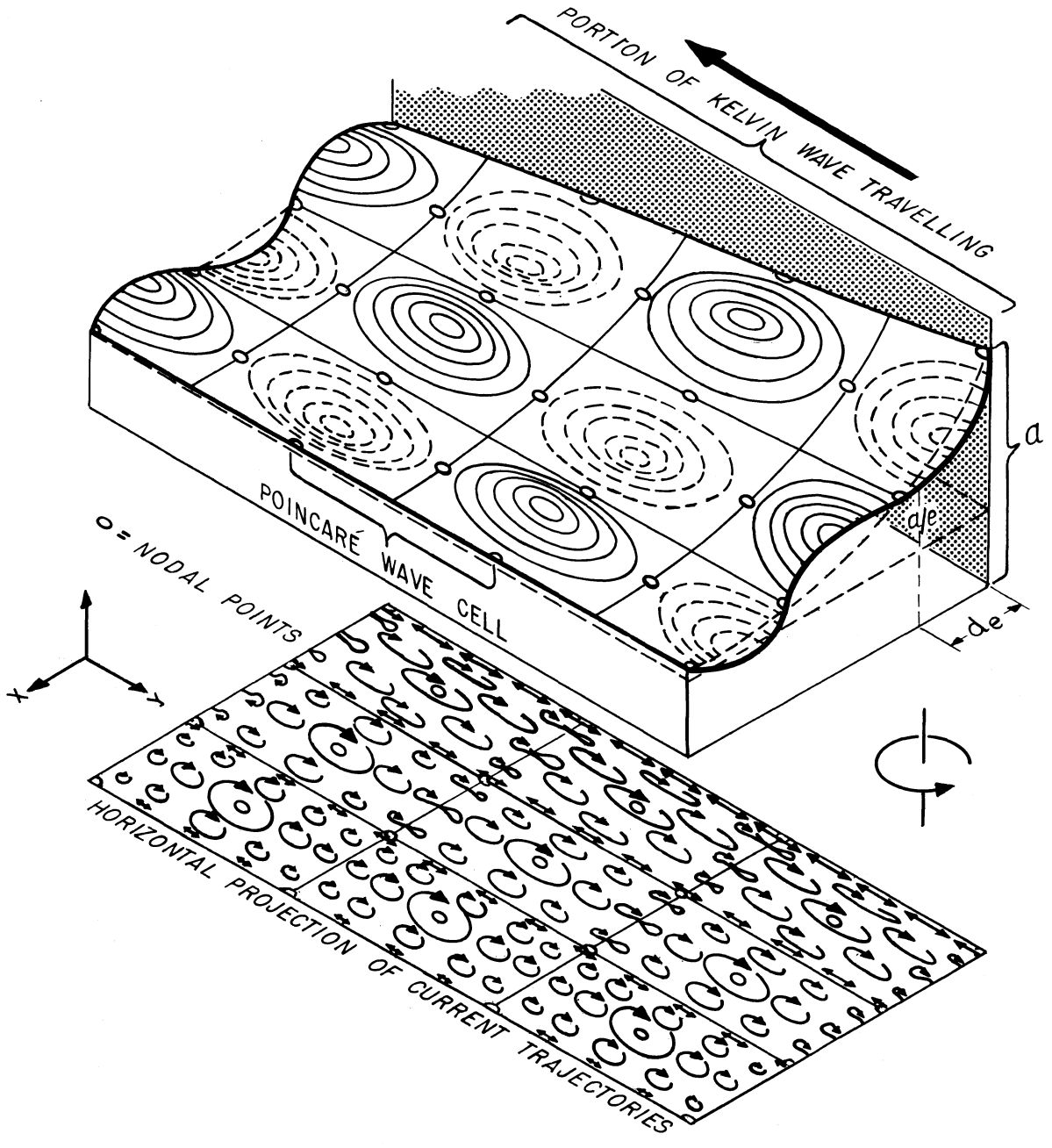

Fig. 87. Combination of a multinodal standing Poincaré wave in a semi-infinite ocean model (or in a very wide channel, of which only one side is shown) and a portion of a Kelvin wave traveling along the side. The elevation and current amplitudes associated with the Kelvin wave are at a maximum at the channel side (elevation amplitude, a) and decrease exponentially away from the side in the x-direction, falling to 1/e of the "onshore" value at a distance d_e from the side. (The note in the legend in fig. 47 applies.) The figure (adapted from Mortimer 1968) illustrates the transition, in current trajectories, from a nearshore pattern dominated by the K wave to a pattern dominated by the P wave at distances > $2d_e$ offshore.

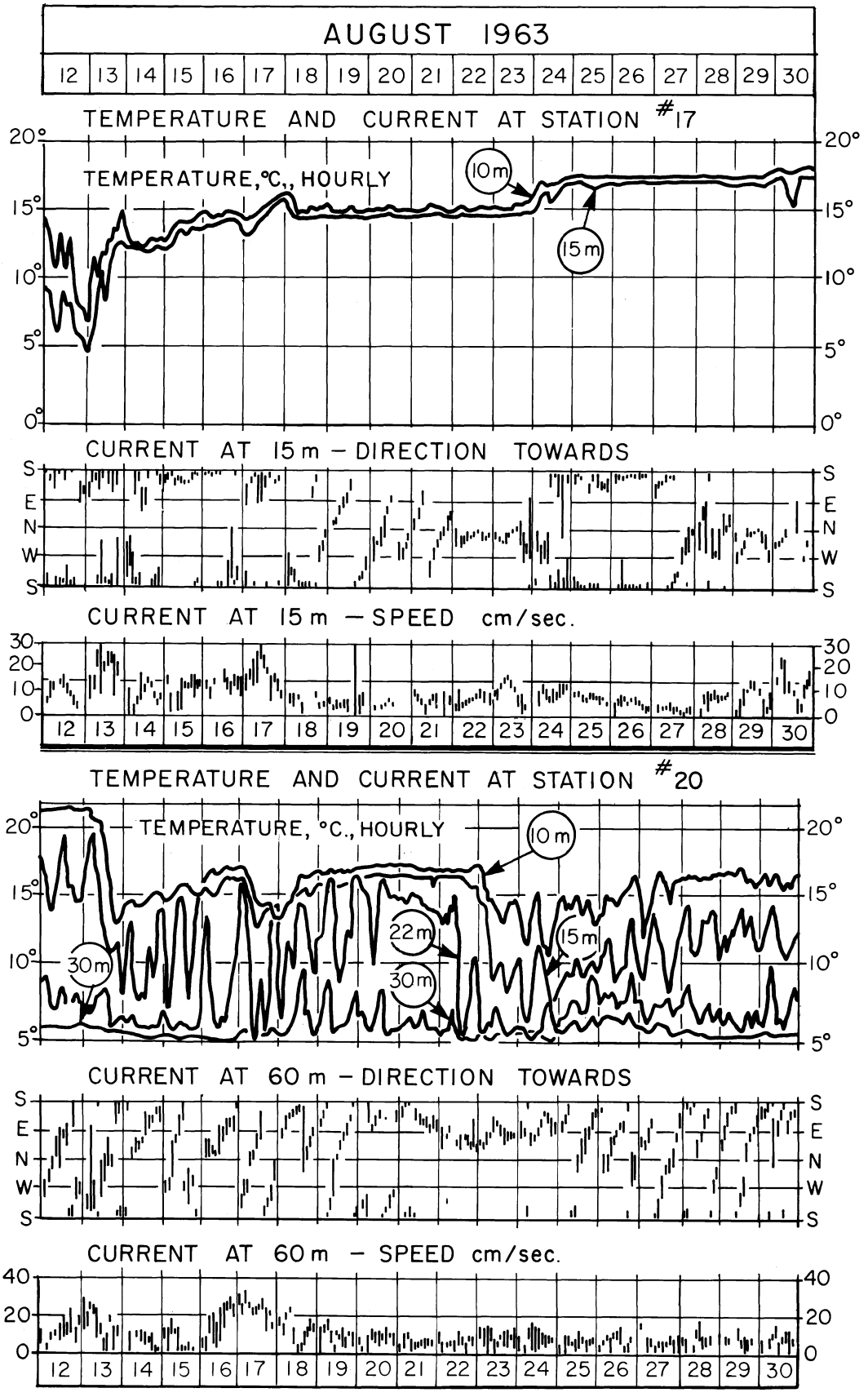

Fig. 88. Lake Michigan, stations 17 and 20 (U.S. Dept. Int. 1967), 12-30 August 1963. Temperature (°C, hourly) at 10 and 15 m (sta. 17) and 10, 15, 22, and 30 m (sta. 20); current direction and speed at 15 m (sta. 17) and 60 m (sta. 20).

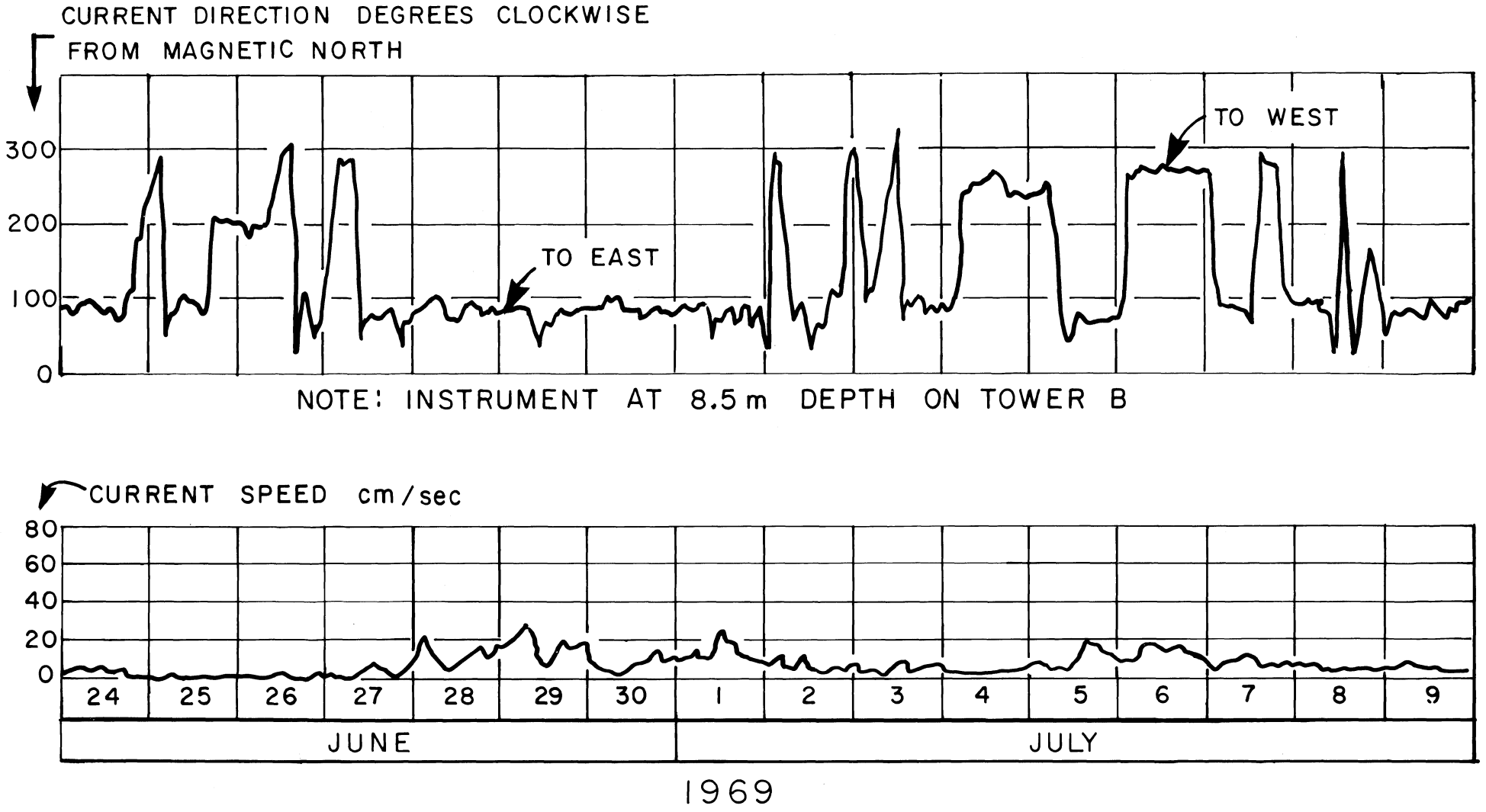

Fig. 89. Lake Ontario, 24 June - 9 July 1969. Current direction and speed at 8.5 m depth on a tower close to shore (in about 13 m of water) at Nine Mile Point, Oswego, N.Y. (from Gunwaldsen, et al.1970).

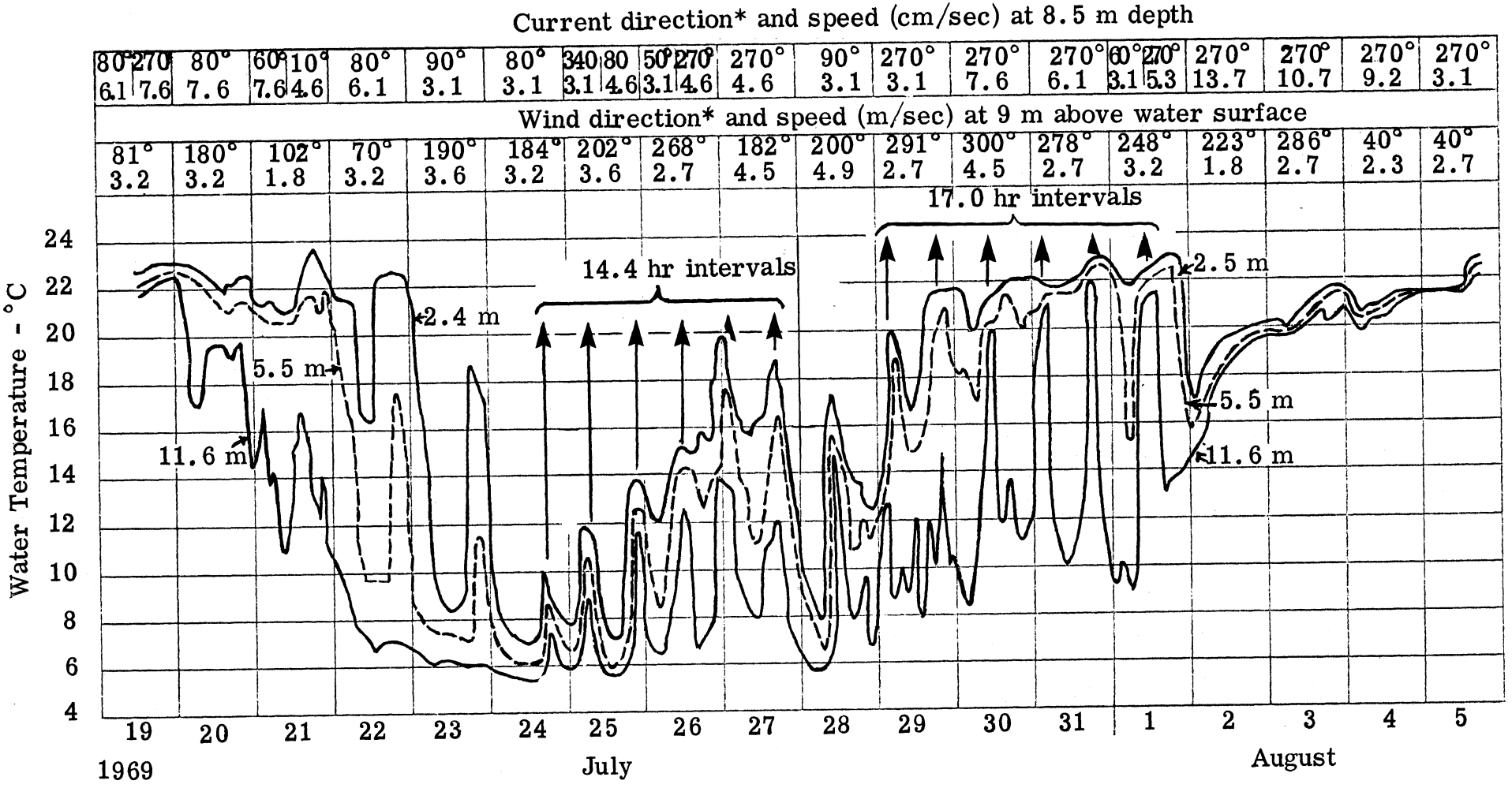

*Degrees relative to magnetic N and from the direction indicated

Fig. 90. Lake Ontario, 19 July - 5 August 1969. Temperature oscillations at three depths (2.4, 5.5 and 11.6 m) on a tower in 13 m of water near Nine Mile Point, Oswego, N.Y. (adapted from Gunwaldsen, et al. 1970). Daily (or 12 hr) mean speeds and direction of wind and current are also shown. Vertical arrows indicate mean periodicities of 14.4 hr during 24-27 July and 17.0 hr during 29 July - 1 August.

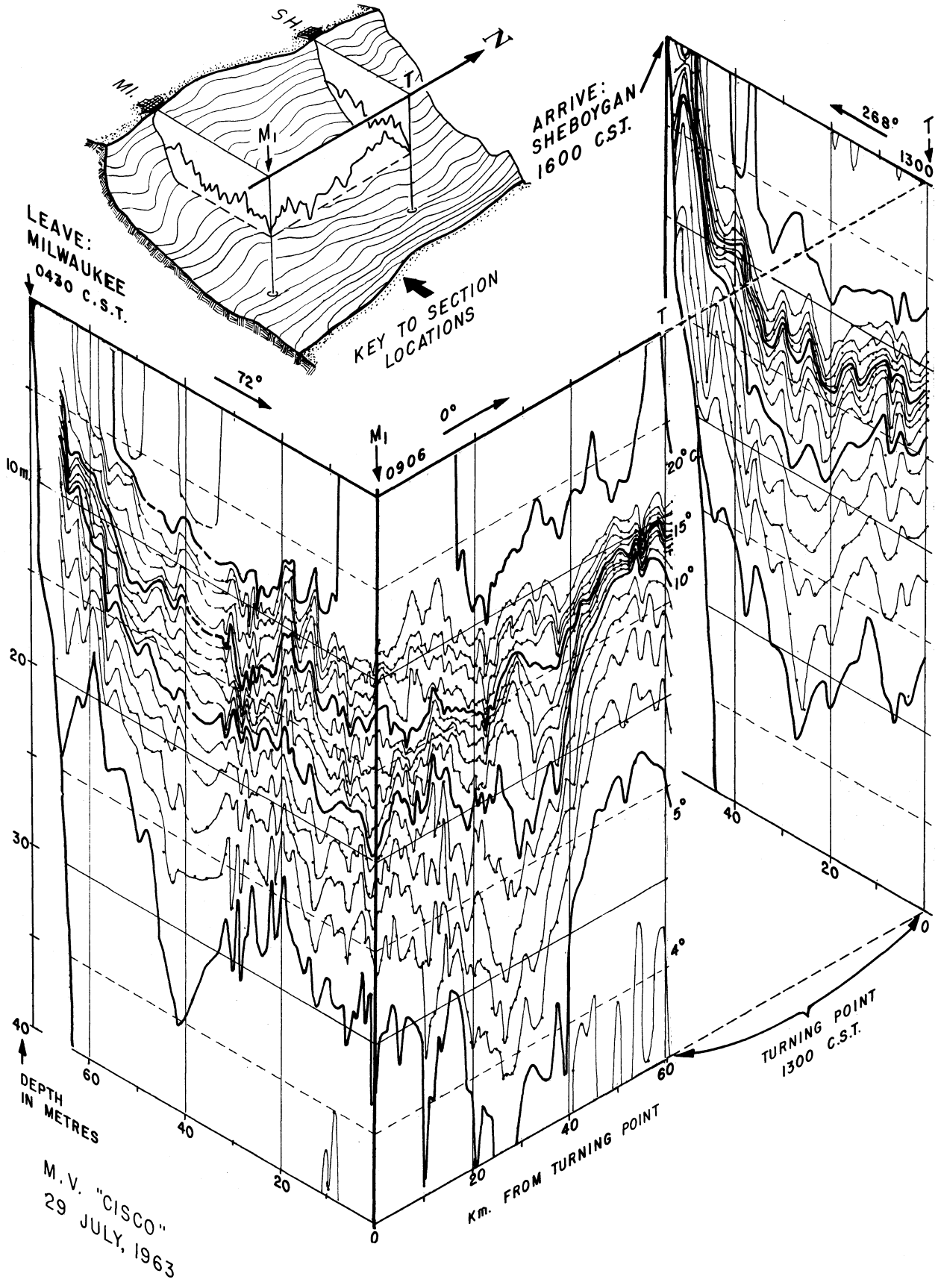

Fig. 91. Lake Michigan, 29 July 1963. Distribution of temperature, °C, observed from R. V. "Cisco", on a cruise from Milwaukee to mid-Lake, then north for 60 km, then west to Sheboygan. Isometric projection; directions °(true); adapted from Mortimer (1968).

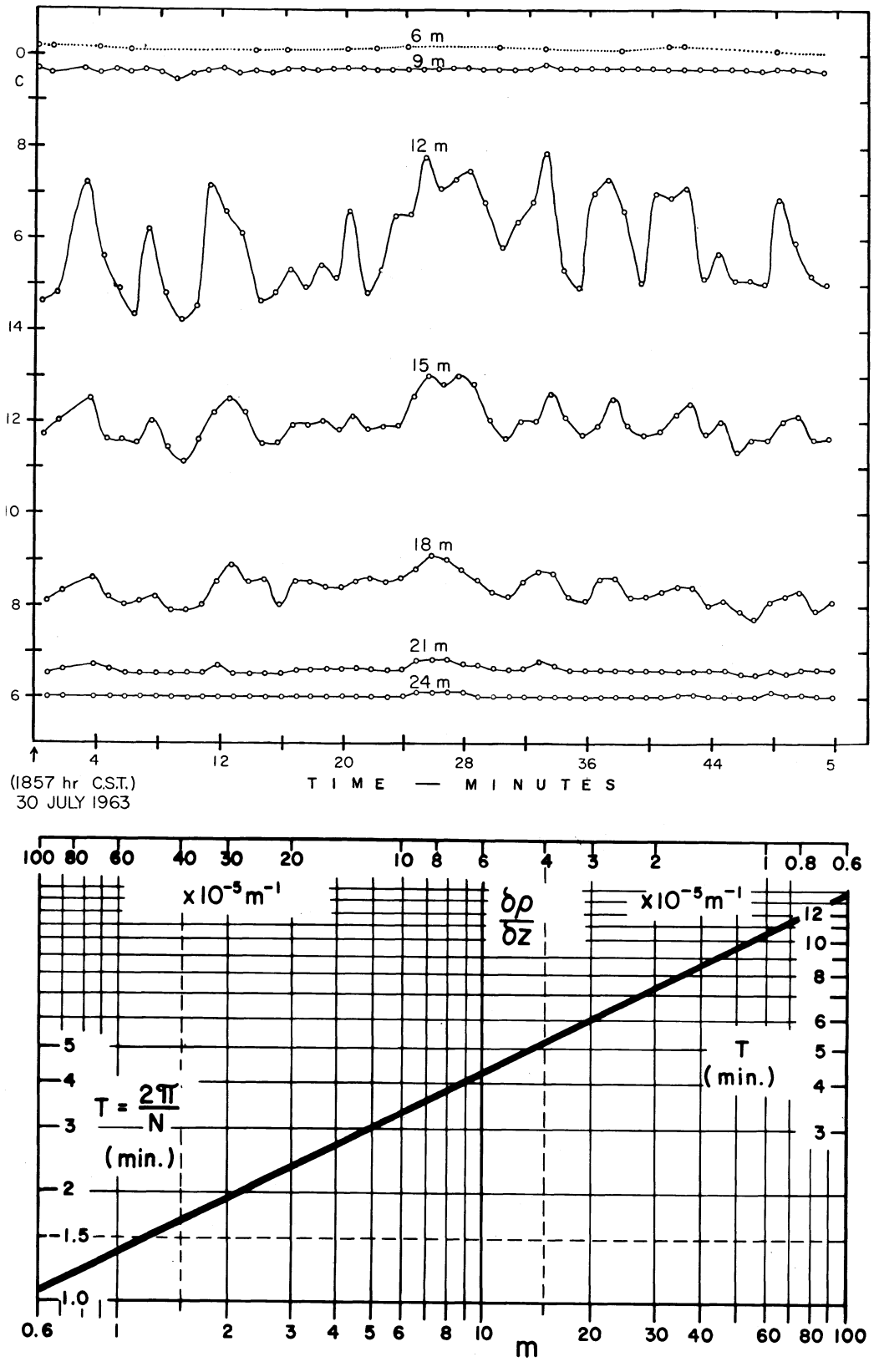

Fig. 92. Upper portion: Lake Michigan, 30 July 1963. Temperature, °C, at several depths ranging from 6 to 24 m at anchor station M_2 (see fig. 65) during a 54 min interval, Brunt-Väisälä diagram.
Lower portion: relation between the Brunt-Väisälä period ($2\pi/N$) and the vertical density gradient($\partial\rho/\partial z$, upper scale) or the thickness of a model "thermocline" (lower scale) defined as a uniform gradient between the 10° and 15°C isotherms (from Mortimer et al. 1968).